

Electronic Thesis and Dissertation Repository

7-7-2021 10:00 AM

Self-Immolative Dendritic Hydrogels

Karanpreet Gill, *The University of Western Ontario*

Supervisor: Gillies, Elizabeth R., *The University of Western Ontario*

A thesis submitted in partial fulfillment of the requirements for the Master of Science degree in Chemistry

© Karanpreet Gill 2021

Follow this and additional works at: <https://ir.lib.uwo.ca/etd>

Recommended Citation

Gill, Karanpreet, "Self-Immolative Dendritic Hydrogels" (2021). *Electronic Thesis and Dissertation Repository*. 7902.

<https://ir.lib.uwo.ca/etd/7902>

This Dissertation/Thesis is brought to you for free and open access by Scholarship@Western. It has been accepted for inclusion in Electronic Thesis and Dissertation Repository by an authorized administrator of Scholarship@Western. For more information, please contact wlsadmin@uwo.ca.

Abstract

Stimuli-responsive hydrogels have attracted significant research interest as they exhibit triggerable drug release or changes in mechanical properties. Hydrogels containing dendrimers have also been targeted as their multiple functional groups provide enhanced crosslinking or chemical conjugation. Self-immolative dendrimers (SIDs) fragment in response to a stimulus event, but they have not been explored for the preparation of stimuli-responsive hydrogels. This thesis reports the preparation of hydrogels from a 4-arm poly(ethylene glycol) polymer and SIDs composed of a photosensitive *o*-nitrobenzyl carbonate core. The gel content and equilibrium water content were examined as a function of the hydrogel formulation. Hydrogel degradation was demonstrated using ¹H NMR spectroscopy and measurements of the mechanical properties before and after degradation. The loading and release of the drug celecoxib from the hydrogels was also investigated. This work introduces a new implantable stimuli-responsive dendritic hydrogel platform that can potentially be used for the delivery of celecoxib or cell encapsulation and release.

Keywords

Hydrogels, self-immolative dendrimers, poly(ethylene glycol), photosensitive, drug delivery.

Summary for Lay Audience

Certain molecules with tree-like morphologies have attracted a lot of interest due to their structural precision and functional diversity. Such characteristics afford them various applications in drug delivery, catalysis, sensors, and agriculture. This group of molecules has recently been extended to include a new class of materials, which are comprised of three components: (i) central core (ii) interior branches and (iii) peripheral functional groups from which molecules are released. The novel species fragment in a domino-like fashion in response to a trigger event, such as UV light irradiation, at the core. However, their incorporation into hydrogels has not yet been explored. Hydrogels are of significant interest for biomedical applications due to their high water content, which resembles that of tissues. They have been investigated for both cell and drug delivery. This thesis describes the synthesis of hydrogels that contain photosensitive tree-shaped moieties. Upon exposure to UV light, the fragmentation of the networks was assessed. The scaffolds were made to ensure the degradation products were not toxic to the human body. Also, the durability of the scaffolds in the presence and absence of UV light was examined. Finally, the hydrogels were loaded with drug molecules to investigate the networks' drug release behaviour with and without irradiation. Overall, the materials produced in this thesis are proof-of-concept for the development of future biomaterials for cell and drug delivery.

Co-Authorship Statement

The work presented in this thesis was written by the author and revised by Dr. Elizabeth Gillies. Compression data for the hydrogels was collected by Xueli Mei, a graduate student in the Gillies lab, while size exclusion chromatographic runs were performed by Aneta Borecki, a lab technician in the Gillies lab.

Dedication

This thesis is dedicated to the memory of my father who never saw this adventure. He taught me to be optimistic and persevere through any setback. I miss you every day, Dad.

Acknowledgments

First and foremost, I would like to thank my supervisor, Dr. Elizabeth Gillies. Her mentorship and invaluable expertise have undoubtedly helped me overcome many hurdles in my research and has shaped me to be a better chemist. She always encouraged me to think outside the box when research didn't go as planned. The past two years in her group have been an amazing learning experience.

Thank you to past and present members of the Gillies group for all the great times spent in lab. I especially want to thank Quinton and Xiaoli, who were always available to teach me techniques and answer my endless questions about polymer and organic chemistry. Also, I must thank Monica, Trent, Charmaine, Echo, Eric, Jared, Jue, Andrew, Jan, Farshid, and Terry for their continuous support in lab. I'd also like to extend my appreciation to Aneta for helping me with the instrumental setup for numerous experiments.

I would also like to show my gratitude towards all the amazing friends I've made while at Western University. Thank you to my friends from undergrad for being there during the hard and easy times. I would also like to thank the friends I've made in the Chemistry department for their advice, support, and simply distractions when research got stressful. My time at Western wouldn't be the same without the wonderful company of members from the Baines, Ding, FLL, and Wren groups.

Last but not least, I must thank my mom, sister, and brother for their unwavering encouragement and support. Thank you for teaching me the meaning of hard work, but also reminding me to take breaks and relax when things got stressful.

Table of Contents

Abstract.....	i
Summary for Lay Audience.....	ii
Co-Authorship Statement.....	iii
Dedication.....	iv
Acknowledgments.....	v
Table of Contents.....	vi
List of Tables.....	ix
List of Figures.....	x
List of Schemes.....	xiv
List of Abbreviations.....	xv
Chapter 1.....	1
1 Introduction.....	1
1.1 Dendrimers: Structure, Synthesis, and Properties.....	1
1.2 Self-immolative Dendrons (SIDs).....	3
1.2.1 Structure and Properties.....	3
1.2.2 SID Fragmentation Methods.....	4
1.2.3 Poly(ethylene glycol) (PEG).....	5
1.2.4 Photosensitive SIDs.....	6
1.2.5 Chemically-responsive SIDs.....	7
1.2.6 Benzyl Carbamate/Carbonate Backbones.....	8
1.2.7 Benzyl Ether Backbones.....	10
1.2.8 Cinnamyl Carbamate/Carbonate Backbones.....	12
1.2.9 Applications of SIDs.....	14
1.2.10 Rotational Isomers.....	15

1.3	Hydrogels	16
1.3.1	Background	16
1.3.2	Synthesis	16
1.3.3	Properties	22
1.3.4	Stimuli-responsive Hydrogels for Biomedical Applications	24
1.3.5	Dendritic Hydrogels for Biomedical Applications	28
1.4	Motivation for Thesis.....	31
1.5	References.....	33
Chapter 2	39
2	Development of SID Hydrogels as Drug Delivery Systems.....	39
2.1	Introduction.....	39
2.2	Results and Discussion	41
2.2.1	Synthesis and Characterization of G1 and G2 SIDs	41
2.2.2	Degradation of G1 and G2 SIDs.....	44
2.2.3	Synthesis and Characterization of PEG Derivatives.....	46
2.2.4	Synthesis and Characterization of Hydrogels	48
2.2.5	Copper Content in SID Hydrogels	49
2.2.6	Degradation of the Hydrogels.....	50
2.2.7	Compression Moduli of TEG-alkyne and SID Hydrogels.....	52
2.2.8	Drug Release	54
2.3	Conclusion	56
2.4	Experimental	57
2.4.1	General Experimental Details	57
2.4.2	Synthesis of Crosslinkers and Polymers.....	58
2.4.3	Degradation of SIDs	64

2.4.4 Hydrogel Synthesis, Characterization, and Degradation	64
2.4.5 Trace Elemental Analysis	66
2.4.6 Drug Release	66
2.5 References	70
Chapter 3	74
3 Conclusions and Future Work	74
3.1 References	76
Appendix: Supplementary Figures	77
Curriculum Vitae	102

List of Tables

Table 1. Gel content (%) and EWC of the different hydrogel formulations.....	49
Table 2. Average loading of CXB (%) in hydrogel systems prepared from 15% (w/w) of 4-arm-PEG-azide and TEG or SID alkynes.....	55

List of Figures

Figure 1.1. a) Dendron, b) Dendrimer.	1
Figure 1.2. Divergent and convergent synthesis of dendrimers.....	2
Figure 1.3. Amphiphilic Janus dendrimer reported by Najafi and coworkers. Red and blue correspond to non-polar and polar moieties, respectively. ⁷	2
Figure 1.4. A core is cleaved off in response to an external stimulus; b) Removal of the core results in the disassembly of the SID; c) The fragmentation products include the core and derivatives of the interior and terminal groups.	3
Figure 1.5. SID fragmentation by a) 1,4-elimination, b) 1,6-elimination, c) 1,8-elimination, d) 1,5- cyclization.	5
Figure 1.6. Chemical structure of PEG.....	6
Figure 1.7. a) <i>o</i> -Nitrobenzyl, b) 4-Bromo-7-hydroxycoumarin photosensitive moieties (red).....	6
Figure 1.8. Photosensitive a) First-, b) Second-generation SIDs reported by Brochet and Kastrati, R corresponds to <i>p</i> -nitrophenoxy moieties. ¹⁷	7
Figure 1.9. Enzymatically activated second-generation SID reported by Shabat and coworkers. ²⁰	8
Figure 1.10. Third-generation SID containing a Boc core and peripheral 4-nitroaniline moieties, as reported by Shabat and coworkers. ²¹	10
Figure 1.11. a) Zeroth-, b) First-, c) Second-generation SIDs containing a 4-allyloxy trigger group, benzyl ether backbones and a terminal <i>p</i> -nitrophenoxy unit as reported by McGrath and coworkers. ²²	11

Figure 1.12. Second-generation dendron containing a 4-allyloxy trigger group, benzyl ether backbone and four terminal <i>p</i> -nitrophenoxy units, as reported by McGrath and coworkers. ²³	12
Figure 1.13. First-generation SID with a cinnamyl-based backbone as reported by Shabat and coworkers. ²⁴	13
Figure 1.14. Second-generation SID with a cinnamyl-based backbone as reported by DeGroot and coworkers. ²⁵	14
Figure 1.15. A trimeric SID developed by Shabat and researchers. ²⁷	15
Figure 1.16. Bond rotation about the a) α -carbon in peptides, b) C-N bond in carbamates.	16
Figure 1.17. Hydrogel structure.	16
Figure 1.18. Photopolymerization reaction between 4-arm-PEG norbornene and PEG thiol using the LAP initiator to form a hydrogel containing lysozyme and TGF β molecules in the scaffold, as reported by Anseth and coworkers. ³⁸ Purple and red circles correspond to lysozyme and TGF β , respectively.....	19
Figure 1.19. CuAAC click reaction.	20
Figure 1.20. (a) Azide or (b) Alkyne modified PVAs used for CuAAC reaction for hydrogel formation, as reported by Hilborn and coworkers. ⁴¹	20
Figure 1.21. Types of physical crosslinking include a) Ionic interactions, b) Hydrogen bonding, c) Hydrophobic interactions.....	21
Figure 1.22. Crosslinked alginate via ionic interactions with divalent calcium cations. Blue squares correspond to the alginate backbone.	22
Figure 1.23. Compression stress-strain curve.	23

Figure 1.24. LCST phase transition of a thermoresponsive polymer in aqueous solution. Green and blue correspond to hydrophobic and hydrophilic moieties, respectively.	24
Figure 1.25. Free radical polymerization of NIPAM and PEGDA initiated by ABCA to form a thermoresponsive hydrogel, as reported by Georgieva and coworkers. ⁵⁰	25
Figure 1.26. Chemical structure of pH-responsive polymers ionized under acid conditions to afford swollen hydrogels, as reported by Peppas and coworkers. ⁵¹	26
Figure 1.27. Photoisomerization of azobenzene.	27
Figure 1.28. Photoisomerization of the azobenzene moiety in the hydrogel leading to the release of hydrophobic drug molecules, as reported by Gupta and coworkers. ⁵³ Blue lines and purple markers correspond to dextran and aspirin drug molecules, respectively.	27
Figure 1.29. Photolabile macromonomer containing PEG, <i>o</i> -nitrobenzyl moieties, and terminal acrylate groups which crosslink with monoacrylated PEG to form a hydrogel for tissue regeneration, as reported by Anseth and researchers. ⁵⁴	28
Figure 1.30. a) Functionalized G4.0 PAMAM dendrimer, b) Copolymer of PEG and PLA containing peripheral acrylate groups, as reported by Wang and coworkers. ⁵⁵	30
Figure 1.31. Synthesis route of the modified G3.0 PAMAM dendrimer functionalized with PEG and acrylate moieties, as reported by Yang and coworkers. ⁵⁶	31
Figure 2.1. Schematic depiction of the UV light triggered fragmentation of a G1 SID hydrogel. Red lines, green pentagons, and orange circles represent PEG, triazole moieties, and interior branching units of the dendrimer, respectively.	40
Figure 2.2. ¹ H NMR spectra of (a) G1 SID and (b) G2 SID (400 MHz, CDCl ₃). Asterisks correspond to ethyl acetate. Rotamers are observed about the carbamate bonds.	44
Figure 2.3. ¹ H NMR degradation profile of the G1 SID in deuterated PBS:DMSO-d ₆ (1:1.25) (D ₂ O, 400 MHz). *denotes an irradiation exposure of 0.5 h. Red and green	

markers correspond to methylene and methyl protons, respectively, in the <i>N,N'</i> -dimethylimidazolidinone degradation product.	46
Figure 2.4. ¹ H NMR spectra of (a) non-irradiated, (b) irradiated G1 SID hydrogel in deuterated PBS:acetonitrile (100:1) (D ₂ O, 400 MHz). *denotes an irradiation exposure of 0.5 h followed by 1 h incubation at 37 °C. Red and green markers correspond to methylene and methyl protons, respectively, in the <i>N,N'</i> - dimethylimidazolidinone degradation product.	51
Figure 2.5. Degradation (%) of G1 and G2 SID hydrogels over time in deuterated PBS: acetonitrile (100:1). Arrows denote an irradiation exposure of 0.5 h followed by incubation at 37 °C for 1 h before measurement at the subsequent time point.....	52
Figure 2.6. Compressive moduli (n = 3) of non-irradiated and irradiated TEG-alkyne, G1 SID, and G2 SID hydrogels in PBS. TEG-alkyne hydrogels were irradiated for 0.5 h and incubated at 37 °C for 1 day while SID gels were exposed to UV light for four hours for four days and incubated overnight following each irradiation event. Non-irradiated hydrogels were incubated for the same time as irradiated systems of the same formulation. *denotes a statistically significant difference between hydrogel systems. Data was analyzed by a two-way ANOVA with a Tukey’s post-hoc test comparison of the means (p < 0.05).	53
Figure 2.7. Structure of CXB.....	54
Figure 2.8. Release of CXB from the TEG-alkyne hydrogel, as well as irradiated and non-irradiated G2 SID hydrogels in PBS containing 2 wt % polysorbate80. The dissolution rate of free CXB is included for comparison.	56

List of Schemes

Scheme 1.1. Fragmentation of a photolabile first-generation SID by 1,5-intramolecular cyclization followed by two 1,4-quinone-methide rearrangements resulting in the release of terminal pyrene molecules, as reported by Shabat and coworkers.	9
Scheme 1.2. Mechanism of initiation, propagation, and termination for free radical polymerization.	17
Scheme 1.3. Mechanism of the UV-light activated type I photoinitiator Irgacure 2959..	18
Scheme 1.4. Mechanism of the UV-light activated type I photoinitiator LAP.....	18
Scheme 1.5. Mechanism of the UV-light activated type II photoinitiator eosin Y.	19
Scheme 2.1. Synthesis of the G1 SID.	42
Scheme 2.2. Synthesis of the G2 SID.	43
Scheme 2.3. Proposed degradation products of G1 SID exposed to 0.5 h of UV irradiation in PBS:DMSO-d ₆ (1:1.25).	45
Scheme 2.4. Synthesis of 4-arm-PEG-azide.	47
Scheme 2.5. Synthesis of TEG-alkyne.	47
Scheme 2.6. Hydrogel formation by a click reaction between an alkyne species and 4-arm-PEG-azide.....	48

List of Abbreviations

Carbon-thirteen	^{13}C
Celecoxib	CXB
Centimetre	cm
Chemical shift	δ
Copper (I) alkyne-azide cycloaddition	CuAAc
Day	d
Dendritic chain reaction	DCR
Dichloromethane	CH_2Cl_2
Dimethylsulfoxide	DMSO
Dispersity	\bar{D}
Extracellular matrix	ECM
Equilibrium Water Content	EWC
Fourier transform infrared spectroscopy	FTIR
Gram	g
High performance liquid chromatography	HPLC
Hour	h
Infrared	IR
Kilopascal	kPa
Kilogram	kg
Lithium phenyl-2,4,6-trimethylbenzoylphosphinate	LAP
Lower critical solution temperature	LCST
Mass spectrometry	MS

Metre	m
Milimole	mmol
Millimetre	mm
Mole	mol
Molecular weight	MW
Multiplet	m
Nanometre	nm
Near-infrared	NIR
Nuclear magnetic resonance	NMR
Number average molecular weight	M_n
Phosphate-buffered saline	PBS
Poly(amidoamine)	PAMAM
Poly(ethylene glycol)	PEG
Poly(lactic acid)	PLA
Proton	^1H
Second	s
Self-immolative dendrimer	SID
Tert-butyloxycarbonyl	Boc
Thin-layer chromatography	TLC
Triethylamine	Et_3N
Trifluoroacetic acid	TFA
Ultraviolet-visible spectroscopy	U-vis
Watts	W

Weight average molecular weight	M_w
Weight by volume	w/v
Weight by weight	w/w
Weight percent	wt %

Chapter 1

1 Introduction

1.1 Dendrimers: Structure, Synthesis, and Properties

Since the 1980s, dendrimers have garnered much interest due to their structural precision and functional diversity.¹ Dendrimers are a special group of molecules known for their compact tree-like structures and large number of peripheral groups.² A dendrimer is comprised of three components: (i) a central core (ii) interior branches (generations) and (iii) peripheral functional groups (Figure 1.1).³ Diverse combinations of these components and structural precision make dendrimers of interest for various applications.⁴ Identical fragments called dendrons grow from or are attached to the central core to produce the globular dendritic macromolecule.⁴

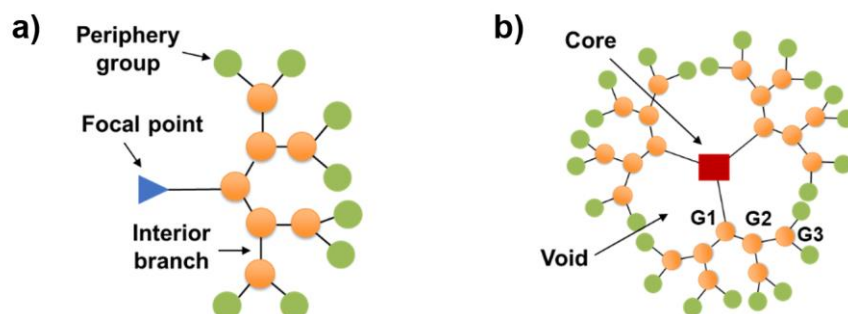


Figure 1.1. a) Dendron, b) Dendrimer.

Dendrimers are synthesized by either divergent or convergent syntheses (Figure 1.2).⁴⁻⁵ In divergent synthesis, the core molecule reacts with dendron repeating units called monomers to produce a first-generation dendrimer.⁴⁻⁵ Then, after the activation of peripheral groups on the dendrimer, they are reacted with monomers to afford the second-generation dendrimer.⁴⁻⁵ This process is repeated to grow the dendrimer layer-by-layer. In contrast, convergent synthesis begins from the periphery and moves inwards towards the core.⁴⁻⁵ Dendrimers with high generations are often prepared more easily by divergent synthesis due to the sterics introduced by the convergent method.¹

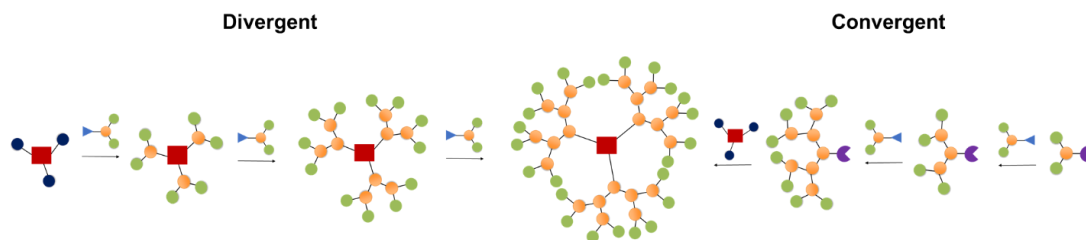


Figure 1.2. Divergent and convergent synthesis of dendrimers.

The type and number of peripheral groups strongly influence the solubility, biocompatibility, and reactivity of dendrimers.^{4, 6} Introducing hydrophilic or hydrophobic functional groups at the termini or along the dendritic backbone can diversify the macromolecule's applications.⁴ Najafi and coworkers synthesized an amphiphilic Janus dendrimer containing triazole branching points and a polar and non-polar wedge comprised of terminal hydroxyl and benzyl phenyl ether moieties, respectively (Figure 1.3).⁷ The dendrimers self-assembled into vesicles in aqueous solution where manipulation of spacer length and dendrimer generation influenced the assembly shape.⁷ The versatile Janus dendrimer affords potential applications in drug delivery and catalysis.⁷

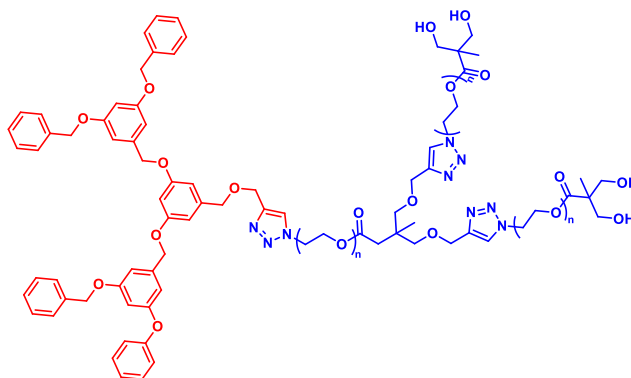


Figure 1.3. Amphiphilic Janus dendrimer reported by Najafi and coworkers. Red and blue correspond to non-polar and polar moieties, respectively.⁷

Dendrimers with particular terminal functional groups, such as primary amines, are found to exhibit toxic effects to various cell types, while hydroxyl and carboxyl groups demonstrate reduced cytotoxicity.⁶ At low pH, amine terminated polyamidoamine (PAMAM) dendrimers become cationic and demonstrate toxicity in the body.⁸ Toxic

effects on red blood cell membrane proteins tends to increase with higher generations, more peripheral groups, and large concentrations of dendrimer.⁸ In contrast, carboxylic acid terminated PAMAM dendrimers did not exhibit cell toxicity over a broad concentration range.⁸

1.2 Self-immolative Dendrons (SIDs)

1.2.1 Structure and Properties

A dendron that disassembles into small molecule components upon a cleavage event at the core is known as a self-immolative dendron (SID) (Figure 1.4).⁹ Notably, this amplified response from a single cleavage event makes SIDs desirable for biological applications, among other fields, as they are sensitive to low stimulus concentrations.⁸ Furthermore, the structural precision of dendrimers allows for predictable disassembly behaviour. De Groot et al. and Amir et al. were the first to introduce self-immolative systems that produced an amplified response when exposed to an external trigger.^{3,9} For the past decade, researchers have developed various scaffold designs that employ unique stimuli-responsive cores, disassembly systems, and tail units.

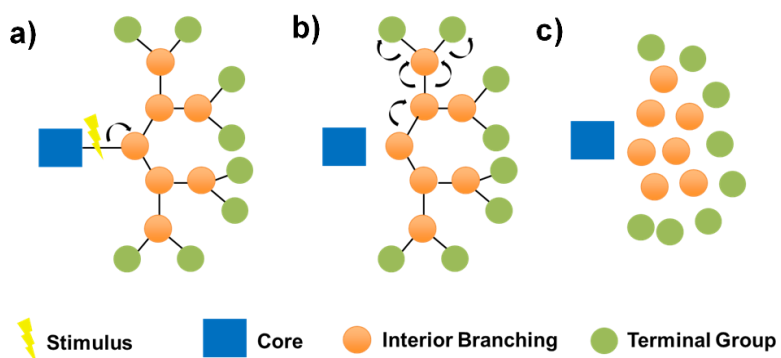


Figure 1.4. A core is cleaved off in response to an external stimulus; b) Removal of the core results in the disassembly of the SID; c) The fragmentation products include the core and derivatives of the interior and terminal groups.

1.2.2 SID Fragmentation Methods

Specific chemical functionalities must be incorporated into the SID to achieve a cascade mechanism that results in the release of molecules at the periphery.² These functionalities are incorporated into the structure of the core, interior branches (spacers), and periphery of the dendrimer. The spacer is an important component of SIDs as it relays a cleavage event from one end of the spacer to the other. Spacers rely on an electronic cascade or intramolecular cyclization for disassembly.⁹ Among other functionalities, SIDs containing an aromatic moiety with a hydroxyl, amino, or thiol substituent in the *ortho* or *para* location undergo electronic cascade disassembly.⁹ Upon activation, degradation occurs by either 1,4-, 1,6-, or 1,8-elimination reactions (Figure 1.5).⁹ Intramolecular cyclization involves a nucleophilic attack on an electrophilic aliphatic carbon or carbonyl carbon.⁹ The *N,N'*-dimethylethylenediamine cyclization spacer is commonly used in SIDs and its cyclization has proven to be the rate-limiting step in various SID fragmentation mechanisms.⁶ Furthermore, increasing the spacer length has been shown to reduce steric hindrance along the SID scaffold.⁶ Electronic cascade and intramolecular cyclization can both be employed for SID fragmentation. Researchers have investigated various backbones that degrade using the methods mentioned above. Commonly used backbones include benzyl carbamates/carbonates, benzyl ethers, and cinnamyl carbamates/carbonates.⁸⁻¹¹

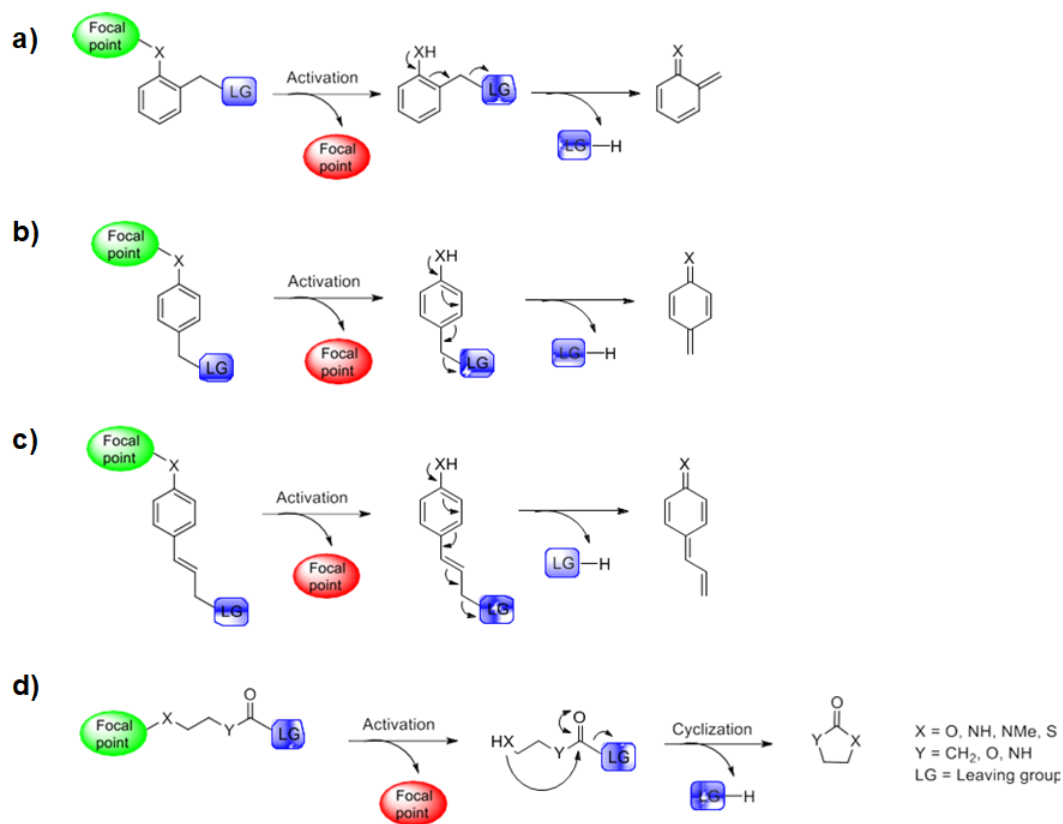


Figure 1.5. SID fragmentation by a) 1,4-elimination, b) 1,6-elimination, c) 1,8-elimination, d) 1,5- cyclization.

1.2.3 Poly(ethylene glycol) (PEG)

PEG is an FDA approved linear hydrophilic polymer (Figure 1.6).¹² PEG can be synthesized by the anionic polymerization of ethylene oxide and hydroxyl initiators.¹³ The polymer is commercially available in various molecular weights and architectures, such as branched, star, and comb geometries.¹³ Properties of PEG vary depending on the molar mass of the polymer where between 200-700 g/mol PEGs are liquids, 700-2000 g/mol PEGs are semi-solid, and > 2000 g/mol PEGs are crystalline solids.¹⁴ PEG's solubility in water and organic solvents, as well as its low toxicity and compatibility with the human immune system makes it ideal for drug delivery applications.^{12, 14} Additionally, PEG is often coupled with substrates to improve the substrate's hydrophilicity and prevent aggregation in aqueous solution.¹² The Gillies group developed amphiphilic block copolymers by capping the ends of poly(ethyl glyoxylate) (PEtG) with PEG chains.¹⁵ The

copolymer self-assembled into nanoparticles in aqueous solution and could be triggered by external stimuli to release drug molecules.¹⁵

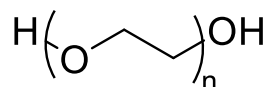


Figure 1.6. Chemical structure of PEG.

1.2.4 Photosensitive SIDs

Photosensitive SIDs fragment into various molecular fragments upon exposure to a light stimulus.¹⁶ Light activation is attractive due to its simple application and tunable parameters like wavelength, intensity, and exposure time.¹⁶ Notably, irradiation allows for a predictable fragmentation event as the trigger typically only effects the targeted portion of the SID.¹⁶ UV and near-infrared (NIR) are commonly used light stimuli, but NIR is often favoured for biological applications since the former is more damaging to tissues.¹⁶ SIDs that undergo photocleavage from UV or NIR irradiation have either *o*-nitrobenzyl or 4-bromo-7-hydroxycoumarin (Bhc) moieties (Figure 1.7).¹⁶ Upon light exposure, the SID disassembles into small molecules in a domino-like fashion.¹⁶

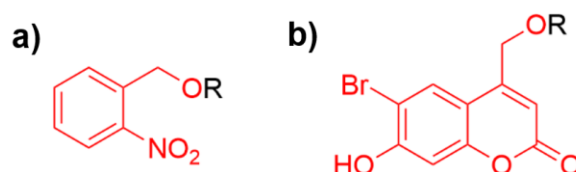


Figure 1.7. a) *o*-Nitrobenzyl, b) 4-Bromo-7-hydroxycoumarin photosensitive moieties (red).

Bochet and Kastrati synthesized a first-, second-, and third-generation SIDs composed of a *o*-nitrobenzyl unit at the focal point, benzyl ether spacers, and nitrophenol moieties at the peripheries (Figure 1.8).¹⁷ A single trigger event by UV irradiation led to an electron cascade disassembly by 1,4-elimination.¹⁷ The authors reported a third-generation SID that releases the highest number of peripheral groups to date. The first-, second-, and third-

generation SIDs released three, nine, and twenty-seven nitrophenol moieties, respectively.¹⁷ Release of *p*-nitrophenol reporter molecules was monitored by Ultraviolet-visible (UV-vis) spectroscopy.¹⁷

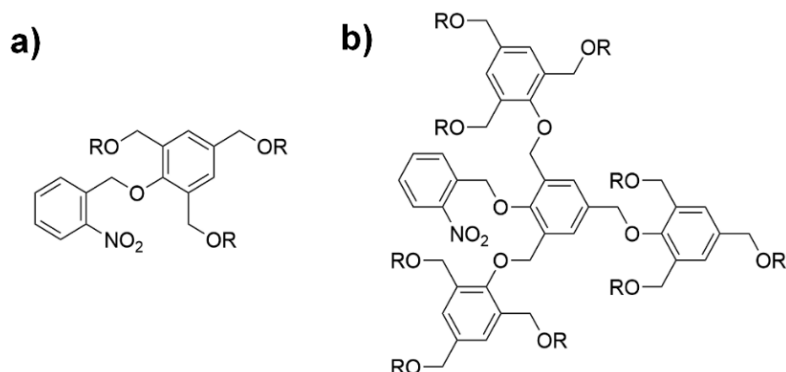


Figure 1.8. Photosensitive a) First-, b) Second-generation SIDs reported by Brochet and Kastrati, R corresponds to *p*-nitrophenoxy moieties.¹⁷

1.2.5 Chemically-responsive SIDs

SID fragmentation initiated by chemical species, such as proteins and bioactive molecules, allow for more versatile *in vitro* and *in vivo* applications.¹⁸ Chemical activation is appealing due to the numerous chemical triggers that are compatible with biological systems.¹⁸ Increased hydrophobicity at higher generations can cause the SID to form aggregates in aqueous solution, thereby hindering the chemical trigger's ability to access the core and disassemble the dendritic network.¹⁹ However, second-generation SIDs with polar attributes have been successfully disassembled by chemical activation.

Shabat and coworkers were the first to report a second-generation SID that released four anticancer drug molecules upon a single enzymatic trigger event by penicillin-G-amidase (PGA) (Figure 1.9).²⁰ The authors prevented aggregation of the scaffold and increased its hydrophilicity by conjugating poly(ethylene glycol) (PEG) chains to the periphery of the SID.²⁰ This modification ensured the enzyme could access the dendritic activation site. Activation triggered a series of intramolecular cyclizations and quinone methide rearrangements to release four camptothecin drug molecules.²⁰ Release of the anticancer agent was monitored by high performance liquid chromatography (HPLC).

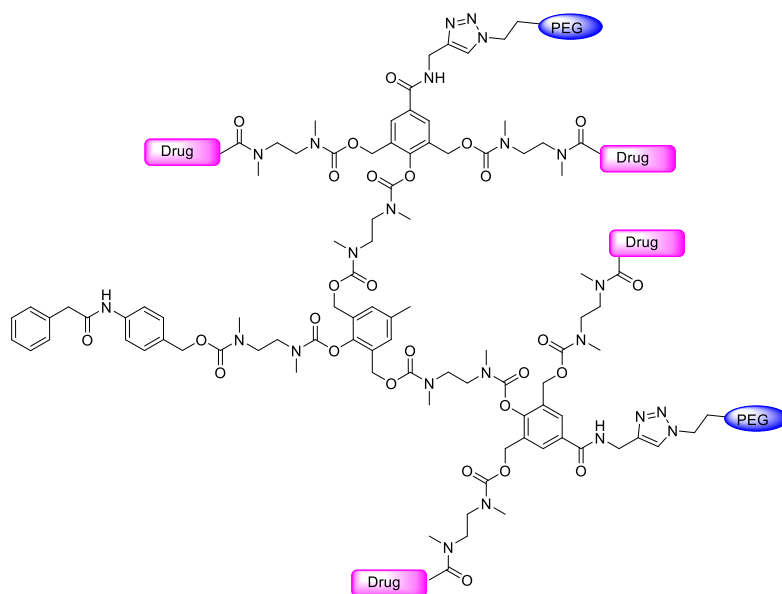
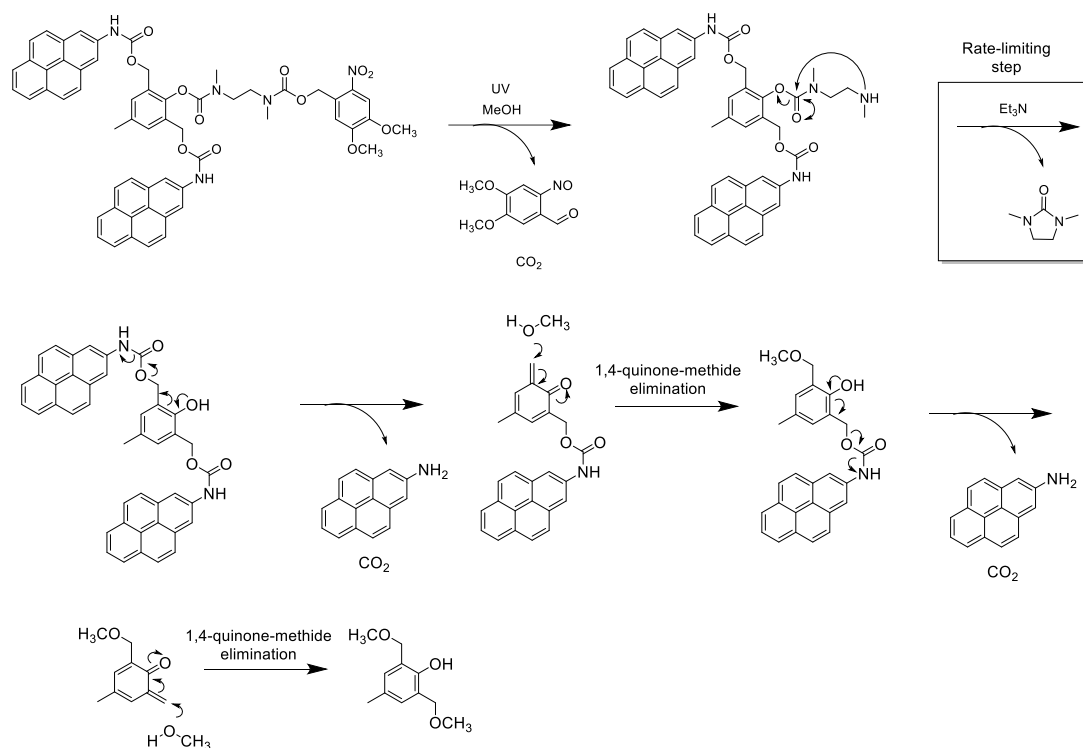


Figure 1.9. Enzymatically activated second-generation SID reported by Shabat and coworkers.²⁰

1.2.6 Benzyl Carbamate/Carbonate Backbones

Shabat and coworkers designed a first-generation SID containing a *N,N'*-dimethylethylenediamine cyclization spacer, a bis(hydroxymethyl)-*p*-cresol moiety on one end up the spacer, a photolabile nitrobenzyl core on the other end, and pyrene reporter molecules (Scheme 1.1).²¹ Upon activation, the spacer undergoes cyclization to afford a phenol to ultimately releases the peripheral groups through a 1,4-quinone-methide elimination.²¹ The single cleavage event was amplified by introducing two hydroxymethyl substituents on the bis(hydroxymethyl)-*p*-cresol moiety.²¹ The dual substitution allows for a double 1,4-quinone-methide elimination and increases the number of peripheral groups compared to a single substitution.²¹ Kinetic studies revealed that intramolecular cyclization is the rate-limiting step.²¹ Release of the pyrene reporter molecules was monitored by HPLC.²¹



Scheme 1.1. Fragmentation of a photolabile first-generation SID by 1,5-intramolecular cyclization followed by two 1,4-quinone-methide rearrangements resulting in the release of terminal pyrene molecules, as reported by Shabat and coworkers.²¹

The group also successfully synthesized a third-generation SID using a *tert*-butoxycarbonyl (Boc) trigger group, a *N,N'*-dimethylethylenediamine cyclization spacer, and a bis(hydroxymethyl)-*p*-cresol amplifying unit.²¹ However, the pyrene reporter molecules were exchanged for 4-nitroaniline units to circumvent steric problems associated with higher generation SIDs (Figure 1.10).²¹ For activation, trifluoroacetic acid (TFA) was used to deprotect the Boc group to form an amine.²¹ Upon activation, the third-generation SID fragmented through intramolecular cyclization and a series of 1,4-quinone-methide eliminations.²¹ Release of the 4-nitroaniline reporter molecules was monitored by HPLC and UV-vis spectroscopy.²¹

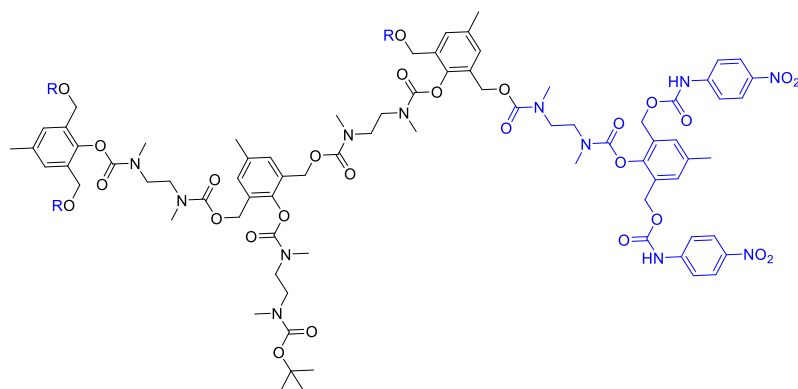


Figure 1.10. Third-generation SID containing a Boc core and peripheral 4-nitroaniline moieties, as reported by Shabat and coworkers.²¹

1.2.7 Benzyl Ether Backbones

McGrath and coworkers reported SIDs with benzyl ether backbones in 2003.²² The authors synthesized zeroth- to second-generation SIDs with a 4-allyloxy group at the trigger site and *p*-benzyl ether linkages, leading to a *p*-nitrophenoxy unit (Figure 1.11).²² A *p*-nitrophenoxy moiety was installed at the end opposite to the allyl group such that allyl deprotection led to a fragmentation mechanism towards the release of *p*-nitrophenoxide.²² Allyl deprotection triggered by Pd(PPh₃)₄ and NaBH₄ initiated SID disassembly by a 1,6-elimination mechanism.²² A single cleavage event resulted in complete disassembly of the SID within 15 minutes.²² Release of the *p*-nitrophenoxide reporter molecule was monitored by UV-vis spectroscopy.²²

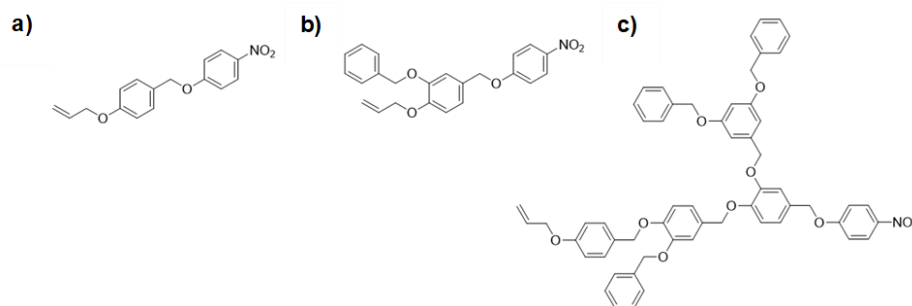


Figure 1.11. a) Zeroth-, b) First-, c) Second-generation SIDs containing a 4-allyloxy trigger group, benzyl ether backbones and a terminal *p*-nitrophenoxy unit as reported by McGrath and coworkers.²²

The McGrath group enhanced the SID design above by developing a dendritic amplification system.²³ They designed a first- and second-generation SID containing an allyloxy moiety at the core with benzyl ether subunits leading to numerous *p*-nitrophenoxy groups at the peripheries (Figure 1.12).²³ Activation by allyl deprotection induced SID fragmentation through a 1,4-quinone-methide elimination. Disassembly of a single 2,4-branched benzyl ether subunit resulted in the release of two reporter molecules.²³ Complete disassembly was observed by UV-vis spectroscopy where a decrease in absorption at 310 nm with an increase in the absorption of *p*-nitrophenoxide at 431 nm was monitored.²³ Kinetic studies revealed that allyl deprotection is the rate-limiting step while SID disassembly occurred rapidly.²³

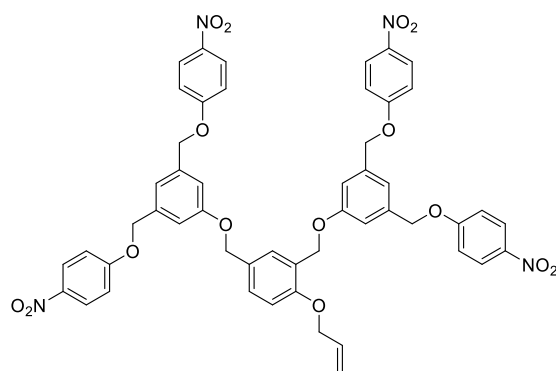


Figure 1.12. Second-generation dendron containing a 4-allyloxy trigger group, benzyl ether backbone and four terminal *p*-nitrophenoxy units, as reported by McGrath and coworkers.²³

1.2.8 Cinnamyl Carbamate/Carbonate Backbones

Shabat and coworkers developed a novel first-generation SID containing a cinnamyl carbamate backbone.²⁴ The SID consisted of a Boc trigger group, a *N,N'*-dimethylethylenediamine cyclization spacer, and a cinnamyl moiety leading to six aminomethylpyrene reporter units (Figure 1.13).²⁴ Activation by Boc deprotection using TFA induced an intramolecular cyclization followed by six quinone methide rearrangements to release the reporter molecules.²⁴ Using HPLC, intramolecular cyclization of the amine was found to be the rate-limiting step.²⁴ Release of free aminomethylpyrene molecules was monitored by fluorescence spectroscopy.²⁴

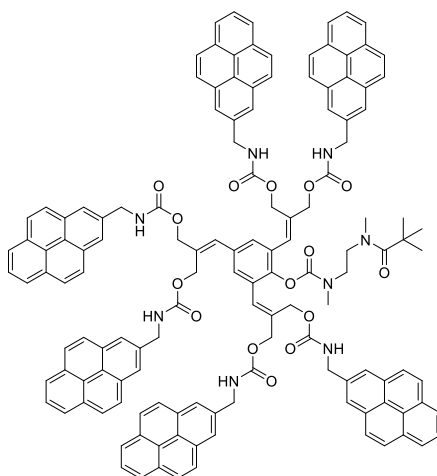


Figure 1.13. First-generation SID with a cinnamyl-based backbone as reported by Shabat and coworkers.²⁴

DeGroot and coworkers developed a novel second-generation SID containing a cinnamyl-based backbone.²⁵ The SID contained a 4-aminobenzyl moiety at the focal point and 4-aminocinnamyl spacer units leading to four paclitaxel drug molecules at the periphery (Figure 1.14).²⁵ A zinc acetic acid mediated reduction of the nitro group at the focal point resulted in a 1,8-elimination along the SID towards the release of the drug molecules.²⁵ Release of paclitaxel was monitored by thin-layer chromatography (TLC), mass spectrometry (MS), and nuclear magnetic resonance (NMR) spectroscopy.²⁵

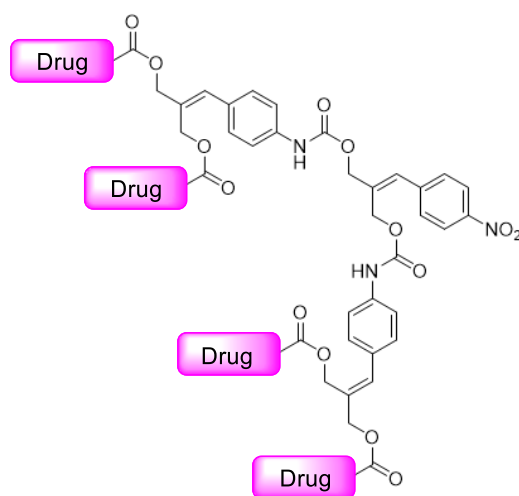


Figure 1.14. Second-generation SID with a cinnamyl-based backbone as reported by DeGroot and coworkers.²⁵

1.2.9 Applications of SIDs

The structural tunability and precision of SIDs allow for applications in biomaterials, agriculture, and catalysis.²⁶ Researchers have spent the past decade investigating the use of SIDs in drug delivery and sensor applications.^{18, 27} Shabat and researchers developed a novel trimeric SID scaffold comprising an enzymatic substrate at the core and three different anticancer drugs at the termini (Figure 1.15).²⁷ A single activation event at the core induced by an enzymatic cleavage led to an intramolecular cyclization and a series of quinone methide rearrangements with the subsequent release of drug molecules.²⁷ Notably, the disassembly was successful under physiological conditions and the release of drug molecules was monitored by HPLC. Additionally, the degradation products had minimal to no toxicity to a human cell line.²⁷ The group has developed a promising drug delivery system to inhibit tumor growth that can be further manipulated to advance research in cancer therapy.

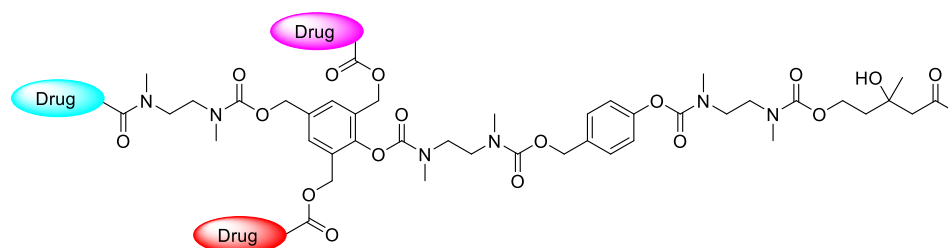


Figure 1.15. A trimeric SID developed by Shabat and researchers.²⁷

SID disassembly can be monitored by the release of fluorescent or UV-visible reporter molecules.¹⁸ Additionally, SIDs can adopt a biosensor model for the detection of contaminants, metals, and pathogens in the environment or harmful biological entities, such as bacteria and viruses.¹⁸ Shabat and researchers have synthesized a novel SID that disassembles through a dendritic chain reaction (DCR) under aqueous conditions.²⁸ The DCR fragmentation technique exponentially amplifies a diagnostic signal where the activation of one SID by an analyte led to the release of reagent and reporter molecules.²⁸ Through a chemical reaction, the reagent molecules are converted to the analyte, which can then go on to activate more SIDs.²⁸ Shabat and coworkers synthesized a SID triggered by hydrogen peroxide and disassembly of the SID released a 4-nitroaniline reporter and two choline units.²⁸ Oxidation of the choline molecules to hydrogen peroxide allowed for further activation while fragmentation was monitored by the release of the yellow reporter molecule.²⁸ Overall, development of a viable signal amplification technique is attractive for diagnostic applications where analyte sensitivity is improved through a feedback system.

1.2.10 Rotational Isomers

Rotational isomers, or rotamers, are isomers produced by rotation about a single bond at room temperature.²⁹ The restricted rotation about a sigma bond affords conformational isomers due to different spatial arrangements of atoms in the molecule.²⁹ Rotations between the amino and carbonyl groups about the α -carbon in peptides is frequently observed (Figure 1.16 a).³⁰ Similarly, restricted rotation about the C-N bond in carbamates can also produce rotamers (Figure 1.16 b).³¹ Typically, ¹H NMR experiments of rotamers conducted

at or below room temperature afford complicated spectra as the different isomers produce different signals.²⁹ However, variable temperature NMR spectroscopy is a possible solution to simplify the ^1H NMR spectra as the high temperature accelerates the rotation, resulting in a coalescence of the separate peaks into a single peak or series of peaks.³¹

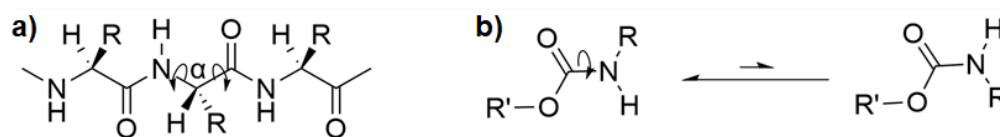


Figure 1.16. Bond rotation about the a) α -carbon in peptides, b) C-N bond in carbamates.

1.3 Hydrogels

1.3.1 Background

Hydrogels are a class of hydrophilic crosslinked polymeric materials that absorb large amounts of water (Figure 1.17).³² The hydrophilicity arises from polar moieties along the polymer backbone while crosslinking contributes to preventing dissolution.³² While naturally occurring hydrogels have been investigated extensively, synthetic forms are becoming more prevalent due to their functional and mechanical tunability.³² The high water content of these three-dimensional networks mimics the composition of soft tissues.³² This characteristic affords them numerous applications in biomaterials, among other fields.³²

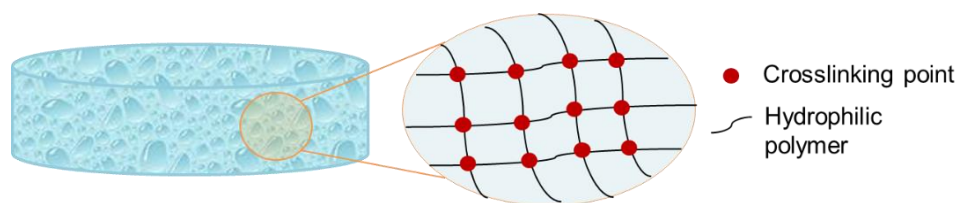
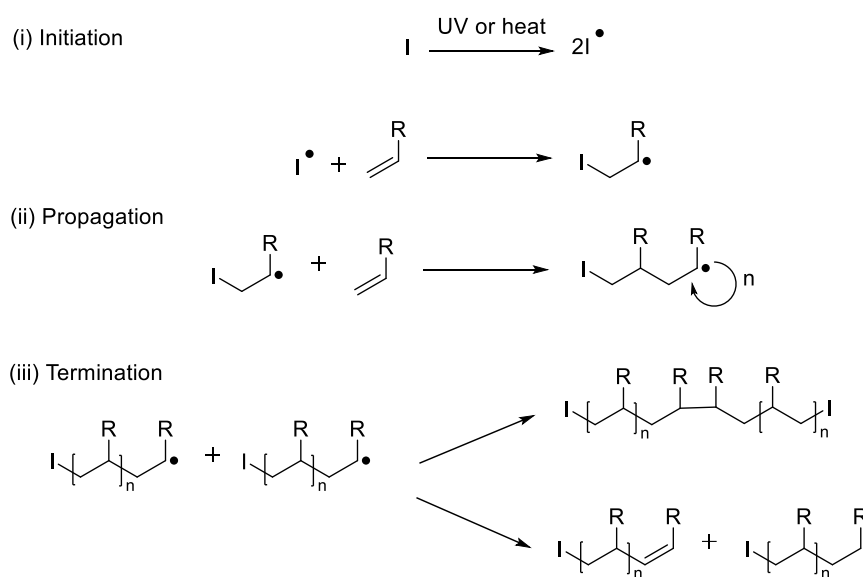


Figure 1.17. Hydrogel structure.

1.3.2 Synthesis

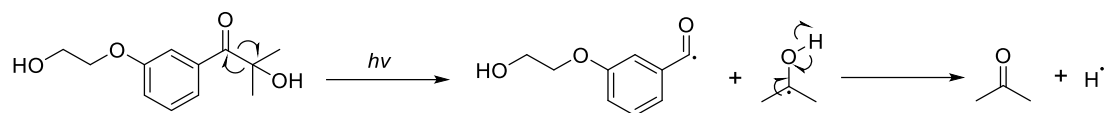
Polymeric hydrogels can be synthesized by either chemical or physical gelation.³³⁻³⁵ Chemical or permanent hydrogels are formed through covalently-crosslinked networks.³³⁻

³⁵ Crosslinking occurs between hydrophilic polymer chains or hydrophobic chains that are made hydrophilic.³³⁻³⁵ The covalent bonds are formed by either free radical polymerization, addition/condensation reactions, or enzymatic crosslinking.³³⁻³⁵ Since the bonds are non-reversible, chemical hydrogels afford strong and stable networks. Mechanical properties of chemical hydrogels can be tuned by modifying the crosslinking method, polymer structure, and crosslinker type.³³⁻³⁵ Free radical polymerizations have been extensively used as crosslinking reactions as they are not technically demanding and the crosslinked site can be selectively identified.³⁶ The polymerization method employs an initiator that forms a radical species when exposed to heat or light.³⁶ The radical initiating species then reacts with an unsaturated monomer to create a propagating site and chain growth proceeds until all or most polymerizable units are consumed (Scheme 1.2).



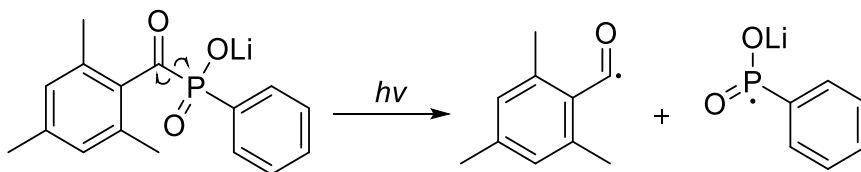
Scheme 1.2. Mechanism of initiation, propagation, and termination for free radical polymerization.³⁶

Irgacure 2959 is a type I photoinitiator frequently employed for photocrosslinkable hydrogels.³⁷ The photoinitiator is ideal for applications in drug delivery and tissue engineering due to its low toxicity, crosslinking efficiency, and adequate water solubility.³⁷ Irgacure 2959 is activated at 365 nm where a homolytic bond cleavage generates two radical species that then initiate polymerization (Scheme 1.3).³⁷



Scheme 1.3. Mechanism of the UV-light activated type I photoinitiator Irgacure 2959.³⁷

The photoinitiator lithium phenyl-2,4,6-trimethylbenzoylphosphinate (LAP) (scheme 1.4) exhibits improved crosslinking efficiency, biocompatibility, and water solubility than Irgacure 2959.³⁷ Additionally, LAP is preferred for biological applications as it absorbs both in the UV-light and visible light range.³⁷⁻³⁸ Anseth and researchers developed hydrogels from a thiol-ene reaction photoinitiated by LAP.³⁸ 4-arm-PEG norbornene was photocrosslinked with PEG thiol using UV-light (wavelength: 365 nm, intensity: 10 mW/cm²) in the presence of two proteins, lysozyme and TGF β (Figure 1.18).³⁸ With a concentration of 40 mM for both thiol and alkene moieties, complete gel formation only required 0.1 mM of LAP and ~60 s of UV-light exposure.³⁸ Furthermore, the gel successfully encapsulated the proteins and the effects of photopolymerization on protein bioactivity were investigated.³⁸ Cell assays indicated that the thiol-ene photopolymerization reaction had no effect on lysozyme or TGF β bioactivity, which may be attributed to the rapid gelation time and low photoinitiator concentration.³⁸ The Anseth group has developed a photocrosslinkable hydrogel with promising features for future biomaterial applications.



Scheme 1.4. Mechanism of the UV-light activated type I photoinitiator LAP.³⁷

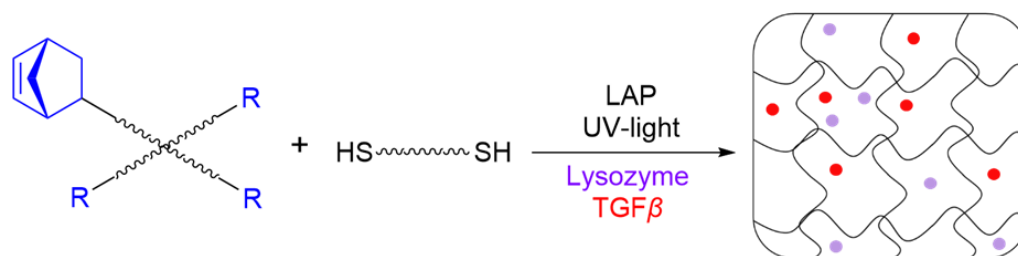
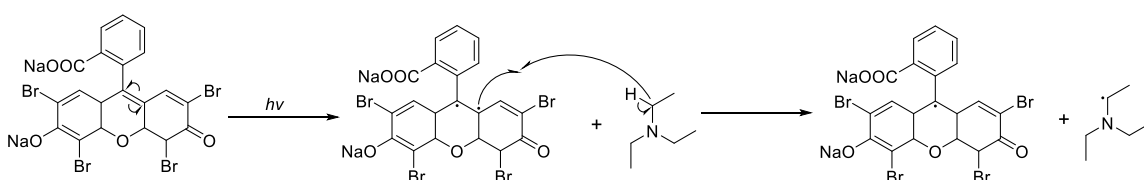


Figure 1.18. Photopolymerization reaction between 4-arm-PEG norbornene and PEG thiol using the LAP initiator to form a hydrogel containing lysozyme and TGF β molecules in the scaffold, as reported by Anseth and coworkers.³⁸ Purple and red circles correspond to lysozyme and TGF β , respectively.

Alternatively, type II photoinitiators, such as eosin Y, are also used for biomedical applications due to their compatibility with living organisms, but they are often less efficient than their type I counterparts due to competing processes during photoinitiation.³⁹ Typically, a co-initiator, such as a hydrogen donor, is needed to activate the type II photoinitiator.³⁹ When irradiated with UV-light, triethylamine (Et₃N) can donate a radical to eosin Y to generate two radicals that then proceed to initiate polymerization (Scheme 1.5).³⁹



Scheme 1.5. Mechanism of the UV-light activated type II photoinitiator eosin Y.³⁹

Click reactions are a simple type of addition reaction that occur under mild conditions and have high selectivity and yield.³⁶ One of the most common click reactions is the copper (I) alkyne-azide cycloaddition (CuAAC) click reaction where a Cu(II) salt and reducing agent are commonly used to produce the Cu(I) species (Figure 1.19).⁴⁰

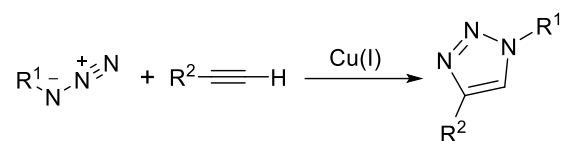


Figure 1.19. CuAAC click reaction.

Hilborn and coworkers were the first to develop hydrogels utilizing click chemistry.⁴¹ The group prepared poly(vinyl alcohol) (PVA) chains with either alkyne or azide moieties (Figure 1.20).⁴¹ The modified PVA chains were crosslinked by a CuAAC reaction in the presence of copper sulfate (CuSO_4), sodium ascorbate, and propargylamine or azidoethylamine functionalized PVA to form hydrogels.⁴¹ Finally, Schiff base formation is commonly used for hydrogel synthesis where an amine reacts with an aldehyde to form an imine bond.³³ The condensation reaction is often reversible and produces pH-sensitive products, making the crosslinking technique ideal for pH-sensitive and self-healing hydrogels.³³

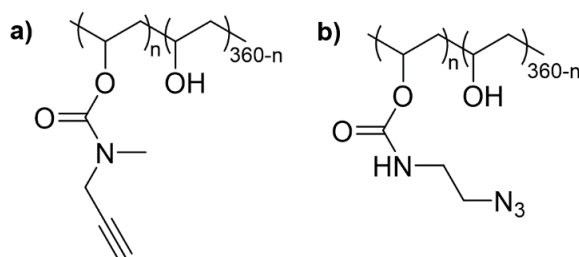


Figure 1.20. (a) Azide or (b) Alkyne modified PVAs used for CuAAC reaction for hydrogel formation, as reported by Hilborn and coworkers.⁴¹

Physical or reversible hydrogels are formed by secondary forces, such as ionic or hydrogen bonding, hydrophobic interactions, or by entanglement of polymer chains (Figure 1.21).³³⁻³⁵ Since the non-covalent bonds and entanglements are reversible, physical hydrogels are weak compared to chemical hydrogels.³³ The reversible interactions degrade in response to environmental changes, such as pH, temperature, and ionic strength or when stress is applied.³³⁻³⁵ Physical hydrogels can be prepared by temperature regulated self-assembly, low pH induced hydrogen-bonding, and oppositely charged polyelectrolytes.³³ Alginate

hydrogels can be synthesized quickly under mild conditions with the use of divalent a cation, such as Ca^{2+} .⁴² When sodium alginate is immersed in a calcium chloride solution, the sodium ions are displaced by Ca^{2+} ions to create a crosslinked polymer network in the form of a hydrogel (Figure 1.22).⁴² Alginate-based hydrogels are attractive for biomedical applications due to their nontoxicity, facile gel synthesis, and resemblance to the extracellular matrix (ECM).⁴³

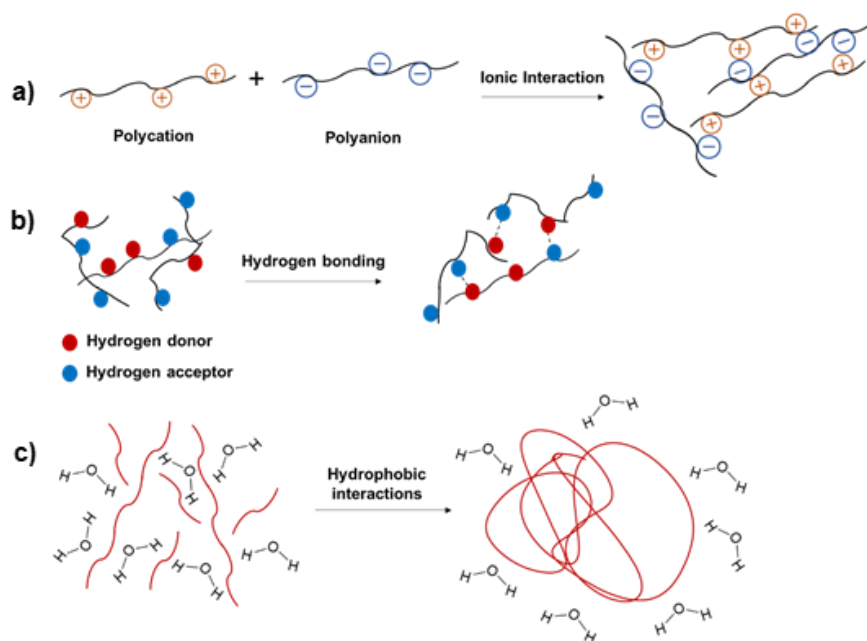


Figure 1.21. Types of physical crosslinking include a) Ionic interactions, b) Hydrogen bonding, c) Hydrophobic interactions.

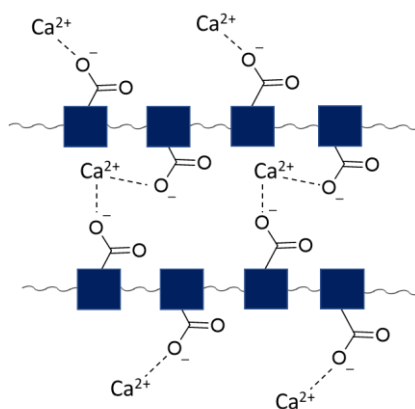


Figure 1.22. Crosslinked alginate via ionic interactions with divalent calcium cations. Blue squares correspond to the alginate backbone.

1.3.3 Properties

A hydrogel's ability to absorb and retain water depends on the network's charge density and degree of crosslinking.³³ Water moves into the pores of a hydrogel containing hydrophilic polymers, causing the network to swell.⁴⁴ The increase in hydrophilicity affords stronger polymer-water interactions and more swelling.⁴⁴ In an aqueous solution, ionic groups of the same charge in the network repel each other, causing the pores to expand.⁴⁴ Differences in ion concentration prompt water absorption and swelling of the gel.⁴⁴ Higher crosslinking density produces a tighter hydrogel, thereby decreasing space for water absorption.⁴⁴ The hydrogel's water content at equilibrium is calculated by equation 1, where m_d is the mass of the dry hydrogel and m_s is the mass of the swollen hydrogel at equilibrium.³³ Equilibrium is achieved when the weight of the swollen hydrogel does not change.³³ Hydrogels are also characterized by gel content, which is the percentage of material incorporated into the network.³³ Gel content is calculated by equation 2, where m_t is the theoretical weight of the hydrogel if all material was incorporated into the network.³³

$$\text{EWC} = \frac{m_s - m_d}{m_s} \times 100\% \quad (1)$$

$$\text{Gel content} = \frac{m_d}{m_t} \times 100\% \quad (2)$$

Hydrogels are viscoelastic materials that exhibit both elastic and viscous properties.⁴⁵ A hydrogel's degree of elasticity can be determined by measuring its resistance to compression, also known as the compression modulus. Compression stress is the amount of force applied divided by the cross-sectional area of the specimen, as shown by equation 3. As a sample experiences compressional stress, it deforms by contracting. Equation 4 describes the percent contraction (strain), which is the change in length of the sample after compression ($L-L_0$) divided by the sample's original length (L_0), times a hundred. Compression strength is the stress needed to fracture the material. As stress is applied to a sample, the strain it experiences can be measured to produce a stress-strain curve (Figure 1.23).⁴⁶ The compression modulus is the slope of the curve while the height is the compression strength.⁴⁶ A steep curve reflects a stiff material with a high modulus and compression strength.⁴⁶ Toughness is the amount of energy the sample absorbs before fracturing.⁴⁶ The area under the curve of a stress-strain curve measures the toughness of a sample.⁴⁶

$$\text{Stress} = \frac{\text{Force}}{\text{Cross-sectional area}} \quad (3)$$

$$\% \text{ Contraction} = \frac{L-L_0}{L_0} \times 100\% \quad (4)$$

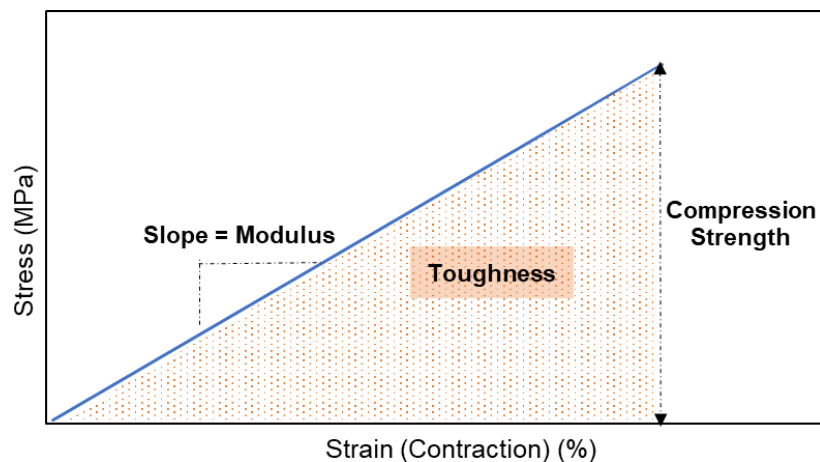


Figure 1.23. Compression stress-strain curve.

Increasing the crosslinking density enhances the mechanical properties of a hydrogel.⁴⁴ Higher crosslinking affords stronger and more durable hydrogels that last longer.³³ However, a higher crosslinking density reduces the swelling capacity of a hydrogel.⁴⁴ Additionally, a fast gel time often produces a weak hydrogel as there is not enough time to form a strong network.³³ Swelling and mechanical properties can be tuned by modifying the hydrogel structure.

1.3.4 Stimuli-responsive Hydrogels for Biomedical Applications

Stimuli-responsive hydrogels undergo changes in their chemical, physical, and mechanical properties when exposed to external stimuli such as pH, temperature, and light.⁴⁷ These materials are referred to as smart hydrogels and have realized numerous applications.⁴⁷ Thermoresponsive hydrogels are attractive for biomedical applications as they can swell under physiological conditions and their administration is non-invasive.⁴⁸⁻⁴⁹ The sol-gel transition describes the transformation from a liquid state to a gel state when a critical temperature is reached.⁴⁸ Many thermoresponsive hydrogels exist as a homogenous solutions below the lower critical solution temperature (LCST) and gels above the LCST (Figure 1.24).

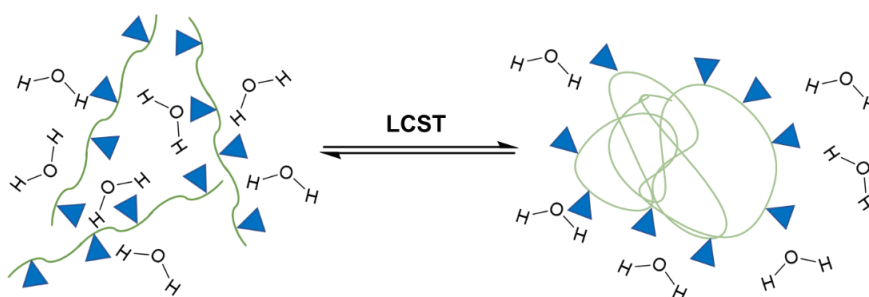


Figure 1.24. LCST phase transition of a thermoresponsive polymer in aqueous solution. Green and blue correspond to hydrophobic and hydrophilic moieties, respectively.

N-isopropyl acrylamide (NIPAM) polymers are often used in thermoresponsive hydrogels since the polymer's LCST lies close to physiological temperature. Georgieva and coworkers developed a thermoresponsive hydrogel containing the monomer NIPAM and

crosslinker poly(ethylene glycol) diacrylate (PEGDA) by use of the initiator 4,4-azobis(4-cyanovaleric acid) (ABCA) for free radical polymerization (Figure 1.25).⁵⁰ The crosslinked network afforded a hydrogel that demonstrated reversible swelling-deswelling phase changes over a temperature range of 10-60 °C.⁵⁰ The hydrogel was loaded with galantamine hydrobromide and the drug's release from the scaffold was investigated.⁵⁰ The network readily released all of the loaded drug within 4 hours at 10 °C.⁵⁰ Overall, the thermoresponsive hydrogel exhibits potential as a transdermal drug delivery system.

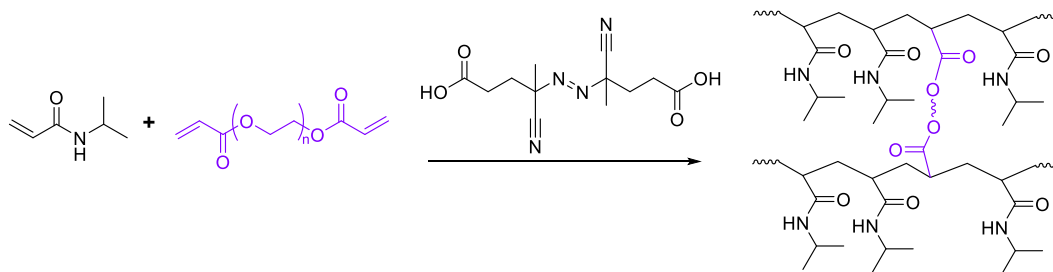


Figure 1.25. Free radical polymerization of NIPAM and PEGDA initiated by ABCA to form a thermoresponsive hydrogel, as reported by Georgieva and coworkers.⁵⁰

Hydrogels containing ionic groups along the polymer backbone can respond to changes in pH through protonation or deprotonation events.⁴⁷ Ionization of pendant groups in the network causes swelling, while deionization collapses the network.⁴⁷ Peppas and coworkers synthesized four pH-responsive nanoparticle hydrogels containing acidic moieties for the oral delivery of the hydrophobic drug doxorubicin to the gastrointestinal (GI) tract.⁵¹ The hydrogels were synthesized by photoinitiated free radical polymerization where the polymer backbones were composed of methacrylic acid, a grafted PEG chain, and one of the four hydrophobic monomers (*tert*-butyl methacrylate, *n*-butyl acrylate, *n*-butyl methacrylate, methyl methacrylate) (Figure 1.26).⁵¹ The hydrophobic component is important to encapsulation and retention of the hydrophobic drug while the methacrylic acid moiety along the polymer backbone responds to changes in external pH.⁵¹ The PEG chains improve the scaffold's biocompatibility, stability in solution, and interaction with the mucus layer of the GI.⁵¹ At pH 7.9, the nanoparticle hydrogel size varied from 120 to 500 nm depending on the size of the hydrophobic moiety along the polymer backbone.⁵¹

All hydrogels demonstrated swelling at pH 4.9, thus the scaffolds are viable drug delivery systems that can retain drug molecules in the acidic stomach and release them at the GI tract.⁵¹

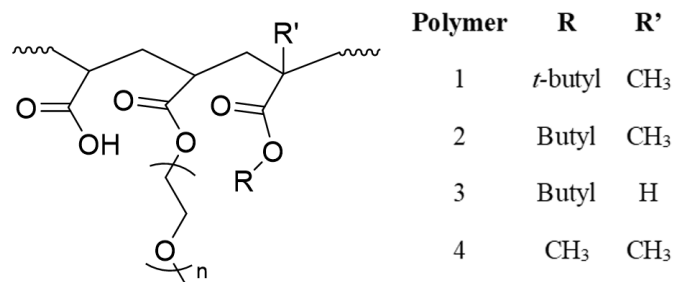


Figure 1.26. Chemical structure of pH-responsive polymers ionized under acid conditions to afford swollen hydrogels, as reported by Peppas and coworkers.⁵¹

Like for SIDs, adjustable wavelength, light intensity, and irradiation time offer control over light-sensitive hydrogels.⁵² Light irradiation can adjust the hydrogel's swelling ratio by modifying the scaffold's crosslinking density and hydrophilicity.⁵² Further, the ability to manipulate hydrogel properties remotely without physical contact afford light-sensitive gels for numerous applications as biomaterials.⁵² Implantable hydrogels can undergo physiochemical changes when exposed to UV or NIR light at the implantation site.⁵² Exposure to UV-light can induce *trans-cis* isomerization where one isomer is converted to the other.⁵² Typically, photoisomerization changes the length of polymer chains, thereby causing the hydrogel to swell or shrink.⁵² For example, photoisomerization of azobenzene moieties in polymer chains has been shown to alter the hydrogel's swelling ratio where the *cis* isomer enhanced swelling (Figure 1.27).⁵² Alternatively, photoinduced cleavage of several crosslinking points or bonds in the polymer backbone also manipulates hydrogel swelling.⁵² Cleavage of all crosslinking points in the hydrogel by light irradiation can afford a liquid solution. Thus, a hydrogel's sol-gel transition can be manipulated by light irradiation.⁵² Sol-gel transitions can also be achieved by the incorporation of reversible covalent bonds, such as disulfide bridges, into the network.⁵²

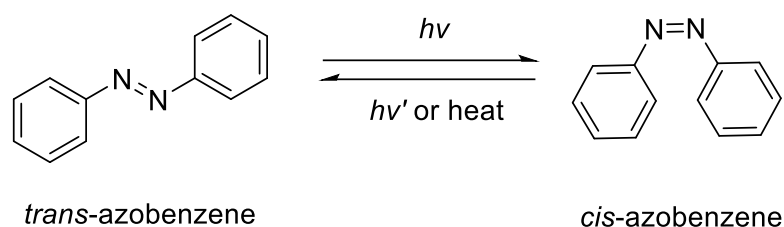


Figure 1.27. Photoisomerization of azobenzene.

Gupta and coworkers developed a photoresponsive hydrogel containing a modified azobenzene linker that was non-covalently crosslinked to dextran, a polysaccharide.⁵³ The effect of UV-light exposure at 365 nm on the release of aspirin from the hydrogel was investigated.⁵³ The group found drug release was controlled by photoisomerization of the azobenzene group in the scaffold's crosslinker.⁵³ UV-light irradiation disrupted the hydrophobic interactions between azobenzene side chains, leading to disassembly of the network followed by the release of encapsulated drug molecules (Figure 1.28).⁵³ While the azobenzene moiety did isomerize back to the *trans* form in the dark, the transition was too slow to afford significant drug release.⁵³ Overall, the group regulated the release of a hydrophobic drug from pores of the hydrogel by photoisomerization of the azobenzene moiety.

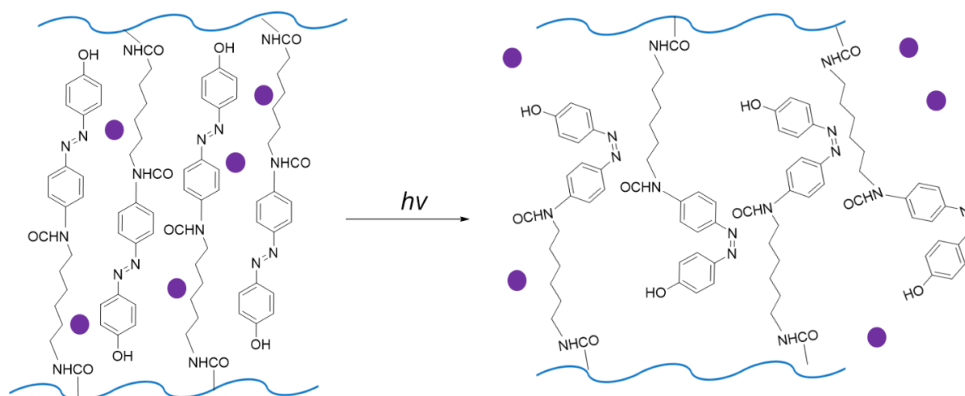


Figure 1.28. Photoisomerization of the azobenzene moiety in the hydrogel leading to the release of hydrophobic drug molecules, as reported by Gupta and coworkers.⁵³ Blue lines and purple markers correspond to dextran and aspirin drug molecules, respectively.

Similar to SIDs, photolabile *o*-nitrobenzyl moieties are employed in photoresponsive hydrogels.⁵² Anseth and coworkers incorporated *o*-nitrobenzyl ether moieties into a PEG-based polymer functionalized with terminal acrylate groups (Figure 1.29).⁵⁴ The macromonomer was crosslinked with monoacrylated PEG by redox-initiated free radical polymerization to afford a photodegradable hydrogel.⁵⁴ Exposure to UV light decreased the network's crosslinking density and physical durability.⁵⁴ Further, hydrogels loaded with human stem cells demonstrated cell viability and migration in response to UV irradiation.⁵⁴ However, unlike the photolabile azobenzene, UV irradiation of the *o*-nitrobenzyl moiety is irreversible and these photoresponsive hydrogels may not accurately reproduce the dynamic environment of the ECM. Nonetheless, the work by Anseth and coworkers presents a framework for photolabile hydrogels as biomaterials for drug delivery and tissue engineering.

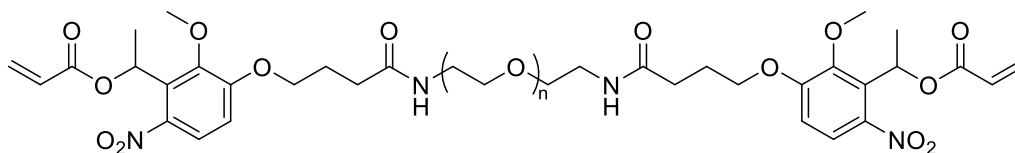


Figure 1.29. Photolabile macromonomer containing PEG, *o*-nitrobenzyl moieties, and terminal acrylate groups which crosslink with monoacrylated PEG to form a hydrogel for tissue regeneration, as reported by Anseth and researchers.⁵⁴

1.3.5 Dendritic Hydrogels for Biomedical Applications

Hydrogels containing dendritic macromolecules exhibit specific properties due to the structural precision and branched architecture of dendrimers.³⁴ Dendrimers can crosslink with each other or with other polymer chains to form a hydrogel network.³⁴ Multiple crosslinking points can be introduced by modifications to dendrimer size, peripheral groups, and shape.³⁴ The structural precision of the dendrimers aids in understanding the network's properties and applications.³⁴ For instance, mechanisms underlying the scaffold's drug loading and release are better understood when the network's structure is well defined.³⁴

Dendritic hydrogels are synthesized by either physical or chemical gelation.³⁴ Similar to other hydrogels, dendritic hydrogels synthesized by chemical gelation tend to be stronger and more stable than those formed by physical gelation.³⁴ Properties of dendritic hydrogels, such as the degree of swelling, crosslinking density, and mechanical strength can be tuned by structural modifications to the dendrimer.³⁴ Numerous crosslinking points can be introduced by tuning the number and functionality of surface groups on the dendrimer.³⁴ As a result, dendrimer-based hydrogels can produce scaffolds with higher crosslinking densities, enhanced mechanical properties, and reduced swelling.³⁴ Furthermore, dendritic hydrogels containing hydrophobic building blocks are attractive for the encapsulation and retention of hydrophobic drug molecules.

Wang and coworkers combined the versatility of dendrimers and biocompatibility of PEG-based polymers to produce a novel poly(amido amine) (PAMAM) dendritic hydrogel as a mimic for the ECM.⁵⁵ The group developed a multifunctional fourth-generation (G4.0) PAMAM dendrimer through PEGylation and alkene and amino acid functionalization of peripheral amine groups (Figure 1.30 a).⁵⁵ The introduction of PEG improved the dendrimer's biocompatibility while the conjugation of the peptide (RGDyC) triggered proliferation of osteoblast cells.⁵⁵ The terminal alkene moieties underwent photoinitiated crosslinking with a copolymer of PEG and poly(lactic acid) (PLA) to form a dendritic hydrogel (Figure 1.30 b).⁵⁵ The dendrimer's multiple crosslinking points improved the gel's mechanical properties and degree of swelling while the PEG and peptide moieties enhanced the scaffold's biocompatibility and cell proliferation when compared to a control with no dendritic component.⁵⁵ Overall, the researchers developed a dendritic hydrogel that could be functionalized to tune its mechanical properties while still mimicking the ECM and promoting cell growth.

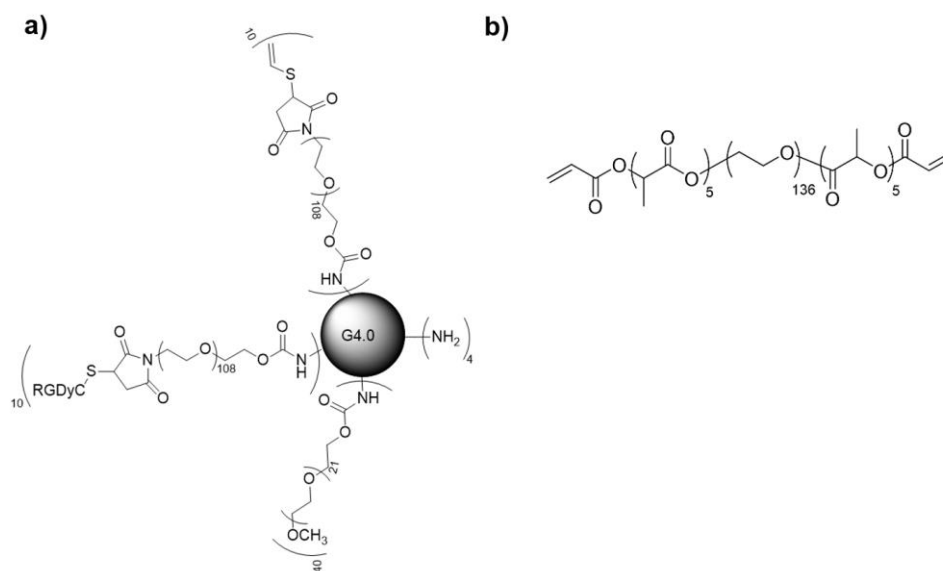


Figure 1.30. a) Functionalized G4.0 PAMAM dendrimer, b) Copolymer of PEG and PLA containing peripheral acrylate groups, as reported by Wang and coworkers.⁵⁵

The highly branched structure and functionality of PAMAM dendrimers was further exploited by Yang and coworkers for ocular drug delivery.⁵⁶ To ensure successful crosslinking, acrylate groups were first conjugated to the termini of PEG chains rather than the amine moieties around a third-generation (G3.0) PAMAM dendrimer to avoid shielding effects by polymer chains. Thus, PEG was first reacted with acryloyl chloride, followed by 4-nitrophenyl chloroformate to afford a functionalized PEG (Figure 1.31).⁵⁶ Using the eosin Y photoinitiator, UV-light triggered crosslinking between terminal acrylate groups afforded a viscous gel-like solution ideal for ocular drug delivery.⁵⁶ The PEG moieties provided good biocompatibility and water solubility while the hydrophobic network of the PAMAM dendrimer aided in the encapsulation of hydrophobic antiglaucoma drugs such as brimonidine.⁵⁶ The dendritic hydrogel demonstrated a sustained release of the drug when compared to traditional eye drop treatments, thereby requiring less doses administered and better efficacy.⁵⁶

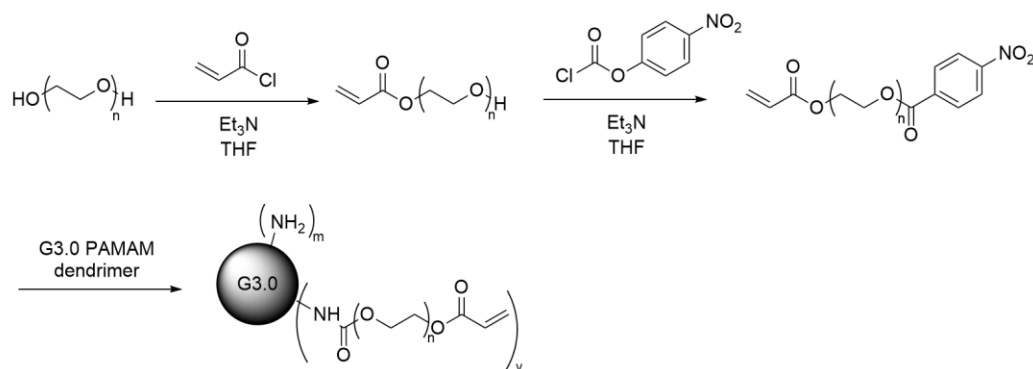


Figure 1.31. Synthesis route of the modified G3.0 PAMAM dendrimer functionalized with PEG and acrylate moieties, as reported by Yang and coworkers.⁵⁶

1.4 Motivation for Thesis

Researchers have extensively investigated the use of dendrimers, SIDs, and hydrogels as biomaterials for applications in tissue engineering and drug delivery. Hydrogels containing dendritic macromolecules exhibit specific properties due to the structural precision and branched architecture of dendrimers.³⁴ Furthermore, the dendrimer structure has been exploited to tune the scaffold's degree of swelling, crosslinking density, and mechanical strength. While conventional dendrimer-based systems require multiple cleavage events to release molecules from the network's termini, self-immolative dendrimers (SIDs) release all terminal molecules in a domino-like fashion in response to a single trigger event at the dendron's core.⁸⁻⁹ However, hydrogels synthesized using SIDs as a component of the hydrogel network have yet to be reported. Here, we propose the synthesis of a photosensitive SID hydrogel comprised of a first-generation or second-generation SID and 4-arm PEG. The hypothesis for this project is that the photosensitive SID hydrogels, synthesized by a CuAAC click reaction, will afford scaffolds with enhanced mechanical properties, fragment through a well-documented disassembly mechanism, and demonstrate the regulated release of hydrophobic drugs when irradiated.

Chapter 2 describes the synthesis, characterization, and fragmentation of the photolabile SID hydrogels. The mechanical durability was also investigated by measuring the compression moduli of SID hydrogels with and without UV-light exposure. Finally, the

nonsteroidal anti-inflammatory drug celecoxib (CXB) was incorporated into the hydrogels and its release was examined in the presence and absence of UV-light irradiation. Chapter 3 summarizes the results obtained from chapter 2 and proposes future work for this project.

1.5 References

1. Fréchet, J. M. J., Dendrimers and supramolecular chemistry *Proc. Natl. Acad. Sci.* **2002**, *99*, 4782-4787.
2. Avital-Shmilovici, M.; Shabat, D., Self-immolative dendrimers: A distinctive approach to molecular amplification. *Soft Matter* **2010**, *6*, 1073-1080.
3. Wang, R. E.; Costanza, F.; Niu, Y.; Wu, H.; Hu, Y.; Hang, W.; Sun, Y.; Cai, J., Development of self-immolative dendrimers for drug delivery and sensing. *J. Controlled Release* **2012**, *159*, 154-163.
4. Klajnert, B.; Bryszewska, M., Dendrimers: properties and applications. *Acta. Biochim. Pol.* **2001**, *48*, 199-208.
5. Abbasi, E.; Aval, S. F.; Akbarzadeh, A.; Milani, M.; Nasrabadi, H. T.; Joo, S. W.; Hanifehpour, Y.; Nejati-Koshki, K.; Pashaei-Asl, R., Dendrimers: synthesis, applications, and properties. *Nanoscale Res. Lett.* **2014**, *9*, 247-257.
6. Kono, K., Dendrimer-based bionanomaterials produced by surface modification, assembly and hybrid formation. *Polym. J.* **2012**, *44*, 531-540.
7. Liu, X.; Gitsov, I., Thermosensitive amphiphilic janus dendrimers with embedded metal binding sites. synthesis and self-assembly. *Macromolecules* **2018**, *51*, 5085-5100.
8. Roth, M. E.; Green, O.; Gnaim, S.; Shabat, D., Dendritic, oligomeric, and polymeric self-immolative molecular amplification. *Chem. Rev.* **2016**, *116*, 1309-1352.
9. Amir, R. J.; Pessah, N.; Shamis, M.; Shabat, D., Self-immolative dendrimers. *Angew. Chem. Int. Ed.* **2003**, *42*, 4494-4499.
10. De Groot, F. M. H.; Albrecht, C.; Koekkoek, R.; Beusker, P. H.; Scheeren, H. W.; Amir, R. J.; Pessah, N.; Shamis, M.; Shabat, D., Liberate all end groups upon a

- single triggering event in the dendritic core/self-immolative dendrimers. *Angew. Chem. Int. Ed.* **2003**, *42*, 4411-4411.
11. McGrath, D. V., Dendrimer disassembly as a new paradigm for the application of dendritic structures. *Mol. Pharm.* **2005**, *2*, 253-263.
 12. Dowler, W.; Robison, J.; Fury, J.; Dou, X.; Delong, R.; Sedaghat-Herati, R., Synthesis, characterization, and applications of poly(ethylene glycol)-block-poly(ether-sulfide) dendrimers. *J. Macromol. Sci.* **2015**, *52*, 30-38.
 13. Zia, F.; Anjum, M. N.; Saif, M. J.; Jamil, T.; Malik, K.; Anjum, S.; BiBi, I.; Zia, M. A., Chapter 16 - Alginate-poly(Ethylene) glycol and poly(ethylene) oxide blend materials. *Algae Based Polymers, Blends, and Composites*, Elsevier: 2017; 581-601.
 14. D'Souza A, A.; Shegokar, R., Polyethylene glycol (PEG): a versatile polymer for pharmaceutical applications. *Expert Opin. Drug Deliv.* **2016**, *13*, 1257-1275.
 15. Fan, B.; Gillies, E. R., Poly(ethyl glyoxylate)-poly(ethylene oxide) nanoparticles: stimuli-responsive drug release via end-to-end polyglyoxylate depolymerization. *Mol. Pharm.* **2017**, *14*, 2548-2559.
 16. de Gracia Lux, C.; McFearin, C. L.; Joshi-Barr, S.; Sankaranarayanan, J.; Fomina, N.; Almutairi, A., Single uv or near ir triggering event leads to polymer degradation into small molecules. *ACS Macro Lett.* **2012**, *1*, 922-926.
 17. Kastrati, A.; Bochet, C. G., Photochemical amplifier based on self-immolative dendritic spacers. *J. Org. Chem.* **2019**, *84*, 7776-7785.
 18. Wang, R. E.; Costanza, F.; Niu, Y. H.; Wu, H. F.; Hu, Y. G.; Hang, W.; Sun, Y. Q.; Cai, J. F., Development of self-immolative dendrimers for drug delivery and sensing. *J. Control. Release* **2012**, *159*, 154-163.

19. Roth, M. E.; Green, O.; Gnaim, S.; Shabat, D., Dendritic, oligomeric, and polymeric self-immolative molecular amplification. *Chem. Rev.* **2016**, *116*, 1309-1352.
20. Gopin, A.; Ebner, S.; Attali, B.; Shabat, D., Enzymatic activation of second-generation dendritic prodrugs: conjugation of self-immolative dendrimers with poly(ethylene glycol) via click chemistry. *Bioconjug. Chem.* **2006**, *17*, 1432-1440.
21. Amir, R. J.; Pessah, N.; Shamis, M.; Shabat, D., Self-immolative dendrimers. *Ange. Chem. Int. Edit.* **2003**, *42*, 4494-4499.
22. Li, S.; Szalai, M. L.; Kevwitch, R. M.; McGrath, D. V., Dendrimer disassembly by benzyl ether depolymerization. *J. Am. Chem. Soc.* **2003**, *125*, 10516-10517.
23. Szalai, M. L.; Kevwitch, R. M.; McGrath, D. V., Geometric disassembly of dendrimers: dendritic amplification. *J. Am. Chem. Soc.* **2003**, *125*, 15688-15689.
24. Shamis, M.; Shabat, D., Single-triggered ab₆ self-immolative dendritic amplifiers. *Chem. Eur. J.* **2007**, *13*, 4523-4528.
25. de Groot, F. M. H.; Albrecht, C.; Koekkoek, R.; Beusker, P. H.; Scheeren, H. W., "Cascade-release dendrimers" liberate all end groups upon a single triggering event in the dendritic core. *Angew. Chem. Int. Ed.* **2003**, *42*, 4490-4494.
26. Klajnert, B.; Bryszewska, M., Dendrimers: properties and applications. *Acta. Biochim. Pol.* **2001**, *48*, 199-208.
27. Haba, K.; Popkov, M.; Shamis, M.; Lerner, R. A.; Barbas Iii, C. F.; Shabat, D., Single-triggered trimeric prodrugs. *Angew. Chem. Int. Ed.* **2005**, *44*, 716-720.
28. Sella, E.; Shabat, D., Dendritic chain reaction. *J. Am. Chem. Soc.* **2009**, *131*, 9934-9936.
29. Toyota, S., Rotational isomerism involving acetylene carbon. *Chem. Rev.* **2010**, *110*, 5398-5424.

30. Haddad, Y.; Adam, V.; Heger, Z., Rotamer dynamics: analysis of rotamers in molecular dynamics simulations of proteins. *Biophys. J.* **2019**, *116*, 2062-2072.
31. Smith, B. D.; Goodenough-Lashua, D. M.; D'Souza, C. J. E.; Norton, K. J.; Schmidt, L. M.; Tung, J. C., Substituent effects on the barrier to carbamate C–N rotation. *Tetrahedron Lett.* **2004**, *45*, 2747-2749.
32. Ahmed, E. M., Hydrogel: Preparation, characterization, and applications: A review. *J. Adv. Res.* **2015**, *6*, 105-121.
33. Ghobril, C.; Grinstaff, M. W., The chemistry and engineering of polymeric hydrogel adhesives for wound closure: a tutorial. *Chem. Soc. Rev.* **2015**, *44*, 1820-1835.
34. Ghobril, C.; Rodriguez, E. K.; Nazarian, A.; Grinstaff, M. W., Recent advances in dendritic macromonomers for hydrogel formation and their medical applications. *Biomacromolecules* **2016**, *17*, 1235-1252.
35. Hoffman, A. S., Hydrogels for biomedical applications. *Adv. Drug Deliv. Rev.* **2012**, *64*, 18-23.
36. Hu, W.; Wang, Z.; Xiao, Y.; Zhang, S.; Wang, J., Advances in crosslinking strategies of biomedical hydrogels. *Biomater. Sci.* **2019**, *7*, 843-855.
37. Choi, J. R.; Yong, K. W.; Choi, J. Y.; Cowie, A. C., Recent advances in photo-crosslinkable hydrogels for biomedical applications. *BioTechniques* **2019**, *66*, 40-53.
38. McCall, J. D.; Anseth, K. S., Thiol–ene photopolymerizations provide a facile method to encapsulate proteins and maintain their bioactivity. *Biomacromolecules* **2012**, *13*, 2410-2417.
39. Tomal, W.; Ortyl, J., Water-soluble photoinitiators in biomedical applications. *Polymers* **2020**, *12*, 1073-1103.

40. Liang, L.; Astruc, D., The copper(I)-catalyzed alkyne-azide cycloaddition (CuAAC) “click” reaction and its applications. An overview. *Coord. Chem. Rev.* **2011**, *255*, 2933-2945.
41. Ossipov, D. A.; Hilborn, J., Poly(vinyl alcohol)-based hydrogels formed by “click chemistry”. *Macromolecules* **2006**, *39*, 1709-1718.
42. Abasalizadeh, F.; Moghaddam, S. V.; Alizadeh, E.; akbari, E.; Kashani, E.; Fazljou, S. M. B.; Torbati, M.; Akbarzadeh, A., Alginate-based hydrogels as drug delivery vehicles in cancer treatment and their applications in wound dressing and 3D bioprinting. *J. Biol. Eng.* **2020**, *14*, 8-30.
43. Lee, K. Y.; Mooney, D. J., Alginate: properties and biomedical applications. *Prog. Polym. Sci.* **2012**, *37*, 106-126.
44. Okano, T.; Park, P., Biomedical applications of hydrogels handbook. 1 ed.; Springer New York, New York **2010**.
45. Oyen, M. L., Mechanical characterisation of hydrogel materials. *Int. Mater. Rev.* **2014**, *59*, 44-59.
46. Odian, G., Principles of polymerization. John Wiley & Sons Incorporated Hoboken, United States **2004**.
47. Echeverria, C.; Fernandes, S. N.; Godinho, M. H.; Borges, J. P.; Soares, P. I. P., Functional stimuli-responsive gels: hydrogels and microgels. *Gels* **2018**, *4*, 54-91.
48. Klouda, L., Thermoresponsive hydrogels in biomedical applications: a seven-year update. *Eur. J. Pharm. Biopharm.* **2015**, *97*, 338-349.
49. Klouda, L.; Mikos, A. G., Thermoresponsive hydrogels in biomedical applications. *Eur. J. Pharm. Biopharm.* **2008**, *68*, 34-45.
50. Georgieva, D.; Ivanova-Mileva, K.; Ivanova, S.; Kostova, B.; Rachev, D.; Christova, D., Thermoresponsive poly(N-isopropylacrylamide) copolymer

networks for galantamine hydrobromide delivery. *Colloid Polym. Sci.* **2020**, *298*, 377-384.

51. Puranik, A. S.; Pao, L. P.; White, V. M.; Peppas, N. A., Synthesis and characterization of pH-responsive nanoscale hydrogels for oral delivery of hydrophobic therapeutics. *Eur. J. Pharm. Biopharm.* **2016**, *108*, 196-213.
52. Li, L.; Scheiger, J. M.; Levkin, P. A., Design and applications of photoresponsive hydrogels. *J. Adv. Mater.* **2019**, *31*, 54-71.
53. Patnaik, S.; Sharma, A. K.; Garg, B. S.; Gandhi, R. P.; Gupta, K. C., Photoregulation of drug release in azo-dextran nanogels. *Int. J. Pharm.* **2007**, *342*, 184-193.
54. Kloxin, A. M.; Tibbitt, M. W.; Kasko, A. M.; Fairbairn, J. A.; Anseth, K. S., Tunable hydrogels for external manipulation of cellular microenvironments through controlled photodegradation. *Adv. Mater.* **2010**, *22*, 61-66.
55. Wang, Y.; Zhao, Q.; Zhang, H.; Yang, S.; Jia, X., A novel poly(amido amine)-dendrimer-based hydrogel as a mimic for the extracellular matrix. *Adv. Mater.* **2014**, *26*, 4163-4167.
56. Holden, C. A.; Tyagi, P.; Thakur, A.; Kadam, R.; Jadhav, G.; Kompella, U. B.; Yang, H., Polyamidoamine dendrimer hydrogel for enhanced delivery of antiglaucoma drugs. *Nanomedicine: NBM* **2012**, *8*, 776-783.

Chapter 2

2 Development of SID Hydrogels as Drug Delivery Systems

2.1 Introduction

Hydrogels have been of significant interest for numerous applications in the field of biomaterials.¹ Polymers such as poly(ethylene glycol) (PEG), poly(lactic acid) (PLA), and poly(glycolic acid) (PGA) are used in biomaterials due to their low toxicity and compatibility with the human immune system.⁸ These polymers can be functionalized to include stimuli-responsive moieties and form smart hydrogels.⁹ Stimuli-responsive, or smart, hydrogels undergo changes in their chemical, physical, and mechanical properties when exposed to triggers, such as changes in pH, temperature, and irradiation with light.¹⁰ Upon stimulus exposure, they undergo chemical and physical modifications, such as swelling changes, protonation or deprotonation events, and phase changes.¹¹⁻¹² While traditional drug administration methods, such as intravenous and oral delivery typically require multiple doses, smart gels can provide controlled drug release to specific locations in the body.¹⁴

Hydrogels containing dendritic macromolecules exhibit specific properties due to the structural precision and branched architecture of dendrimers.¹⁵ Dendrimers can crosslink with each other or with other polymer chains to form a hydrogel network.¹⁵ Multiple crosslinking points can be introduced by modifications to dendrimer size, peripheral groups, and shape.¹⁵ Furthermore, dendrimer structure has been exploited to tune the scaffold's degree of swelling, crosslinking density, and mechanical strength.¹⁵ Notably, the structural precision of dendrimers aids in understanding the network's drug loading and release behaviour.¹⁵ While conventional dendritic-based drug delivery systems require multiple cleavage events to release molecules from the network's termini, self-immolative dendrimers (SIDs) release all terminal molecules in a domino-like fashion in response to a single trigger event at the network's core.¹⁶⁻¹⁷ The amplified response from a single cleavage event makes SIDs desirable for drug delivery, among other fields, as they are sensitive to low stimulus concentrations.¹⁷

Researchers have used hydrogels to encapsulate a H_2O_2 sensitive SID-enzyme pair where oxidation of enzyme derivatives generates more H_2O_2 , resulting in disassembly of the hydrogel by a dendritic chain reaction.¹⁸ However, hydrogel synthesis using SIDs has yet to be reported and the design of these scaffolds should be carefully planned to ensure the network itself and its degradation products are nontoxic.

Here we proposed the synthesis of a photolabile SID hydrogel composed of a first-generation SID (**G1 SID**) or second-generation SID (**G2 SID**) and 4-arm poly(ethylene glycol) (PEG). Hydrogel synthesis was achieved by a copper catalyzed azide alkyne (CuAAC) click reaction between the SID and PEG. The SID hydrogel fragments through well-documented intramolecular cyclization of the *N,N'*-dimethylethylenediamine spacer and 1,4-quinone methide rearrangements of the *p*-cresol moiety after the *o*-nitrobenzyl core is exposed to UV-light, resulting in triggered breakdown of the gel (Figure 2.1).¹⁹ The SID hydrogels exhibit high gel content and enhanced compressive moduli compared to a control gel not containing the SID. Collectively, this work offers a hydrogel system where the promising aspects of SIDs and hydrogels are combined to afford a scaffold with enhanced mechanical properties, demonstrating its potential in biomedical applications.

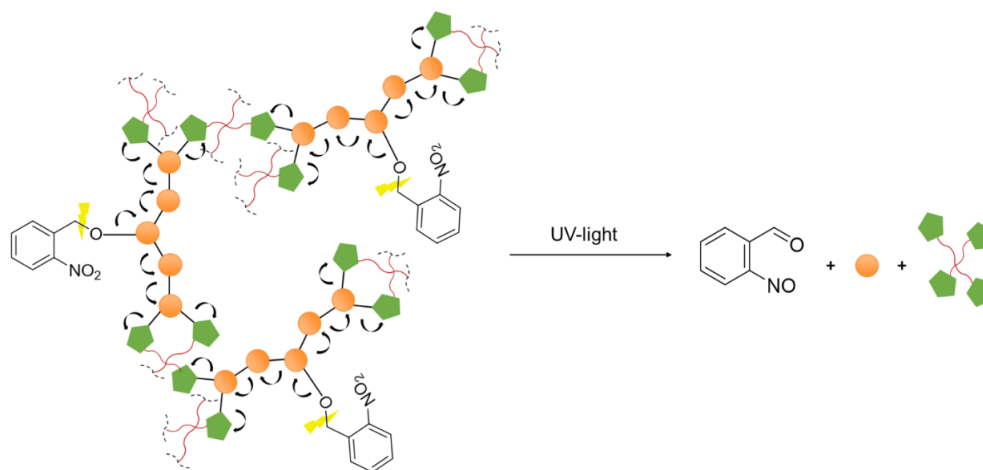
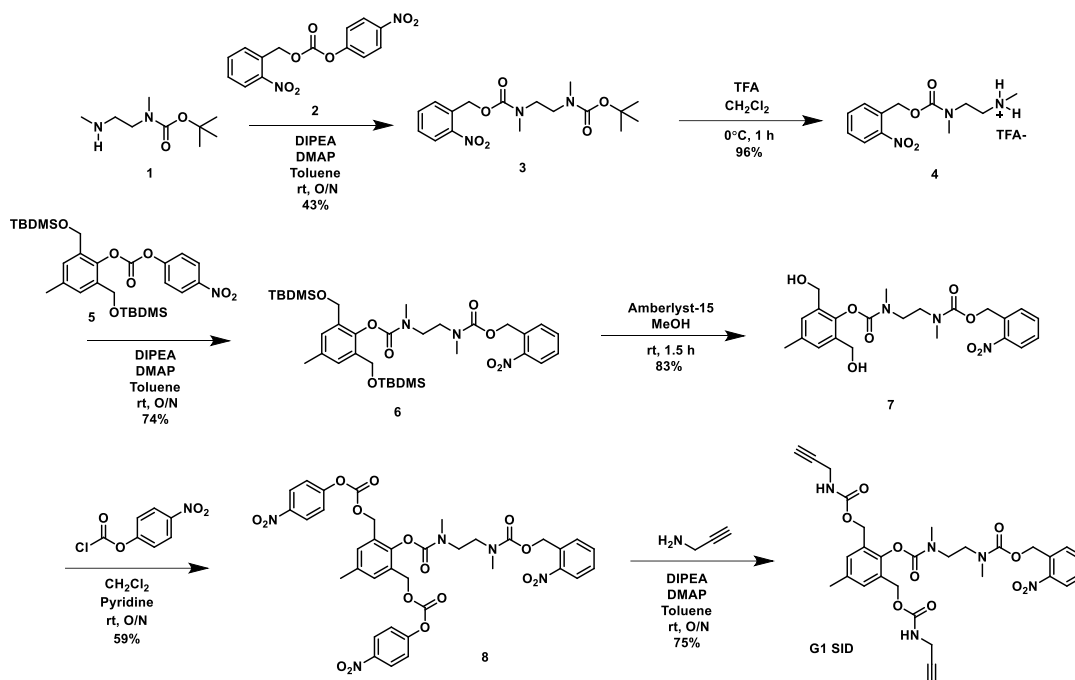


Figure 2.1. Schematic depiction of the UV light triggered fragmentation of a **G1 SID** hydrogel. Red lines, green pentagons, and orange circles represent PEG, triazole moieties, and interior branching units of the dendrimer, respectively.

2.2 Results and Discussion

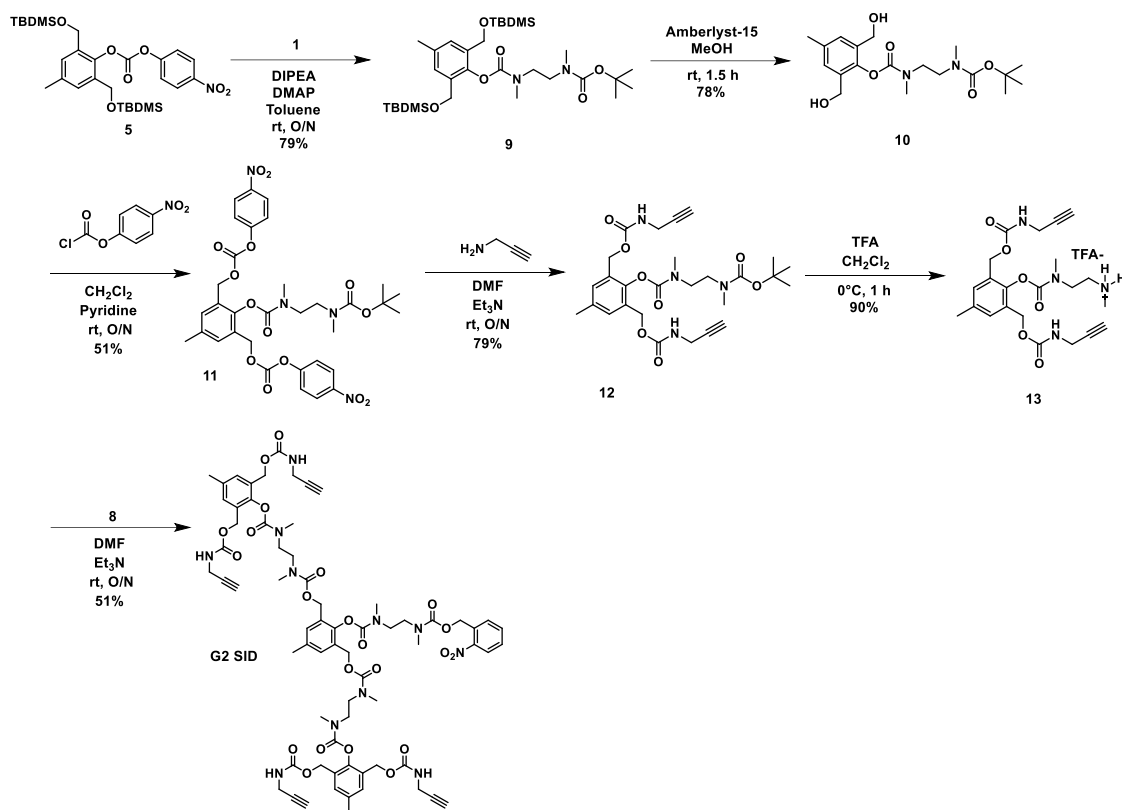
2.2.1 Synthesis and Characterization of G1 and G2 SIDs

To synthesize **G1 SID** (Scheme 2.1), the mono-Boc-protected diamine **1**²⁰ was reacted with the activated carbonate **2**²¹ in a 1:1 ratio in toluene using *N,N*-diisopropylethylamine (DIPEA) and 4-dimethylaminopyridine (DMAP) as the base and catalyst, respectively, to afford the carbamate **3**. Then, the Boc group on **3** was removed using TFA/CH₂Cl₂ at 0 °C for 1 hour to afford the ammonium compound **4**. The low reaction temperature for the synthesis of **3** was important since a previous attempt at room temperature resulted in undesired intramolecular cyclization to afford *o*-nitrobenzyl alcohol and 1,3-dimethyl-2-imidazolidinone. Compound **4** was then reacted with the activated carbonate **5**²² to afford **6**. The *t*-butyldimethylsilyl (TBDMS) protecting groups on **6** were then removed by treatment with Amberlyst-15 in methanol for 1.5 hours to afford compound **7**. The reaction time for this deprotection was carefully controlled, as longer reaction times led to intramolecular cyclization of the deprotected alcohols to form a bicyclic carbonate. Compound **7** was then reacted with six equivalents (equiv.) of 4-nitrophenyl chloroformate in CH₂Cl₂ in the presence of catalytic pyridine to afford compound **8**. Finally, compound **8** was reacted with 4 equiv. of propargylamine in toluene using DIPEA and DMAP as the base and catalyst respectively, to afford the **G1 SID**.



Scheme 2.1. Synthesis of the **G1 SID**.

For the synthesis of **G2 SID** (Scheme 2.2), compounds **9**, **10**, and **11** were synthesized using the procedures reported by Shabat and coworkers with minor modifications.²³ First, the activated carbonate **5** was reacted with mono-Boc-protected diamine **1**²⁰ in the presence of DIPEA and DMAP, then the TBDMS protecting groups were removed by treatment with Amberlyst-15 to give **10**. Activation of the resulting alcohols with 4-nitrophenyl chloroformate in the presence of pyridine provided compound **11**. The reaction of **11** with 4 equiv. of propargylamine in *N,N*-dimethylformamide (DMF) using Et₃N as the base gave compound **12**. Treatment with TFA/CH₂Cl₂ at 0 °C for 1 hour afforded the ammonium salt **13**. Similar to the synthesis of compound **4**, the reaction temperature for the synthesis of **13** was important to avoid intramolecular cyclization. Finally, compound **13** was reacted with compound **8** in DMF using Et₃N as the base to afford the **G2 SID**. The use of 80 equiv. of Et₃N was important to push the reaction to completion as a previous attempt using 40 equiv. gave a derivative of compound **9** where only one arm reacted with compound **13**.



Scheme 2.2. Synthesis of the **G2 SID**.

The chemical structures of the novel compounds were confirmed by ^1H nuclear magnetic resonance (NMR) spectroscopy, ^{13}C NMR spectroscopy, Fourier-transform infrared (FTIR) spectroscopy, and electrospray ionization-mass spectrometry (ESI-MS). The ^1H NMR spectra for the **G1 SID** and **G2 SID** (Figure 2.2) contain peaks with similar chemical shifts, but differences in their peak integrals. Both spectra contain three distinct multiplets from 8.15 - 7.02 ppm which correspond to protons on the aromatic rings. The broad singlets at ~ 5.52 ppm and ~ 5.03 ppm correspond to methylene protons adjacent to the *o*-nitrobenzyl and *p*-cresol moieties, respectively. Multiplets from 4.01 - 2.84 ppm are attributed to protons in the diamine linkers and methylene protons adjacent to the alkyne groups. Finally, signals from 2.37 - 2.14 ppm correspond to methyl protons in the *p*-cresol ring and terminal alkyne protons. For both dendrons, the spectra are complicated by the presence of rotational isomers about the C-N bonds in the carbamates.

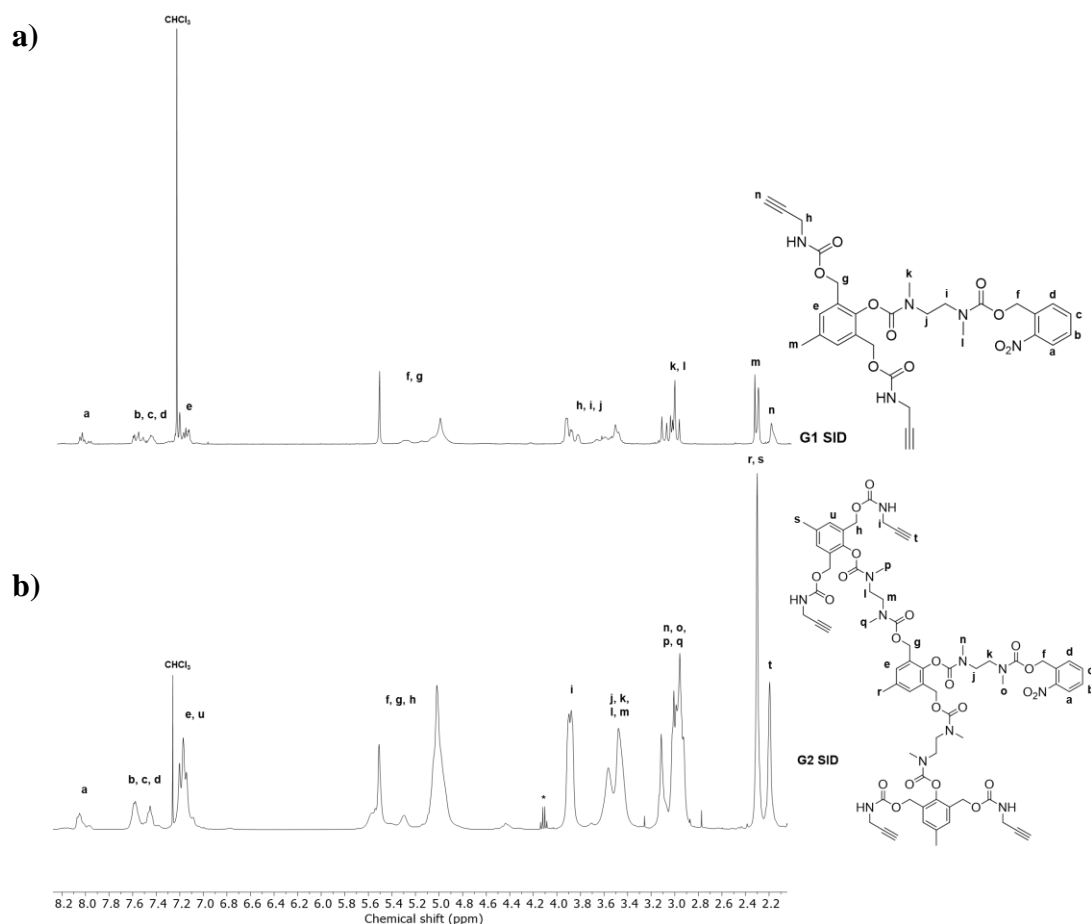


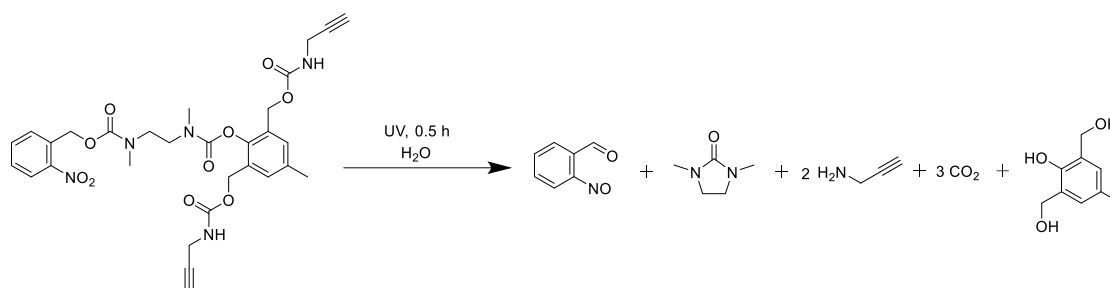
Figure 2.2. ^1H NMR spectra of (a) **G1 SID** and (b) **G2 SID** (400 MHz, CDCl_3).

Asterisks correspond to ethyl acetate. Rotamers are observed about the carbamate bonds.

2.2.2 Degradation of G1 and G2 SIDs

To confirm that the new dendrons would degrade in a similar manner to SIDs with the same polycarbamate backbone but different peripheral and focal point groups,²³ the **G1** and **G2** SIDs were dissolved in deuterated phosphate buffer saline:dimethylsulfoxide ($\text{PBS}:\text{DMSO-}d_6$) (1:1.25 for **G1 SID** and 1:3.5 for **G2 SID**) and degradation was triggered by 0.5 h of UV (365 – 370 nm) light irradiation with an intensity of 10 mW/m^2 . The expected SID degradation products include *o*-nitrosobenzaldehyde, *N,N'*-dimethylimidazolidinone, CO_2 , propargylamine, and *p*-cresol (Scheme 2.3, Figure A1). SID degradation was monitored using ^1H NMR spectroscopy (Figures 2.3, A2), where disappearance of the methylene protons adjacent to the *p*-cresol unit at $\sim 5.52 \text{ ppm}$ and the appearance of singlets at 3.18 and 2.58 ppm indicated cleavage of the photolabile core,

followed by intramolecular cyclization, 1,4-elimination, and decarboxylation reactions of the SID. The degradation time was monitored by using DMSO as the internal standard against which to integrate the singlet at 3.18 ppm, corresponding to the methylene protons in the *N,N'*-dimethylimidazolidinone. These analyses indicated that the **G1 SID** and **G2 SID** took about 10 and 18 days, respectively, to completely degrade. The longer degradation time of the **G2 SID** is attributed to the requirement for a longer sequence of reactions for backbone fragmentation from the core to the periphery, consistent with the results of Shabat and coworkers for SIDs.¹⁶



Scheme 2.3. Proposed degradation products of **G1 SID** exposed to 0.5 h of UV irradiation in PBS:DMSO-*d*₆ (1:1.25).

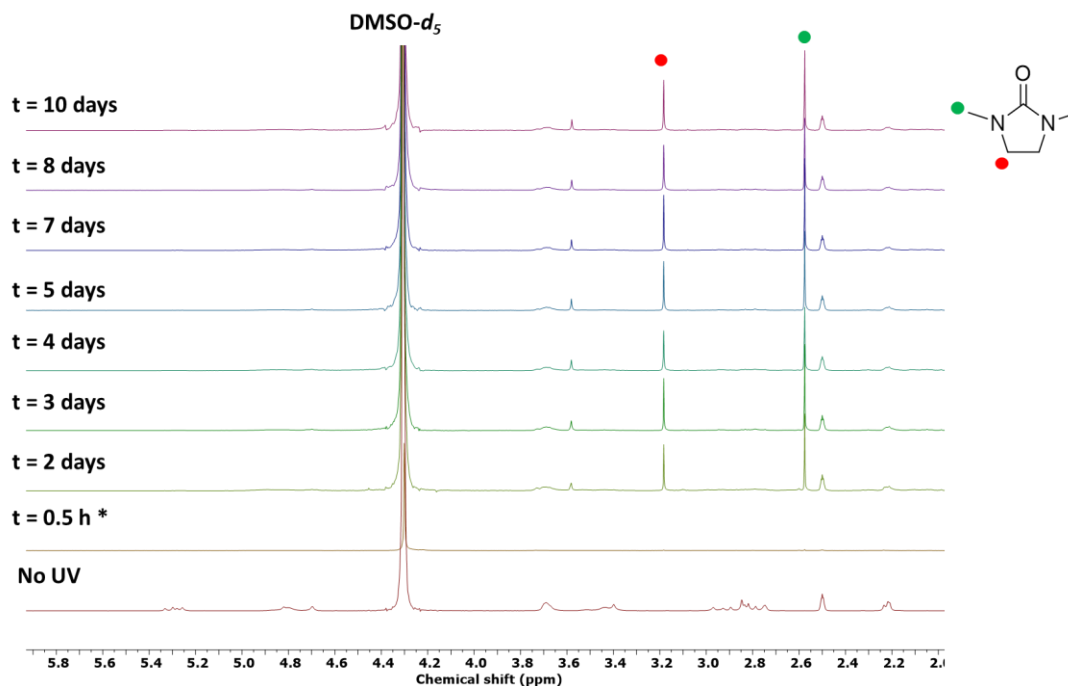
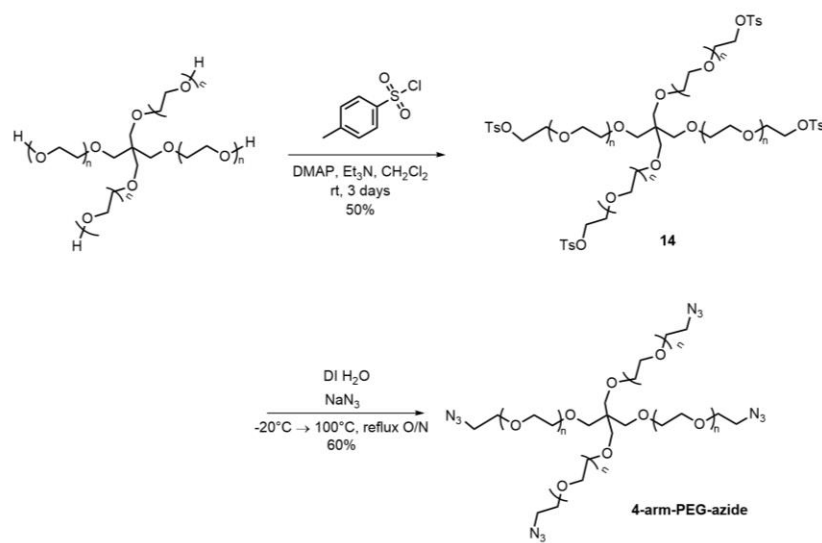


Figure 2.3. ^1H NMR degradation profile of the **G1 SID** in deuterated PBS:DMSO- d_6 (1:1.25) (D_2O , 400 MHz). *denotes an irradiation exposure of 0.5 h. Red and green markers correspond to methylene and methyl protons, respectively, in the N,N' -dimethylimidazolidinone degradation product.

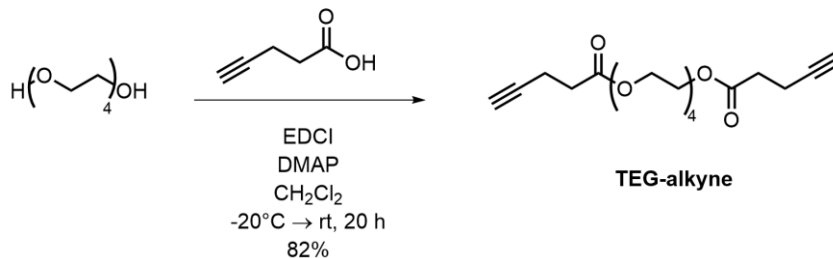
2.2.3 Synthesis and Characterization of PEG Derivatives

Hydrogel synthesis requires network formation, and with the SIDs this network formation requires reaction with a water-soluble molecule having greater than two azides. PEG is widely used in hydrogel preparation as well as many biomedical applications.²⁴⁻²⁵ Therefore, a 2000 g/mol 4-arm-PEG was first activated with tosyl chloride groups to afford the tosylate **14**, which was then reacted with 40 equiv. of sodium azide in deionized (DI) water to provide the **4-arm-PEG-azide** (Scheme 2.4).



Scheme 2.4. Synthesis of 4-arm-PEG-azide.

In addition, a control, non-UV-responsive bisalkyne was prepared to enable the preparation of non-stimuli-responsive hydrogels for comparison with the SID hydrogels. Following a procedure previously reported for TEG monomethyl ether by Opsteen and coworkers,²⁶ TEG was functionalized with two terminal alkyne moieties by reaction with 4 equiv. of 4-pentynoic acid in CH_2Cl_2 using *N*-(3-dimethylaminopropyl)-*N*'-ethylcarbodiimide (EDC) hydrochloride and DMAP as the activating agent and catalyst, respectively, to afford the **TEG-alkyne** (Scheme 2.5).



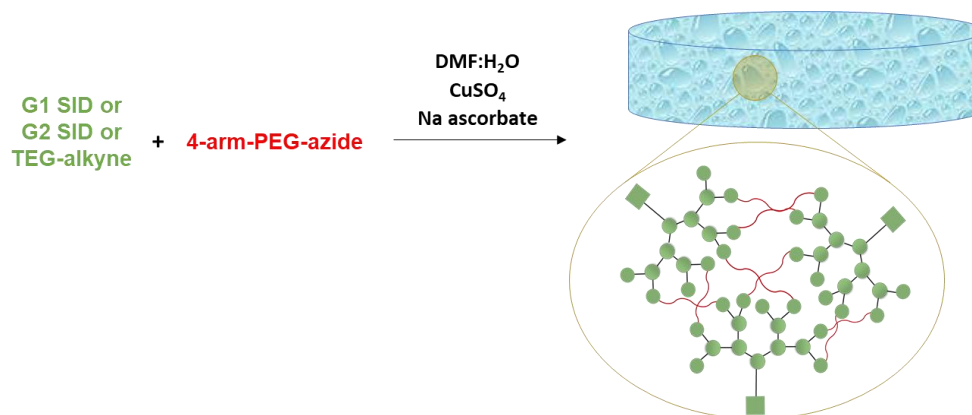
Scheme 2.5. Synthesis of TEG-alkyne.

These PEG derivatives were characterized by ^1H NMR, ^{13}C NMR, and FTIR spectroscopic methods. The **4-arm-PEG-azide** was also characterized by size exclusion chromatography (SEC) (Figure A3) where the number average molar mass (M_n), weight average molar mass

(M_w) and dispersity (D) were obtained using refractive index detection and analyzed relative to poly(methyl methacrylate) (PMMA) standards. The M_n , M_w , and D values obtained were 2814 kg/mol, 2914 kg/mol, and 1.05. Since PMMA standards were used for SEC analysis, molecular weights of the **4-arm-PEG-azide** starting material were overestimated.

2.2.4 Synthesis and Characterization of Hydrogels

The **TEG-alkyne**, **G1 SID**, and **G2 SID** were reacted with the **4-arm-PEG-azide** by a CuAAC click reaction to determine if gelation was possible (Scheme 2.6). The CuAAC click reaction has been extensively employed due to its ease of implementation and high yield.²⁷ Although the use of a copper catalyst is not ideal for biomedical applications, the metal can be efficiently removed using a chelating agent, or the reaction can be replaced with a strain-promoted version quite readily in future work. The reaction was performed in 4:1 DMF:H₂O to dissolve the dendrons and other reagents and a 1:1 stoichiometric ratio of alkyne:azide functional groups was used. Three different formulations were prepared comprising 10, 15, or 25% w/v of **4-arm-PEG-azide**, along with CuSO₄ and sodium ascorbate (Table A1).



Scheme 2.6. Hydrogel formation by a click reaction between an alkyne species and **4-arm-PEG-azide**.

Table 1. Gel content (%) and EWC of the different hydrogel formulations.

Alkyne Hydrogel	Polymer Concentration (% w/v)	Gel Content (%)	EWC (%)
TEG-alkyne	10	92 ± 11	94 ± 1
	15	94 ± 2	91 ± 0.3
	25	91 ± 3	87 ± 3
G1 SID	10	88 ± 5	91 ± 2
	15	94 ± 5	88 ± 1
	25	90 ± 3	80 ± 5
G2 SID	10	95 ± 2	94 ± 1
	15	95 ± 1	89 ± 1
	25	96 ± 1	80 ± 2

The hydrogels were characterized by their gel content and EWC (Table 1). Gel content is the percentage of SID and polymer incorporated into the network while EWC measures the gel's water content at equilibrium.²⁸ The gel content was high ($\geq 88\%$) for all of the formulations, with the **G2 SID** generally giving the highest gel content ($\geq 95\%$) and lowest sample to sample deviation. However, there were no statistically significant differences between any of the samples. The EWC decreased as the polymer concentration increased for each series of hydrogels, which can likely be attributed to the formation of a more densely crosslinked network at higher concentration. In addition, the G1 and G2 SID systems had lower EWC than the **TEG-alkyne** hydrogel, likely due to the dendron component being less hydrophilic than TEG. Although not obvious from the gel content and EWC, the hydrogels synthesized from 10% polymer were soft and susceptible to collapse if handled (Figure A4). However, gels formed from 15 and 25% polymer were more mechanically robust. The improved mechanical properties at higher polymer content can be attributed to the expected higher density of crosslinks. Based on these observations, hydrogels containing 15% polymer were chosen for further studies.

2.2.5 Copper Content in SID Hydrogels

Following the gel synthesis, the SID hydrogels were assessed for copper content by inductively coupled plasma-mass spectrometry (ICP-MS). Copper content in biomaterials should be limited as high concentrations of the metal can result in liver damage and gastrointestinal complications in humans.²⁹ The National Institute of Health determined

that tolerable daily upper intake levels of copper for infants, adolescents, and adults is 1, 5, and 10 mg, respectively.³⁰ Further, the average adult typically has a total body copper content of 50-120 mg.³¹ The ICP-MS instrument detection and reporting limits were 1.26 and 3.78 $\mu\text{g/g}$, respectively. The concentration of copper in the **G1 SID** was determined to be below the testing method's detection limit while the **G2 SID** had a copper concentration of 10.48 $\mu\text{g/g}$. The tighter network formation in the **G2 SID** gel can potentially explain the scaffold's higher copper concentration. Nonetheless, greater than 99.9% of the initial copper was removed from the **G2 SID** gel.

2.2.6 Degradation of the Hydrogels

To evaluate their degradability, accurately measured quantities of the TEG and SID hydrogels were immersed in deuterated PBS containing 1% acetonitrile as an internal standard. Initially, only peaks corresponding to HOD and acetonitrile were observed by ^1H NMR spectroscopy, as the remaining molecules were tied up in the polymer network (Figures 2.4, A5). At defined time points, the hydrogels were then irradiated for 0.5 h with UV light to trigger the fragmentation of the dendrimer backbone, while control hydrogels were stored in the dark. Over time, peaks emerged at 3.72, 3.38, and 2.75 ppm. The peak at 3.72 ppm is attributed to solubilized PEG while the two singlets further upfield correspond to methylene protons in the *N,N'*-dimethylimidazolidinone formed by intramolecular cyclization of the *N,N'*-dimethylethylene diamine spacer. The percent degradation over time was quantified based on the integration of the PEG peak compared to the acetonitrile standard peak at 2.1 ppm. The **G1 SID** hydrogel degraded more than 40% over 1 day after the first irradiation, compared to the **G2 SID** hydrogel which degraded 18% over the same time frame (Figure 2.5). The slower degradation of the **G2 SID** hydrogel, compared to the **G1 SID** hydrogel, can likely be attributed to its more densely crosslinked network, due to it having four reactive alkynes compared to two. In addition, as described above, the **G2 SID** requires longer to degrade, due to a larger number of sequential reactions required to degrade the backbone from core to periphery. Subsequent irradiations resulted in increased hydrogel degradation, indicating that the initial irradiation did not cleave all of the *o*-nitrobenzyl moieties. This feature could be of interest as the hydrogel can be degraded in a controlled manner on demand through multiple irradiations.

In contrast to the irradiated hydrogels, ^1H NMR signals attributed to the degradation products did not appear in the spectra of the non-irradiated SID hydrogels, demonstrating their stability in PBS in the absence of triggering.

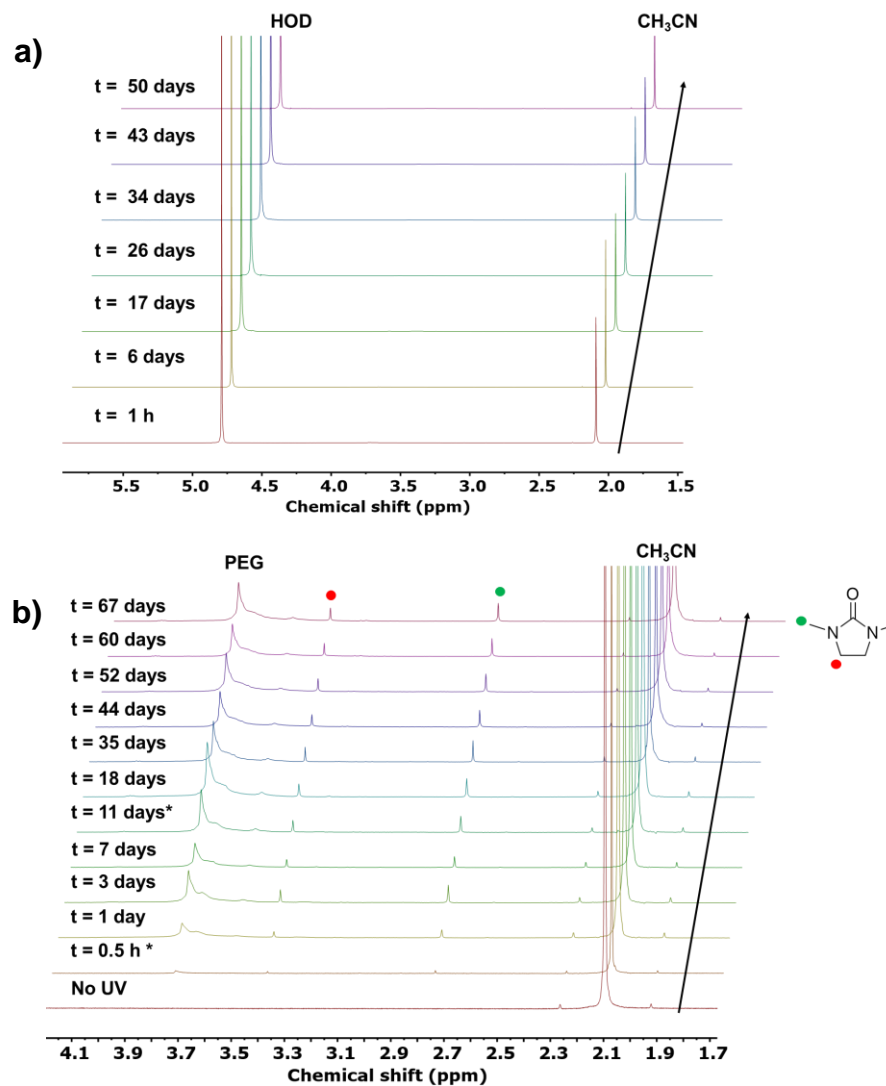


Figure 2.4. ^1H NMR spectra of (a) non-irradiated, (b) irradiated **G1 SID** hydrogel in deuterated PBS:acetonitrile (100:1) (D_2O , 400 MHz). *denotes an irradiation exposure of 0.5 h followed by 1 h incubation at 37 °C. Red and green markers correspond to methylene and methyl protons, respectively, in the N,N' -dimethylimidazolidinone degradation product.

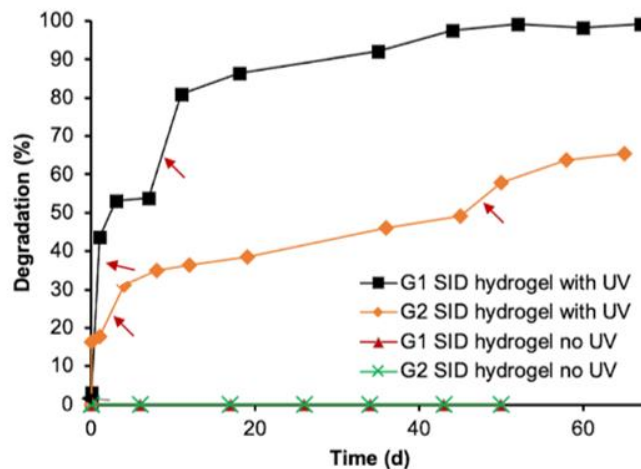


Figure 2.5. Degradation (%) of G1 and G2 SID hydrogels over time in deuterated PBS: acetonitrile (100:1). Arrows denote an irradiation exposure of 0.5 h followed by incubation at 37 °C for 1 h before measurement at the subsequent time point.

While the ^1H NMR spectra of the **TEG-alkyne** hydrogels did not show peaks corresponding to the *N,N'*-dimethylimidazolidinone degradation product, the PEG peak appeared within 7 days for both the non-irradiated and irradiated hydrogels (Figures A6, A7) and can be attributed to the hydrolysis of the ester linkages in the network, whereas the SID hydrogels did not have ester linkages. Thus, although it was a useful comparison for examining the gel content and EWC, the **TEG-alkyne** hydrogel is not highly stable in the PBS.

2.2.7 Compression Moduli of TEG-alkyne and SID Hydrogels

The compressive moduli of the hydrogels were measured in PBS at 37 °C under unconfined compression. The G1 and G2 hydrogels were incubated for six days in PBS either with or without irradiation. Without irradiation, the **G2 SID** had a significantly higher modulus of 144 ± 10 kPa compared to 93 ± 3 kPa for the **G1 SID** hydrogel, which can be attributed to its more densely crosslinked network (Figure 2.6). After irradiation with UV light, the modulus of the **G1 SID** hydrogel decreased more than 2-fold to 42 ± 7 kPa. This decrease can be attributed to substantial degradation of the hydrogel network, as supported by the ^1H NMR spectroscopy results described above. After irradiation, the modulus of the **G2 SID** hydrogel was 123 ± 20 kPa, which was not significantly different statistically from

that of the non-irradiated **G2 SID** hydrogel. The more densely crosslinked network and slow G2 dendron degradation likely contribute to retention of mechanical properties for the **G2 SID** hydrogel. Harsher irradiation conditions, such as longer and more frequent UV exposure events would be required to observe significant differences in compression moduli.

As noted based on the ^1H NMR spectroscopy studies of hydrogel degradation, the **TEG-alkyne** hydrogels were not sufficiently stable to be incubated in PBS for 6 days. However, **TEG-alkyne** based hydrogels incubated for 1 day either with or without UV irradiation showed no significant difference in compressive moduli. Thus, in agreement with ^1H NMR data (Figures A6, A7), UV exposure did not initiate or accelerate hydrolysis of the TEG-based scaffold. It was also noted that the non-irradiated SID hydrogels had significantly higher moduli than the **TEG-alkyne** hydrogel, which suggests that the incorporation of a more hydrophobic crosslinker into the network led to enhanced mechanical properties.

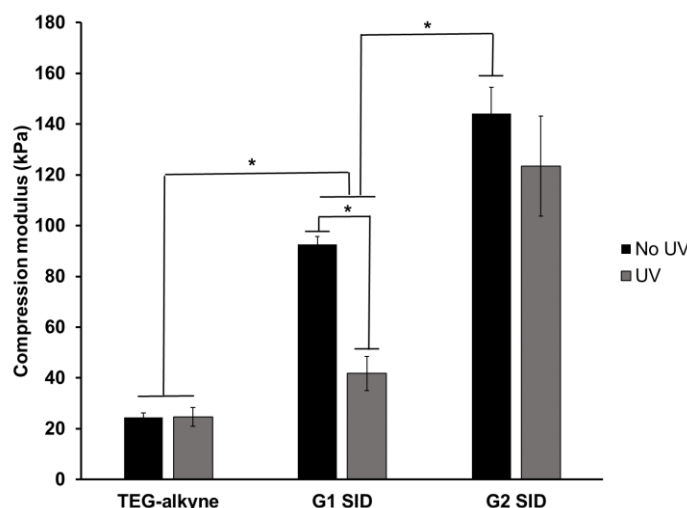


Figure 2.6. Compressive moduli ($n = 3$) of non-irradiated and irradiated **TEG-alkyne**, **G1 SID**, and **G2 SID** hydrogels in PBS. **TEG-alkyne** hydrogels were irradiated for 0.5 h and incubated at 37 °C for 1 day while SID gels were exposed to UV light for four hours for four days and incubated overnight following each irradiation event. Non-irradiated hydrogels were incubated for the same time as irradiated systems of the same formulation. *denotes a statistically significant difference between hydrogel systems. Data was

analyzed by a two-way ANOVA with a Tukey's post-hoc test comparison of the means ($p < 0.05$).

2.2.8 Drug Release

Having demonstrated the ability to trigger degradation of the SID hydrogels in response to UV light, the next step was to determine whether the release of drugs from the hydrogels could potentially be triggered. Celecoxib (CXB) (Figure 2.7) was loaded during the hydrogels during formation through the addition of 10% w/w of CXB relative to polymer. The average loading capacity of celecoxib (CXB) in **TEG-alkyne**, **G1 SID**, and **G2 SID** hydrogel systems was assessed after washing the hydrogels with an ethylenediaminetetraacetic acid (EDTA) solution, followed by dionized water, and then eluting the loaded drug from the hydrogels using CH_2Cl_2 and quantifying it by UV-visible spectroscopy (Table 2). The **TEG-alkyne** hydrogel had the highest average CXB loading at $7.50 \pm 0.03\%$ w/w relative to polymer, which can likely be attributed to the hydrogel's higher EWC and therefore increased space in the network to store CXB. The **G2 SID** hydrogel had a higher CXB content ($5.40 \pm 0.39\%$) than the **G1 SID** hydrogel (3.45 ± 0.24). It is possible that the larger hydrophobic **G2 SID** domains in the hydrogel facilitate the loading of CXB.

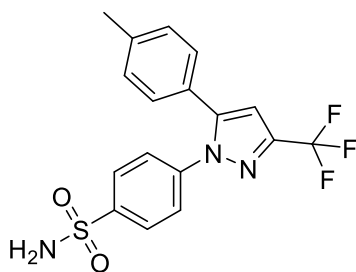


Figure 2.7. Structure of CXB.

Table 2. Average loading of CXB (%) in hydrogel systems prepared from 15% (w/w) of **4-arm-PEG-azide** and TEG or SID alkynes.

Alkyne hydrogel	CXB loading (% w/w relative to polymer)	CXB loading efficiency (%)
TEG-alkyne	7.50 ± 0.03	81.9 ± 0.60
G1 SID	3.45 ± 0.24	35.9 ± 0.41
G2 SID	5.40 ± 0.39	61.9 ± 0.67

Release of CXB from the control **TEG-alkyne** hydrogel was first investigated, using UV-visible spectroscopy to quantify the released drug into 0.1 M PBS solution containing 2% (w/w) of polysorbate 80 to solubilize the CXB. Greater than 90% of the CXB was released over about 10 days (Figure 2.7). As an additional control, free CXB dissolution into the release medium was also investigated, with about 6 days required to completely dissolve the same quantity of CXB as was loaded into the hydrogel. Due to the poor solubility of CXB, its release can be limited by its slow dissolution so this control was important to confirm that the hydrogel rather than solubility was controlling the CXB release. In the case of the SID hydrogels, it was necessary to use HPLC to quantify the released CXB due to the simultaneous generation of dendrimer degradation products whose absorption spectra would overlap with that of CXB in the UV-visible spectroscopy. Initial HPLC studies of the **G1 SID** gels loaded with CXB indicated the presence of a small amount of unconjugated **G1 SID** in the hydrogels. Furthermore, the retention time of free **G1 SID** and CXB on HPLC were quite similar and separation proved difficult. Thus, CXB release studies were only conducted for the **G2 SID** gel systems. Drug release over time from the **G2 SID** hydrogel suggested release of CXB from the irradiated and non-irradiated **G2 SID** hydrogels was similar to the dissolution of the free drug. As supported by the ¹H NMR spectroscopy study of dendrimer and hydrogel degradation, slow degradation of the **G2 SID** and **G2 SID** hydrogel when compared to the smaller **G1 SID** scaffold, could explain the slow release of CXB from the **G2 SID** gel even upon UV light irradiation. Combined with the slow CXB dissolution, it was not possible to demonstrate triggered release of CXB from the SID hydrogels.

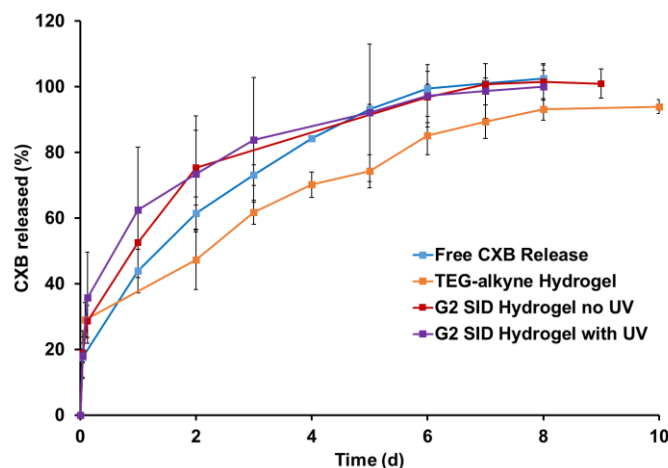


Figure 2.8. Release of CXB from the **TEG-alkyne** hydrogel, as well as irradiated and non-irradiated **G2 SID** hydrogels in PBS containing 2 wt % polysorbate80. The dissolution rate of free CXB is included for comparison.

2.3 Conclusion

We have presented the synthesis of two novel photosensitive **SID** hydrogel systems and investigated their potential as biomaterials for drug delivery. **G1** and **G2 SID**s were successfully synthesized. In addition, a control non-UV-responsive bisalkyne was prepared to develop non-stimuli responsive hydrogels for comparison to **SID** gels. ^1H NMR spectroscopy demonstrated that degradation of the irradiated **G2 SID** gel was slower than the **G1 SID** gel due to the tightly crosslinked network of the former as well as the longer time required for fragmentation of the **G2 SID** backbone. Further, ^1H NMR spectroscopy indicated that the **TEG-alkyne** hydrogel underwent hydrolysis of the ester linkages over time in PBS solution.

Although there were no statistically significant differences between samples, the **G2 SID** hydrogels tended to give the highest and most reproducible gel content values ($\geq 95\%$). Furthermore, the EWC decreased as the polymer concentration increased for each hydrogel system, potentially due to the formation of a denser network at higher concentration. While gels developed from 10% polymer were fragile and susceptible to collapse if handled, scaffolds synthesized from 15 and 25% polymer were stronger due to increased crosslinking density at higher polymer concentration. Similarly, compression testing

indicated that the non-irradiated **G2 SID** hydrogel had a significantly higher modulus than that of the **G1 SID** hydrogel. While irradiation with UV light did not significantly decrease the modulus for the **G2 SID** hydrogel, the modulus for the **G1 SID** hydrogel decreased more than 2-fold. **TEG-alkyne** hydrogels incubated for 1 day either with or without UV irradiation showed no significant differences in compressive moduli. CXB loading was assessed in all three hydrogel systems where the **TEG-alkyne** and **G1 SID** gels provided the highest and lowest loading amount, respectively. Release of CXB from the irradiated and non-irradiated **G2 SID** gels was investigated and found to be similar to the dissolution of the free drug, potentially due to the slow degradation of the G2 dendrimer and hydrogel. Future work will focus on developing a stimuli-responsive dendritic-based hydrogel that demonstrates faster drug release.

2.4 Experimental

2.4.1 General Experimental Details

General Materials. Compounds **1**²⁰, compound **2**²¹, and compound **5**²² were synthesized as previously reported. All reactions were carried out using flame dried glassware under an inert atmosphere of nitrogen unless otherwise stated. Pyridine, Et₃N, Na₂HPO₄, and TFA were purchased from Caledon Laboratory Chemicals (Georgetown, ON, Canada). *N,N'*-dimethylethylenediamine, 4-nitrophenyl chloroformate, and 2-nitrobenzyl alcohol were purchased from TCI Chemicals. Bis(hydroxymethyl)-*p*-cresol, TEG, DMSO, sodium azide, and DIPEA were purchased from Sigma-Aldrich. DMAP was purchased from AK Scientific. Amberlyst-15 and 4-pentynoic acid were purchased from Alfa Aesar. 4-arm-PEG was purchased from JenKem Technology. EDC hydrochloride was purchased from Advanced ChemTech. NaCl was purchased from Fisher Scientific. KH₂PO₄ and KCl were purchased from EMD Millipore. All chemicals were used as received unless otherwise noted. Under a nitrogen atmosphere, toluene was distilled over sodium, while Et₃N and CH₂Cl₂ were distilled over CaH₂.

General Procedures. Dialysis was performed using Spectra/Por 6 dialysis tubing from Spectrum Laboratories (Rancho Dominguez, CA, USA) with a molecular weight cutoff (MWCO) of 3.5 kg/mol. Column chromatography was performed using silica gel

(0.040–0.063 mm particle size, 230–430 mesh). Thin layer chromatography (TLC) was carried out using Siliaplate silica gel F254 plates (20 cm × 20 cm, 250 μm). NMR spectroscopy was conducted on a Bruker AvIII HD 400 MHz Spectrometer (¹H 400.09 MHz, ¹³C 100.5 MHz). The ¹H and ¹³C chemical shifts (δ) are reported in parts per million (ppm) relative to tetramethylsilane and were calibrated against CHCl₃ (7.26 ppm) and CDCl₃ (77 ppm) respectively. Coupling constants (J) are expressed in Hertz (Hz). FTIR spectra were recorded using a PerkinElmer Spectrum Two FTIR spectrometer with an attenuated total reflectance (ATR) attachment and a single reflection diamond. The SEC instrument was equipped with a Viscotek GPC Max VE2001 solvent module. Samples were analyzed using the Viscotek VE3580 RI detector operating at 30°C, and triple detection Malvern 270 Dual detector. The separation technique employed two Agilent Polypore (300 x 7.5 mm) columns connected in series and to a Polypore guard column (50 x 7.5 mm). Samples were dissolved in THF (glass distilled grade) in approximately 5 mg/mL concentration and filtered through 0.22 μm syringe filters. Samples were injected using a 50 μL loop (56 μL volume). The THF eluent was filtered and eluted at 1 ml/min for a total of 30 minutes. The *M_n*, *M_w*, and *D* were determined relative to PMMA standards with molecular weight ranges of 690 – 790,000 g/mol. High-resolution mass spectrometry (HRMS) was conducted on a Synapt high definition mass spectrometer using electrospray (ESI) ionization in either the positive or negative ion mode. The HPLC was equipped with a Waters Separations Module 2695, a Photodiode Array Detector (Waters 2998) and a Kinetex C18 5μm (4.6x100 mm) column connected to a C18 guard column. The PDA detector was used to monitor Celecoxib at 254 nm. Analyte separation was obtained using an isocratic run method with a mobile phase of acetonitrile: 0.1M KH₂PO₄ pH 2.4 (48:52) at 1 ml/min for 15 min. Samples were irradiated in a UV box (wavelength: 365-370 nm, intensity: 10 mW cm⁻²).

2.4.2 Synthesis of Crosslinkers and Polymers

Synthesis of Compound 3. Compound **1**²⁰ (1.85 g, 9.84 mmol, 1.0 equiv), compound **2**²¹ (3.13 g, 9.84 mmol, 1.0 equiv), DIPEA (3.43 mL, 19.68 mmol, 2 equiv) and DMAP (1.20 g, 9.84 mmol, 1.0 equiv) were combined with stirring in dry toluene (90 mL). The reaction mixture was stirred at room temperature overnight. The solvent was removed, and the crude

residue was dissolved in CH_2Cl_2 (100 mL), washed with saturated Na_2CO_3 (3 x 100 mL), and dried over MgSO_4 . The crude product was purified via column chromatography with a gradient from 100% hexane to 50:50 hexane/ethyl acetate as the eluent yielding 1.54 g of a yellow oil. Yield = 43%. ^1H NMR (CDCl_3 , 400 MHz): δ 8.12 – 8.02 (m, 1H), 7.70 – 7.43 (m, 3H), 5.53 (s, 2H), 3.54 – 3.32 (m, 4H), 3.15 – 2.82 (m, 6H), 1.44 (s, 9H). ^{13}C NMR (CDCl_3 , 100 MHz): δ 171.0, 163.1, 155.4, 147.4, 133.6, 132.9, 129.2, 128.6, 128.5, 126.0, 125.0, 124.8, 122.5, 122.1, 115.5, 79.6, 63.9, 63.7, 47.2, 46.9, 46.7, 46.4, 46.9, 45.5, 35.3, 35.0, 34.7, 34.4, 28.3. FTIR: 2957, 1687, 1524, 1399 cm^{-1} . MS positive ion mode (m/z): calcd for $\text{C}_{17}\text{H}_{25}\text{N}_3\text{O}_6$, 366.1660; found, 366.1655 $[\text{M}]^+$.

Synthesis of Compound 4. Compound **3** (180 mg, 0.493 mmol, 1.0 equiv) was dissolved with stirring in dry CH_2Cl_2 (0.63 mL) at 0 °C. TFA (0.75 mL, 9.86 mmol, 20 equiv) was added dropwise and the mixture was stirred for 1 hour. The solution was concentrated to afford 180 mg of a yellow oil. Yield = 96 %. ^1H NMR (CDCl_3 , 400 MHz): δ 8.35 – 8.24 (m, 2H), 8.09 (d, J = 8.1 Hz, 1H), 7.71 – 7.50 (m, 3H), 5.50 (s, 2H), 3.65 (t, J = 3.7 Hz, 2H), 3.36 (bs, 2H), 3.00 (s, 3H), 2.85 (t, J = 2.9 Hz, 3H). ^{13}C NMR (CDCl_3 , 100 MHz): δ 160.4 (q, J = 160), 158.5, 147.1, 134.3, 131.1, 130.4, 129.8, 129.3, 128.9, 125.2, 125.2, 122.5, 122.4, 114.8 (q, J = 115), 65.6, 49.3, 48.9, 47.8, 46.5, 46.4, 45.7, 45.3, 35.5, 35.0, 34.1, 34.0. MS positive ion mode (m/z): calcd for $\text{C}_{12}\text{H}_{17}\text{N}_3\text{O}_4$, 268.1292; found, 268.1293 $[\text{M}]^+$.

Synthesis of Compound 6. Compound **4** (170 mg, 0.636 mmol, 1.0 equiv), compound **5**²² (357 mg, 0.636 mmol, 1.0 equiv), DIPEA (0.22 mL, 1.27 mmol, 2.0 equiv), and DMAP (77.7 mg, 0.636 mmol, 1.0 equiv) were combined in dry toluene (30 mL) and stirred at room temperature overnight. The solvent was removed, and the crude residue was dissolved in CH_2Cl_2 (50 mL), washed with saturated Na_2CO_3 (3 x 50 mL), and dried over MgSO_4 . The product was purified via column chromatography with a 75% hexane/ethyl acetate solvent system yielding 310 mg of a yellow oil. Yield = 74 %. ^1H NMR (CDCl_3 , 400 MHz): δ 8.10 – 8.05 (m, 1H), 7.71 – 7.35 (m, 3H), 7.17 (s, 2H), 5.57 – 5.51 (m, 2H), 4.65 – 4.55 (m, 4H), 3.68 – 3.44 (m, 4H), 3.19 – 2.97 (m, 6H), 2.3 – 2.31 (m, 3H), 0.91 (s, 18H), 0.05 (s, 12H). ^{13}C NMR (CDCl_3 , 100 MHz): δ 155.7, 155.5, 155.3, 154.0, 153.7, 147.8, 147.5, 147.4,

143.0, 142.8, 135.2, 133.6, 133.4, 133.2, 133.0, 132.8, 132.5, 132.3, 129.6, 129.2, 128.7, 128.6, 128.4, 127.1, 127.0, 124.8, 64.0, 63.9, 60.4, 60.2, 60.1, 47.9, 47.7, 47.4, 47.0, 47.0, 46.9, 46.3, 35.8, 35.7, 35.5, 35.3, 35.2, 35.1, 34.7, 34.6, 34.4, 25.8, 21.2, 18.3, -5.4. FTIR: 2910, 1715, 1527, 1400, 1118 cm^{-1} . MS positive ion mode (m/z): calcd for $\text{C}_{34}\text{H}_{55}\text{N}_3\text{O}_8\text{Si}_2$, 690.3600; found, 690.3812 $[\text{M}]^+$.

Synthesis of Compound 7. Compound **6** (300 mg, 0.456 mmol, 1.0 equiv) and 1.53 g of Amberlyst-15 resin were combined with stirring in methanol (5 mL). The reaction was left to stir at room temperature for 1.5 hours. Amberlyst-15 was removed via filtration and the filtrate was concentrated to afford 249 mg of a brown oil. Yield = 83%. ^1H NMR (CDCl_3 , 400 MHz): δ 8.10 – 8.03 (m, 1H), 7.65 – 7.41 (m, 3H), 7.23 – 7.17 (m, 2H), 5.58 – 5.48 (m, 2H), 4.54 – 4.43 (m, 4H), 3.73 – 3.44 (m, 4H), 3.24 – 2.96 (m, 6H), 2.40 – 2.30 (m, 3H). ^{13}C NMR (CDCl_3 , 100 MHz): δ 156.2, 156.0, 155.7, 147.7, 147.5, 145.1, 144.8, 136.2, 133.6, 133.5, 133.2, 132.8, 132.3, 130.5, 130.1, 129.9, 129.2, 129.0, 128.8, 128.5, 124.8, 64.3, 64.1, 60.6, 60.4, 58.2, 50.6, 47.7, 47.3, 47.1, 46.9, 46.7, 45.9, 35.9, 35.7, 35.2, 35.0, 34.9, 34.3, 20.8. FTIR: 3400, 2939, 1691, 1527, 1399 cm^{-1} . MS positive ion mode (m/z): calcd for $\text{C}_{22}\text{H}_{27}\text{N}_3\text{O}_8$, 462.1871; found, 462.2117 $[\text{M}]^+$.

Synthesis of Compound 8. Compound **7** (240 mg, 0.520 mmol, 1.0 equiv), 4-nitrophenyl chloroformate (630 mg, 3.13 mmol, 6.0 equiv) and dry pyridine (380 mg, 4.80 mmol, 9.2 equiv) were combined with stirring in dry CH_2Cl_2 (30 mL). The reaction was stirred at room temperature overnight. The solvent was removed, and the crude residue was dissolved in CH_2Cl_2 (50 mL), washed with saturated NH_4Cl (3 x 50 mL) and Na_2CO_3 (3 x 50 mL), and dried over MgSO_4 . The product was purified by column chromatography with a 50% hexane/ethyl acetate solvent system and then precipitated in pentane to afford 240 mg of a white solid. Yield = 59%. ^1H NMR (CDCl_3 , 400 MHz): δ 8.29 – 8.22 (m, 4H), 8.09 – 8.00 (m, 1H), 7.63 – 7.29 (m, 9H), 5.54 – 5.48 (m, 2H), 5.27 – 5.15 (m, 4H), 3.73 – 3.46 (m, 4H), 3.24 – 2.92 (m, 6H), 2.38 (s, 3H). ^{13}C NMR (CDCl_3 , 100 MHz): δ 155.5, 154.2, 154.0, 152.3, 146.0, 145.4, 136.4, 133.6, 132.0, 131.7, 129.0, 128.6, 127.9, 125.3, 124.9, 121.8, 66.0, 64.1, 64.0, 47.7, 47.5, 47.1, 45.7, 46.1, 35.9, 35.6, 35.3, 34.9, 34.4, 20.8. FTIR: 2946,

1761, 1520, 1347 cm^{-1} . MS positive ion mode (m/z): calcd for $\text{C}_{36}\text{H}_{33}\text{N}_5\text{O}_{16}$, 792.2001; found, 792.1949 $[\text{M}]^+$.

Synthesis of G1 SID. Compound **8** (200 mg, 0.253 mmol, 1.0 equiv), propargylamine (0.065 mL, 1.01 mmol, 4.0 equiv), DIPEA (0.18 mL, 1.01 mmol, 4.0 equiv), and DMAP (30.9 mg, 0.253 mmol, 1.0 equiv) were combined with stirring in dry toluene (30 mL). The reaction was stirred at room temperature overnight. The solvent was removed, and the crude residue was dissolved in CH_2Cl_2 (50 mL), washed with saturated NH_4Cl (3 x 50 mL) and Na_2CO_3 (3 x 50 mL), and then dried over MgSO_4 to afford 150 mg of a yellow solid. Yield = 75%. ^1H NMR (CDCl_3 , 400 MHz): δ 8.10 – 8.03 (m, 1H), 7.70 – 7.30 (m, 3H), 7.24 – 7.14 (m, 2H), 5.54 (s, 2H), 5.14 – 4.92 (m, 4H), 4.00 – 3.46 (m, 8H), 3.26 – 2.95 (m, 6H), 2.38 – 2.31 (m, 3H), 2.21 (s, 2H). ^{13}C NMR (CDCl_3 , 100 MHz): δ 155.7, 133.6, 131.3, 130.5, 129.3, 129.0, 128.8, 128.2, 125.3, 124.9, 79.7, 71.5, 64.2, 62.5, 46.9, 35.1, 30.7, 29.7, 20.8. FTIR: 3294, 2935, 2119, 1699, 1525, 1405 cm^{-1} . MS negative ion mode (m/z): calcd for $\text{C}_{30}\text{H}_{33}\text{N}_5\text{O}_{10}$, 622.2144; found, 622.1957 $[\text{M}]^-$.

Synthesis of Compound 9. Compound **5**²² (1.25 g, 2.22 mmol, 1.0 equiv), compound **1**²⁰ (0.63 g, 3.33 mmol, 1.5 equiv), DIPEA (0.86 g, 6.66 mmol, 3.0 equiv), and DMAP (0.27 g, 2.22 mmol, 1.0 equiv) were combined in dry toluene (60 mL). The reaction was stirred at room temperature overnight. The solvent was removed, and the crude residue was dissolved in CH_2Cl_2 (50 mL), washed with saturated NH_4Cl (3 x 80 mL) and Na_2CO_3 (3 x 80 mL), and dried over MgSO_4 . The product was purified via column chromatography with a 75% hexane/ethyl acetate solvent system to afford 1.07 g of a colourless oil. Yield = 79%. Spectral characterization data agreed with those previously reported.⁴

Synthesis of Compound 10. Compound **9** (1.05 g, 1.72 mmol, 1.0 equiv) and Amberlyst-15 were combined in methanol (20 mL) and the reaction was stirred at room temperature for 1.5 hours. Amberlyst-15 was removed via filtration and the filtrate was concentrated to afford 0.51 g of a brown oil. Yield = 78%. Spectral characterization data agreed with those previously reported.⁴

Synthesis of Compound 11. Compound **10** (800 mg, 1.73 mmol, 1.0 equiv), 4-nitrophenyl chloroformate (2.10 g, 10.42 mmol, 6.0 equiv), and dry pyridine (1.26 g, 16.0 mmol, 9.2 equiv) were combined in dry CH₂Cl₂ (70 mL). The reaction was stirred at room temperature overnight. The solvent was removed, and the crude residue was dissolved in CH₂Cl₂ (70 mL), washed with saturated NH₄Cl (3 x 70 mL) and Na₂CO₃ (3 x 70 mL), and dried over MgSO₄. The product was purified by column chromatography with a gradient from 85% hexane to 100% ethyl acetate as the eluent yielding 629 mg of a white powder. Yield = 51%. Spectral characterization data agreed with those previously reported.⁴

Synthesis of Compound 12. Compound **11** (500 mg, 0.702 mmol, 1.0 equiv), propargylamine (0.18 mL, 7.81 mmol, 4.0 equiv), and Et₃N (1.09 mL, 7.81 mmol, 4.0 equiv) were combined in dry DMF (30 mL). The reaction was stirred at room temperature overnight. The crude product was dissolved in CH₂Cl₂ (50 mL), washed with saturated NH₄Cl (3 x 50 mL) and Na₂CO₃ (3 x 50 mL), and dried over MgSO₄. The product was purified by column chromatography with a 40% hexane/ethyl acetate solvent system to afford 256 mg of a yellow powder. Yield = 79%. ¹H NMR (CDCl₃, 400 MHz): δ 7.25 – 8.7.14 (m, 2H), 5.70 – 5.16 (m, 2H), 5.03 (s, 4H), 3.99 – 3.87 (m, 4H), 3.17 – 2.88 (m, 6H), 2.31 (s, 3H), 2.21 (s, 2H), 1.51 – 1.41 (m, 9H). ¹³C NMR (CDCl₃, 100 MHz): δ 155.8, 154.2, 154.0, 146.8, 135.7, 131.3, 130.8, 129.2, 79.9, 79.7, 71.4, 62.6, 62.4, 62.2, 47.7, 47.2, 45.8, 46.2, 35.6, 35.3, 35.2, 34.8, 30.7, 29.9, 28.4, 20.8. FTIR: 3298, 2956, 2119, 1701 cm⁻¹. MS positive ion mode (*m/z*): calcd for C₂₇H₃₆N₄O₈, 567.2425; found, 567.2403 [M + Na]⁺.

Synthesis of Compound 13. Compound **12** (200 mg, 0.37 mmol, 1.0 equiv) was dissolved with stirring in dry CH₂Cl₂ (0.60 mL) at 0 °C. TFA (0.75 mL, 7.34 mmol, 20 equiv) was added dropwise and the mixture was stirred for 1 hour. The solution was concentrated to afford 148 mg of a yellow oil. Yield = 90%. ¹H NMR (CDCl₃, 400 MHz): δ 7.25 – 7.16 (m, 2H), 5.33 – 4.93 (m, 4H), 4.02 – 3.82 (m, 4H), 3.80 – 3.22 (m, 4H), 3.20 – 2.73 (m, 6H), 2.35 (s, 3H), 2.29 – 2.18 (m, 2H). ¹³C NMR (CDCl₃, 100 MHz): δ 160.7 (q, *J* = 160.8), 156.9, 156.2, 155.1, 145.8, 136.7, 132.9, 132.2, 131.9, 129.1, 125.1, 122.5, 115.6 (q, *J* = 115.33 Hz), 79.2, 71.9, 71.6, 63.0, 62.8, 62.4, 45.0, 47.3, 46.2, 45.8, 35.9, 33.6,

33.4, 33.1, 31.2, 30.8, 20.7. FTIR: 3304, 2879, 2130, 1699 cm^{-1} . MS positive ion mode (m/z): calcd for $\text{C}_{22}\text{H}_{28}\text{N}_4\text{O}_6$, 445.2082; found, 445.2034 $[\text{M}]^+$.

Synthesis of Compound G2 SID. Compound **13** (140 mg, 0.315 mmol, 6.0 equiv), compound **11** (41.6 mg, 0.05 mmol, 1.0 equiv), and Et_3N (0.56 mL, 4 mmol, 80 equiv) were combined in dry DMF (10 mL). The reaction was stirred at room temperature overnight. The crude product was dissolved in CH_2Cl_2 (50 mL), washed with saturated NH_4Cl (3 x 50 mL) and Na_2CO_3 (3 x 50 mL), and dried over MgSO_4 . The product was purified via column chromatography with a gradient from 15% hexane:ethyl acetate to 80% ethyl acetate: CH_2Cl_2 as the eluent yielding 37 mg of a yellow powder. Yield = 54%. ^1H NMR (CDCl_3 , 400 MHz): δ 8.11 – 7.99 (m, 1H), 7.66 – 7.42 (m, 3H), 7.24 – 7.10 (m, 6H), 5.62 – 5.45 (m, 4H), 5.10 – 4.93 (m, 10H), 3.96 – 3.79 (m, 8H), 3.67 – 3.38 (m, 12H), 3.17 – 2.89 (m, 18H), 2.36 – 2.14 (m, 13H). ^{13}C NMR (CDCl_3 , 100 MHz): δ 156.1, 155.8, 155.4, 153.8, 147.4, 146.2, 145.5, 135.7, 133.6, 133.0, 132.4, 131.3, 130.4, 129.6, 129.3, 128.8, 128.5, 124.8, 79.8, 71.4, 64.0, 62.4, 62.1, 47.3, 46.9, 46.7, 46.0, 35.6, 35.3, 35.1, 34.8, 34.5, 31.3, 30.7, 20.8. FTIR: 3290, 2939, 2246, 1700, 1520, 1397 cm^{-1} . MS positive ion mode (m/z): calcd for $\text{C}_{68}\text{H}_{79}\text{N}_{11}\text{O}_{22}$, 1424.5293; found, 1424.5241 $[\text{M} + \text{Na}]^+$.

Synthesis of Compound 14. 4-arm-PEG (2.00 g, 1.00 mmol, 1.0 equiv), 4-toluenesulfonyl chloride (1.53 g, 8.00 mmol, 8.0 equiv), Et_3N (0.81 g, 8.00 mmol, 8.0 equiv), and DMAP (0.12 g, 1 mmol, 1.0 equiv) were combined in dry CH_2Cl_2 (10 mL). The reaction was stirred at room temperature for 3 days. 1M HCl (50 mL) was added and the reaction mixture was stirred at room temperature for 2 hours. The resulting solution was extracted with CH_2Cl_2 (3 x 50 mL), dried over MgSO_4 , and then precipitated in diethyl ether to afford 1.31 g of an oil. Yield = 50%. ^1H NMR (CDCl_3 , 400 MHz): δ 7.74 (d, $J = 7.7$ Hz, 8H), 7.29 (d, $J = 7.7$ Hz, 8H), 4.10 (t, $J = 4.1$ Hz, 8H), 3.65 – 3.47 (m, 172H), 2.39 (s, 12H). ^{13}C NMR (CDCl_3 , 100 MHz): δ 144.3, 132.4, 129.4, 127.5, 70.5, 70.1, 69.8, 68.8, 68.2, 21.2 cm^{-1} . $M_n = 2814$ kg/mol, $M_w = 2941$ kg/mol, $D = 1.05$.

Synthesis of 4-arm-PEG-azide. Compound **14** (0.50 g, 0.191 mmol, 1.0 equiv) and sodium azide (0.50 g, 7.64 mmol, 40 equiv) were combined with stirring in deionized water (10 mL) at room temperature. The reaction mixture was heated at reflux (100 $^\circ\text{C}$) overnight.

The resulting solution was extracted with CH_2Cl_2 (3 x 50 mL) and dried over MgSO_4 . The crude product was purified by dialysis against deionized H_2O (500 mL), changing the solution 3 times over 24 hours, using a 3.5 kg/mol MWCO membrane. The resulting solution was freeze-dried to afford 0.25 g of an oil. Yield = 60%. ^1H NMR (CDCl_3 , 400 MHz): δ 3.71 – 3.33 (m, 180H). ^{13}C NMR (CDCl_3 , 100 MHz): δ 70.6, 70.2, 69.7, 60.3, 45.2. FTIR: 2864, 2103 cm^{-1} .

Synthesis of TEG-alkyne. TEG (500 mg, 2.57 mmol, 1.0 equiv), 4-pentynoic acid (610 mg, 6.22 mmol, 2.4 equiv), and DMAP (83.0 mg, 0.679 mmol, 0.26 equiv) were combined in dry CH_2Cl_2 (5 mL) at -20 °C. A solution of EDC hydrochloride (960 mg, 6.18 mmol, 2.4 equiv) in CH_2Cl_2 (2 mL) was added dropwise and the mixture was stirred at room temperature for 20 hours. The resulting solution was washed with 1 M NaOH (2 x 50 mL), deionized H_2O (2 x 50 mL) and NH_4Cl (2 x 50 mL), and dried over MgSO_4 to afford 746 mg of an oil. Yield = 82%. ^1H NMR (CDCl_3 , 400 MHz): δ 4.26 (t, J = 4.3 Hz, 4H), 3.73 – 3.68 (t, J = 3.7 Hz, 4H), 3.68 – 3.64 (m, 8 H), 2.61 – 2.55 (m, 4H), 2.54 – 2.48 (m, 4H), 1.98 (t, J = 2.0 Hz, 2H). ^{13}C NMR (CDCl_3 , 100 MHz): δ 82.2, 72.3, 70.3, 68.9, 68.8, 63.4, 33.0, 14.0 cm^{-1} . FTIR: 3272, 2885, 2123, 1731 cm^{-1} .

2.4.3 Degradation of SIDs

G1 SID (10 mg) and G2 SID (11 mg) were dissolved in a 1.25:1 or 3.5:1 solution of $\text{DMSO}-d_6$:deuterated PBS, respectively. The SIDs were then exposed to 0.5 hr of UV irradiation (wavelength: 365-370 nm, intensity: 10 mW cm^{-2}) and then incubated at 37 °C. SID degradation was monitored by ^1H NMR spectroscopy using the DMSO signal as the internal standard. SID degradation was quantified by integration of the singlet at ~ 2.6 ppm relative to $\text{DMSO}-d_6$.

2.4.4 Hydrogel Synthesis, Characterization, and Degradation

Synthesis of the Hydrogels. Hydrogels were prepared using 10, 15, and 25% w/v of **4-arm-PEG-azide** in 4:1 DMF: H_2O , with the specific formulations provided in Table A1. The amount of **TEG-alkyne**, **G1 SID**, and **G2 SID** were determined based on maintaining a 1:1 molar ratio of azide:alkyne functional group was used in each case. First, the alkyne

and azide were dissolved in DMF (240 μL). Sodium ascorbate and CuSO_4 were each dissolved separately in 30 μL of H_2O and vortexed. The sodium ascorbate solution was then added to the DMF solution and mixed by vortexing, followed by the CuSO_4 solution. The reaction mixture was bubbled with a stream of N_2 gas and vented for one hour and then left under nitrogen overnight. The resulting gels were immersed in a 0.1 M EDTA solution (5 mL), changing the solution 3 times over 24 hours to remove copper. The gels were then immersed in deionized H_2O (5 mL), changing the solution 3 times over 24 hours. The gels were then lyophilized.

Measurement of Gel Content and Equilibrium Water Content (EWC). Gel content and equilibrium water content were measured in triplicate. After gelation as described above, the initial mass (m_i) of each hydrogel was recorded and the theoretical mass (m_t) of polymers involved in crosslinking was calculated as m_i x the m/v % in the formulation. The hydrogels were then immersed in 0.1M EDTA, followed by water as described above. After the third deionized H_2O treatment, the swollen mass (m_s) was recorded to determine the EWC. The hydrogels were then lyophilized and their dry masses (m_d) were measured. The gel content and EWC were calculated using equations (1) and (2), respectively.

$$\text{Gel content} = \frac{m_d}{m_t} \times 100\% \quad (1)$$

$$\text{EWC} = \frac{m_s - m_d}{m_s} \times 100\% \quad (2)$$

Measurement of Compressive Moduli under Unconfined Compression. Cylindrical samples with diameters of ~ 4 mm and heights of ~ 6 mm for the SID gels ($n=3$) were prepared in 1 mL syringes as described above and equilibrated in PBS. Gels ($n = 3$) were irradiated with UV light (wavelength: 365-370 nm, intensity: 10 mW cm^{-2}) for four hours for four days and incubated at 37 $^\circ\text{C}$. The gels were then incubated for an additional two days. Non-irradiated gels ($n=3$) were also incubated for a total of six days at 37 $^\circ\text{C}$. Before compression, the dimensions of the swollen hydrogels were accurately measured using calipers. The compressive moduli were then determined using a UniVert system (CellScale, Waterloo, ON, Canada) equipped with a 0.5 N load cell. During the measurement, the samples were immersed in a 37 $^\circ\text{C}$ PBS bath, preloaded at 0.1 N and

compressed to a total strain of 20% at a rate of $0.6\% \text{ s}^{-1}$. The compression moduli were calculated from the slope of the linear region of the stress-strain curve between 10 and 15% strain.

Degradation of SID Hydrogels. First-generation (11.3 mg) and second-generation (12.1 mg) SID hydrogels were immersed in a 1.00 mL of deuterated PBS and 10.0 μL of acetonitrile was added as an internal standard. The immersed gels were then exposed to 0.5 h of UV irradiation (wavelength: 365-370 nm, intensity: 10 mW cm^{-2}) at $t = 0$ and 7 days. The second-generation SID gel was again irradiated at 50 days. The samples were incubated at $37 \text{ }^\circ\text{C}$. Gel degradation was monitored by ^1H NMR spectroscopy with degradation quantified based on the percentage of solubilized PEG, based on integration of the peak at 3.75 – 3.65 ppm corresponding to the protons on PEG, compared to the integration of the acetonitrile internal standard peak at 2.09 ppm.

2.4.5 Trace Elemental Analysis

First-generation (50 mg) and second-generation (45 mg) SID hydrogels were prepared as mentioned above and analyzed for the presence of copper by ICP-MS (Agilent 7700 Series) with helium gas as the plasma. The method detection and reporting limit was 1.26 and 3.78 $\mu\text{g/g}$, respectively.

2.4.6 Drug Release

Calibration Curve for Celecoxib in PBS-polysorbate 80 Solution. The calibration curve for UV-vis was obtained from the CXB standard solutions of 1, 5, 10, 15, 20, and 25 $\mu\text{g/mL}$ in 0.1 M PBS solution containing 2% w/w of polysorbate 80. Absorbance at 260 nm for each sample was determined using UV-visible spectroscopy with the instrument method described above ($\epsilon = 14454 \text{ M}^{-1}\text{cm}^{-1}$). The calibration curve for RP-HPLC was obtained from CXB standard solutions of 5, 10, 25, 75, and 100 $\mu\text{g/mL}$ in the same PBS-polysorbate 80 solution mentioned above. CXB levels in the samples were obtained by diluting 10 μL of each sample 10 times with mobile phase and then through a 0.2 μm Supor membrane filter. The samples were injected at 100 μL using the instrument method described above.

Calibration Curve for Celecoxib in CH₂Cl₂. The calibration curve was obtained from the CXB standard solutions of 1, 5, 7.5, 10, 15, 20 µg /mL in CH₂Cl₂. Absorbance at 260 nm for each sample was determined using UV-visible spectroscopy with the instrument method described above ($\epsilon = 18497 \text{ M}^{-1}\text{cm}^{-1}$).

Preparation of CXB-loaded hydrogels and quantification of loaded drug. The hydrogels were prepared as described above, with the addition of 10% w/w (Table A1) of CXB relative to polymer to the DMF solution containing **4-arm-PEG-azide** and either **G1 SID**, **G2 SID**, or **TEG-alkyne** and then the solution was vortexed for 30 seconds. Following hydrogel synthesis, non-loaded drug, copper, and other impurities were removed by incubation in EDTA solution, followed by water as described above. To quantify the loading of CXB, the hydrated gels (n = 3) were accurately weighed and then immersed in CH₂Cl₂. The samples were incubated overnight at room temperature in a sealed vial to release the loaded CXB. CXB levels in the CH₂Cl₂ solutions were then determined using UV-visible spectroscopy and comparison to the calibration curve determined as described above. The samples of hydrogel swollen in CH₂Cl₂ were then dried and weighed to determine the mass of polymer. The CXB loading and loading efficiency were determined by equations (3) and (4) respectively:

$$\text{CXB loading} = \frac{\text{Mass of CXB calcd from UV-vis}}{M_d \text{ of gel containing CXB}} \times 100\% \quad (3)$$

$$\text{Loading efficiency} = \frac{\text{Mass of CXB calcd from UV-vis}}{4.5 \text{ mg}} \times 100\% \quad (4)$$

Release of Free CXB. A 12.6 x 8.0 x 0.80 cm nylon bag (Supreme Rosin) (n = 3) was cut to form a ~ 5 cm pocket square that was then loaded with 4.5 mg of CXB and sealed with a 2.7 inch bag clip. The drug-loaded bag was immersed in 8 mL of 0.1 M PBS solution containing 2% w/w of polysorbate 80. A 0.5 mL aliquot of each sample was diluted 5 times with fresh PBS-polysorbate solution and the CXB content was determined using UV-visible spectroscopy by measuring the absorbance at 260 nm using the instrument method described above. Following each reading, the drug-loaded bag was immersed in fresh PBS-polysorbate solution and incubated overnight at 37 °C.

CXB Release from the Non-irradiated TEG-alkyne and G2 SID Hydrogel Systems. The experiments were performed in triplicate. CXB-loaded hydrogels were prepared as described above. The **TEG-alkyne** (46.7 ± 1.6 mg) and **G2 SID** hydrogels (53.8 ± 1.8 mg) were immersed in 4.8 and 5.0 mL of 0.1 M PBS solution containing 2% w/w of polysorbate 80, respectively to maintain a constant amount of hydrogel-encapsulated CXB (same as that used to measure the solubilization rate of free CXB) in the release medium. At defined time points, a 0.2 mL aliquot of each sample was diluted 11 times with fresh PBS-polysorbate solution and the CXB content was determined using UV-visible spectroscopy by measuring the absorbance at 260 nm using the instrument method described above. Following each time point, the gels were immersed in fresh PBS-polysorbate solution and incubated overnight at 37 °C.

CXB Release from the Irradiated G2 SID Hydrogel System. The experiments were performed in triplicate. CXB-loaded hydrogels were prepared as described above. 55.0 ± 1.5 mg of hydrogel was immersed in 5.0 mL of 0.1 M PBS solution containing 2% w/w of polysorbate 80, exposed to 1 h of UV irradiation (wavelength: 365-370 nm, intensity: 10 mW cm⁻²), and then incubated at 37 °C for 1 h. CXB content in the PBS-polysorbate mixture was determined using RP-HPLC where 100 µl of the solution was diluted 10 times using the mobile phase and then filtered through a 0.2 µm Supor membrane filter. The samples were injected (100 µL) using the instrument method described above. After each time point, the hydrogels were immersed in fresh PBS-polysorbate solution, exposed to 1 h of UV irradiation (wavelength: 365-370 nm, intensity: 10 mW cm⁻²), and then incubated at 37 °C. The experiment was performed in triplicate.

Statistical Analyses. Data are reported as the mean \pm standard deviation (SD), and the statistical analyses were conducted using GraphPad Prism 6 (GraphPad Software, San Diego, CA, USA) by one-way and two-way ANOVA with a Tukey's post-hoc test. Differences were considered statistically significant at $p < 0.05$.

2.5 References

1. Spicer, C. D., Hydrogel scaffolds for tissue engineering: the importance of polymer choice. *Polym. Chem.* **2020**, *11*, 184-219.
2. Ahmed, E. M., Hydrogel: Preparation, characterization, and applications: A review. *J. Adv. Res.* **2015**, *6*, 105-121.
3. Liang, N.; Flynn, L. E.; Gillies, E. R., Neutral, water-soluble poly(ester amide) hydrogels for cell encapsulation. *Eur. Polym. J.* **2020**, *136*, 109899-109908.
4. Catoira, M. C.; Fusaro, L.; Di Francesco, D.; Ramella, M.; Boccafoschi, F., Overview of natural hydrogels for regenerative medicine applications. *J. Mater. Sci. Mater. Med.* **2019**, *30*, 115-125.
5. Chai, Q.; Jiao, Y.; Yu, X., Hydrogels for biomedical applications: their characteristics and the mechanisms behind them. *Gels* **2017**, *3*, 6-21.
6. Tan, H.; Marra, K. G., Injectable, biodegradable hydrogels for tissue engineering applications. *Materials* **2010**, *3*, 1746-1767.
7. Geckil, H.; Xu, F.; Zhang, X.; Moon, S.; Demirci, U., Engineering hydrogels as extracellular matrix mimics. *Nanomed. J.* **2010**, *5*, 469-484.
8. Kundu, J.; Pati, F.; Hun Jeong, Y.; Cho, D.-W., Chapter 2 - Biomaterials for biofabrication of 3D tissue scaffolds. *Biofabrication*, Andrew Publishing: Boston, **2013**, 23-46.
9. Echeverria, C.; Fernandes, S. N.; Godinho, M. H.; Borges, J. P.; Soares, P. I. P., Functional stimuli-responsive gels: hydrogels and microgels. *Gels* **2018**, *4*, 54-91.
10. Sood, N.; Bhardwaj, A.; Mehta, S.; Mehta, A., Stimuli-responsive hydrogels in drug delivery and tissue engineering. *Drug Deliv.* **2016**, *23*, 748-770.
11. Mohamed, M. A.; Fallahi, A.; El-Sokkary, A. M. A.; Salehi, S.; Akl, M. A.; Jafari, A.; Tamayol, A.; Fenniri, H.; Khademhosseini, A.; Andreadis, S. T.;

- Cheng, C., Stimuli-responsive hydrogels for manipulation of cell microenvironment: from chemistry to biofabrication technology. *Prog. Polym. Sci.* **2019**, *98*, 101147-101183.
12. Klouda, L.; Mikos, A. G., Thermoresponsive hydrogels in biomedical applications. *Eur. J. Pharm. Biopharm.* **2008**, *68*, 34-45.
 13. Kloxin, A. M.; Kasko, A. M.; Salinas, C. N.; Anseth, K. S., Photodegradable hydrogels for dynamic tuning of physical and chemical properties. *Science* **2009**, *324*, 59-63.
 14. Tiwari, G.; Tiwari, R.; Sriwastawa, B.; Bhati, L.; Pandey, S.; Pandey, P.; Bannerjee, S. K., Drug delivery systems: an updated review. *Int. J. Pharm. Investig.* **2012**, *2*, 2-11.
 15. Ghobril, C.; Rodriguez, E. K.; Nazarian, A.; Grinstaff, M. W., Recent advances in dendritic macromonomers for hydrogel formation and their medical applications. *Biomacromolecules* **2016**, *17*, 1235-1252.
 16. Amir, R. J.; Pessah, N.; Shamis, M.; Shabat, D., Self-immolative dendrimers. *Angew. Chem. Int. Ed.* **2003**, *42*, 4494-4499.
 17. Roth, M. E.; Green, O.; Gnaim, S.; Shabat, D., Dendritic, oligomeric, and polymeric self-immolative molecular amplification. *Chem. Rev.* **2016**, *116*, 1309-1352.
 18. Yoshii, T.; Onogi, S.; Shigemitsu, H.; Hamachi, I., Chemically reactive supramolecular hydrogel coupled with a signal amplification system for enhanced analyte sensitivity. *J. Am. Chem. Soc.* **2015**, *137*, 3360-3365.
 19. Sagi, A.; Segal, E.; Satchi-Fainaro, R.; Shabat, D., Remarkable drug-release enhancement with an elimination-based AB₃ self-immolative dendritic amplifier. *Bioorg. Med. Chem.* **2007**, *15*, 3720-3727.

20. Sun, W.; Bandmann, H.; Schrader, T., A fluorescent polymeric heparin sensor. *Chem. Eur. J.* **2007**, *13*, 7701-7707.
21. Barra, T.; Arrue, L.; Urzúa, E.; Ratjen, L., Synthesis of photocaged diamines and their application in photoinduced self-assembly. *J. Phys. Org. Chem.* **2019**, *32*, 3935-3943.
22. Fomina, N.; McFearin, C. L.; Almutairi, A., Increasing materials' response to two-photon NIR light via self-immolative dendritic scaffolds. *Chem. Comm.* **2012**, *48*, 9138-9140.
23. Perry, R.; Amir, R. J.; Shabat, D., Substituent-dependent disassembly of self-immolative dendrimers. *New J. Chem.* **2007**, *31*, 1307-1312.
24. Reyes-Reveles, J.; Sedaghat-Herati, R.; Gilley, D. R.; Schaeffer, A. M.; Ghosh, K. C.; Greene, T. D.; Gann, H. E.; Dowler, W. A.; Kramer, S.; Dean, J. M.; Delong, R. K., mPEG-PAMAM-G4 Nucleic acid nanocomplexes: enhanced stability, RNase protection, and activity of splice switching oligomer and poly I:C RNA. *Biomacromolecules* **2013**, *14*, 4108-4115.
25. Gopin, A.; Ebner, S.; Attali, B.; Shabat, D., Enzymatic activation of second-generation dendritic prodrugs: conjugation of self-immolative dendrimers with poly(ethylene glycol) via click chemistry. *Bioconjug. Chem.* **2006**, *17*, 1432-1440.
26. Opsteen, J. A.; van Hest, J. C. M., Modular synthesis of block copolymers via cycloaddition of terminal azide and alkyne functionalized polymers. *Chem. Comm.* **2005**, 57-59.
27. Castro, V.; Rodríguez, H.; Albericio, F., CuAAC: an efficient click chemistry reaction on solid phase. *ACS Comb. Sci.* **2016**, *18*, 1-14.
28. Katime, I.; Mendizábal, E., Swelling properties of new hydrogels based on the dimethyl amino ethyl acrylate methyl chloride quaternary salt with acrylic acid and 2-methylene butane-1,4-dioic acid monomers in aqueous solutions. *MSA* **2010**, *1*, 162-167.

29. Institute of Medicine, Food, and Nutrition Board. Dietary reference intakes for vitamin A, vitamin K, arsenic, boron, chromium, copper, iodine, iron, manganese, molybdenum, nickel, silicon, vanadium, and zinc. Washington, DC: National Academies Press; **2001**.
30. Institute of Medicine. Food and Nutrition Board. Dietary reference intakes for thiamin, riboflavin, niacin, vitamin B(6), folate, vitamin B(12), pantothenic acid, biotin, and choline. Washington, DC: National Academies Press; **1998**.
31. Ross, A.C.; Caballero, B.; Cousins, R.J.; Tucker, K.L.; Ziegler, T.R. Modern Nutrition in Health and Disease. Baltimore, MD: Lippincott Williams & Wilkins **2014**, *11*, 206-216.

Chapter 3

3 Conclusions and Future Work

Overall, this thesis presented the synthesis of novel UV-responsive SIDs functionalized with alkyne moieties at the termini for hydrogel synthesis and investigated their application as drug delivery systems.

Chapter 2 presented two new photolabile SIDs, **G1 SID** and **G2 SID**, that were constructed with a *o*-nitrobenzyl core, *N,N'*-dimethylethylenediamine spacers extending from a *p*-cresol moiety, and alkyne peripheries. A non-photosensitive **TEG-alkyne** species was developed as a control. Moreover, a **4-arm-PEG-azide** was synthesized with an M_n and D of approximately 2814 kg/mol and 1.05, respectively. The double bonds on the peripheries of the SIDs and bisalkyne were photochemically crosslinked with **4-arm-PEG-azide** by a CuAAC reaction. Hydrogel properties, such as gel content, EWC, and durability were tuned by manipulating gel synthesis techniques and formulations. However, hydrogels containing 15 and 25% (w/v) of **4-arm-PEG-azide** demonstrated greater structural integrity than scaffolds comprised of 10% (w/v) of polymer. As a result, hydrogels containing 15% (w/v) of **4-arm-PEG-azide** were selected for compression testing while only **G2 SID** and **TEG-alkyne** scaffolds were used in drug release studies. Compression results demonstrated that UV-light exposure afforded a statistically significant decrease in compression modulus for only the **G1 SID** hydrogel. The durability of the **G2 SID** scaffold is attributed to the slow degradation of the gel and SID backbone. Similarly, drug release studies of the irradiated **G2 SID** hydrogel did not demonstrate an accelerated release of CXB from the scaffold, potentially due to the slow fragmentation of the network. However, these SID-based hydrogels are a promising proof-of-concept for the development of other dendritic-based hydrogels as biomaterials for drug delivery.

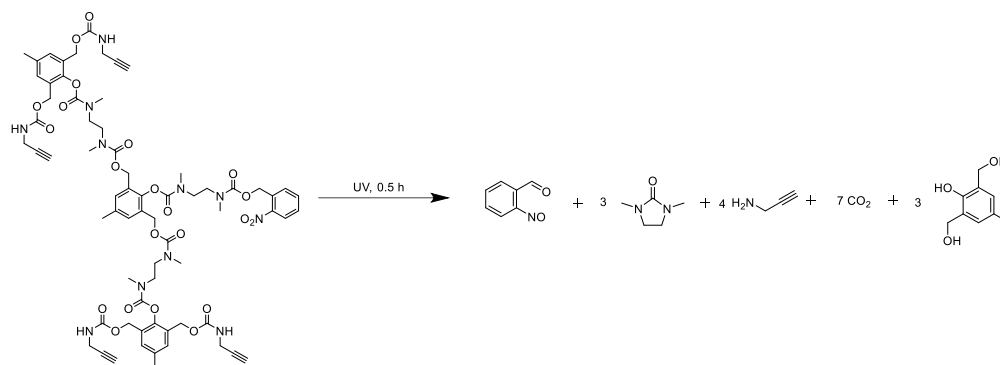
Possible future work includes developing a hydrogel with a shorter synthesis route or a faster network disassembly in response to an external stimulus. Ethyl glyoxylate is a commercially available monomer and can be used to synthesize poly(ethyl glyoxylate) in one-step.¹ Poly(glyoxylates) can be end-capped with UV-responsive groups, such as 6-nitroveratryl carbonate, to provide rapid depolymerization in response to irradiation.¹ By

introducing poly(glyoxylate) moieties into **SIDs** synthesized in this work, perhaps quicker fragmentation upon exposure to UV-light would result in faster drug release. Alternatively, star polymers containing a stimuli-responsive core may provide a more facile synthetic pathway to producing a densely crosslinked hydrogel with improved mechanical properties. Perhaps compound **12**, an intermediate in the **G2 SID** synthesis, could be crosslinked to thiol moieties extending from a central core, resulting in a pH-sensitive star-like scaffold that could potentially demonstrate faster degradation. Finally, drugs more hydrophobic than **CXB** may be used for drug release studies of the **G2 SID** gel to ensure stronger binding to the hydrophobic domains of the scaffold and avoid premature drug leakage. Alternatively, the **G2 SID** could be synthesized to include more hydrophobic moieties along the interior branches to also ensure drug retention.

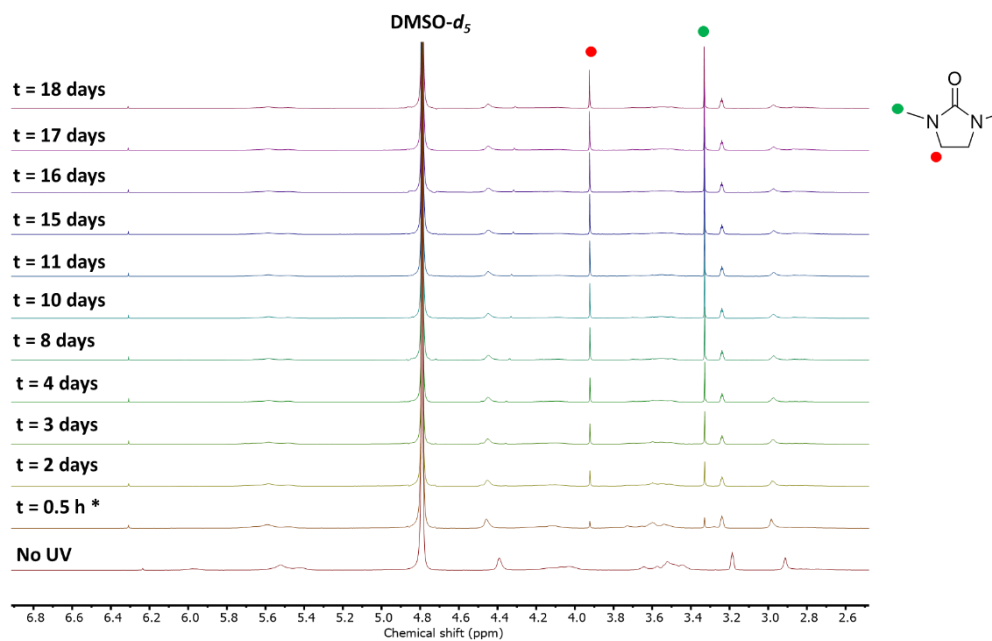
3.1 References

1. Fan, B.; Trant, J. F.; Wong, A. D.; Gillies, E. R., Polyglyoxylates: a versatile class of triggerable self-immolative polymers from readily accessible monomers. *J. Am. Chem. Soc.* **2014**, *136*, 10116-10123.

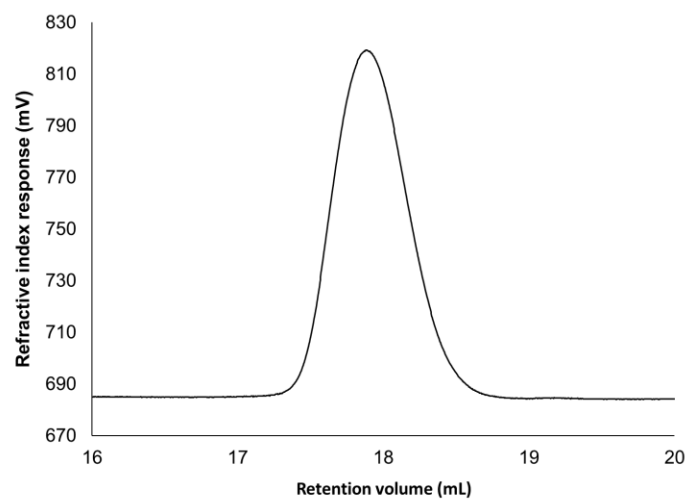
Appendix: Supplementary Figures



A1. Degradation products of irradiated G2 SID.



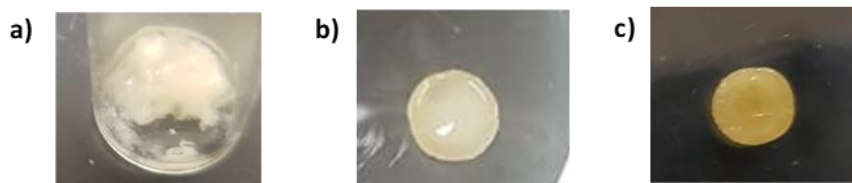
A 2. ¹H NMR degradation profile of the **G2 SID** in deuterated PBS:DMSO-*d*₆ (1:3.5) (D₂O, 400 MHz). *denotes an irradiation exposure of 0.5 h. Red and green markers correspond to methylene and methyl protons, respectively, in the *N,N'*-dimethylimidazolidinone degradation product.



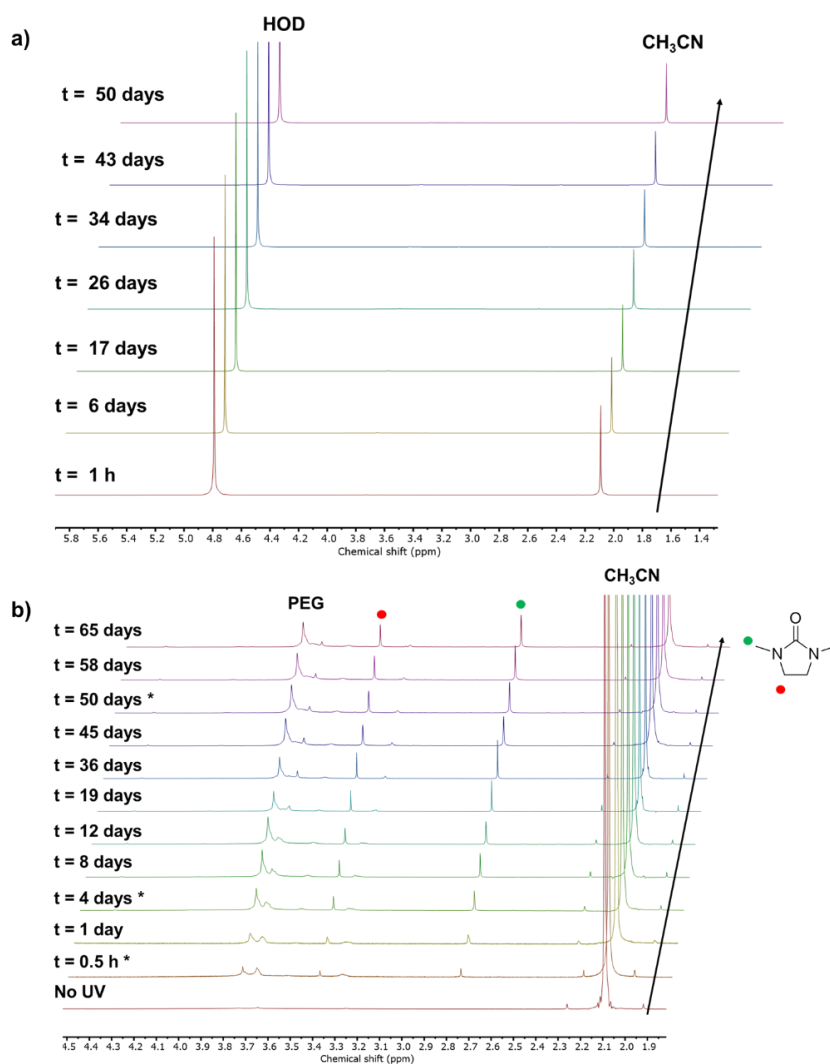
A3. SEC trace of 4-arm-PEG-azide.

Table A1. Formulations of the **TEG-alkyne**, **G1 SID**, and **G2 SID** hydrogels in a DMF:H₂O (240:60 μ L) solution.

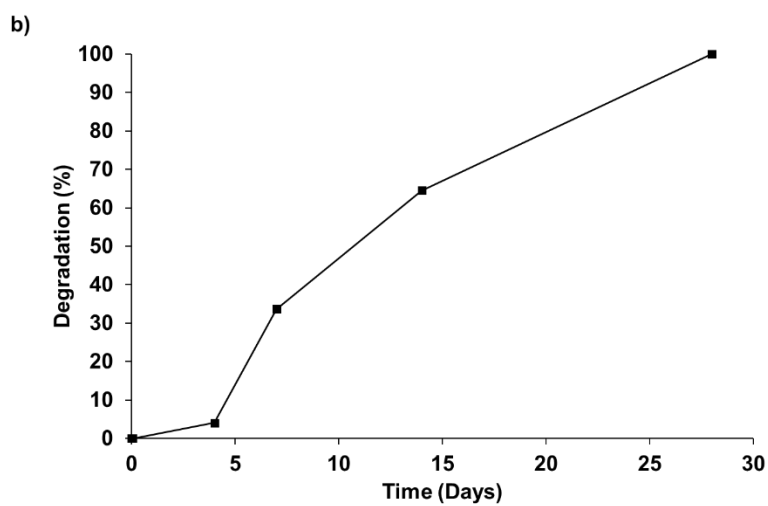
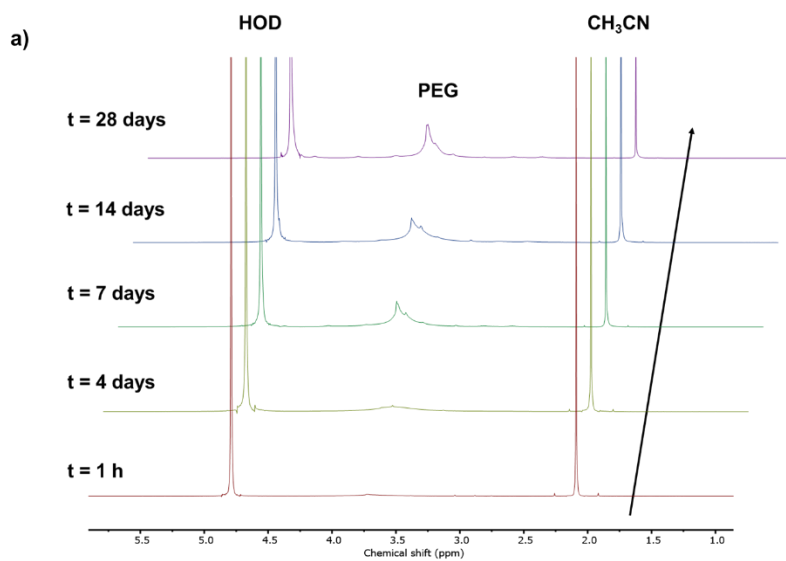
TEG-alkyne Gels					
	4-arm-PEG-azide	TEG	CuSO₄	Na ascorbate	CXB
MM (g/mol)	2614	386	160	198	381
mass (mg)					
10 (% w/v)	30	8.9	1.8	2.3	
15 (% w/v)	45	13	2.8	3.4	4.5
25 (% w/v)	75	22	4.6	5.7	
mmol					
10 (% w/v)	0.012	0.023	0.012	0.012	
15 (% w/v)	0.017	0.034	0.017	0.017	0.012
25 (% w/v)	0.029	0.057	0.029	0.029	
equivalents	1	2	1	1	0.7
G1 SID Gels					
	4-arm-PEG-azide	G1 SID	CuSO₄	Na ascorbate	CXB
MM (g/mol)	2614	624	160	198	381
mass (mg)					
10 (% w/v)	30	14	1.8	2.3	
15 (% w/v)	45	22	2.8	3.4	4.5
25 (% w/v)	75	36	4.6	5.7	
mmol					
10 (% w/v)	0.012	0.023	0.012	0.012	
15 (% w/v)	0.017	0.034	0.017	0.017	0.012
25 (% w/v)	0.029	0.057	0.029	0.029	
equivalents	1	2	1	1	0.7
G2 SID Gels					
	4-arm-PEG-azide	G2 SID	CuSO₄	Na ascorbate	CXB
MM (g/mol)	2614	1402	160	198	381
mass (mg)					
10 (% w/v)	30	16	1.8	2.3	
15 (% w/v)	45	24	2.8	3.4	4.5
25 (% w/v)	75	40	4.6	5.7	
mmol					
10 (% w/v)	0.012	0.012	0.012	0.012	
15 (% w/v)	0.017	0.017	0.017	0.017	0.012
25 (% w/v)	0.029	0.029	0.029	0.029	
equivalents	1	1	1	1	0.7



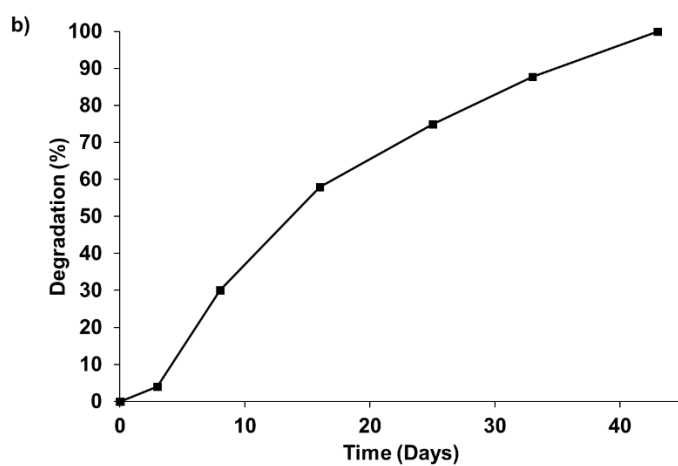
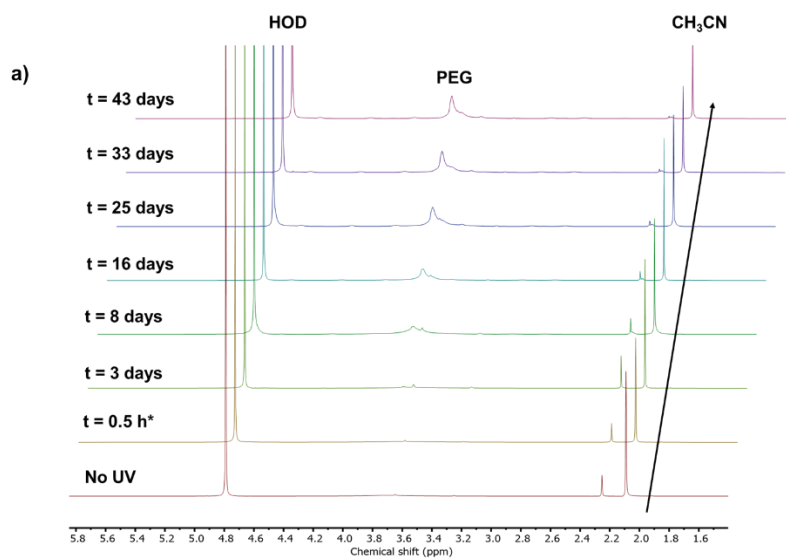
A4. Representative images of **G2 SID** hydrogels containing a) 10, b) 15, c) 25% polymer.



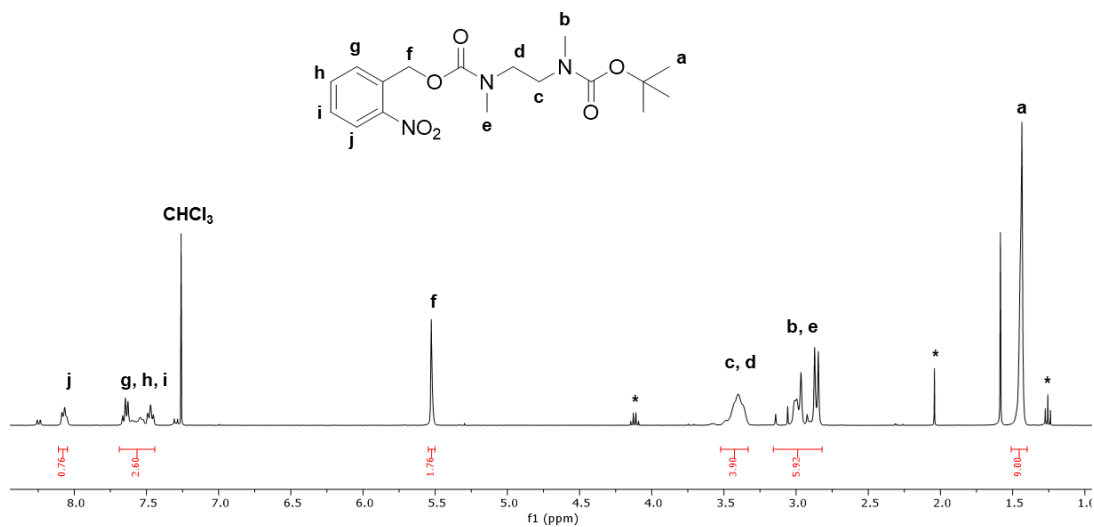
A5. ¹H NMR spectra of (a) non-irradiated, (b) irradiated **G2 SID** hydrogel in deuterated PBS:acetonitrile (100:1) (D₂O, 400 MHz). *denotes an irradiation exposure of 0.5 h followed by 1 h incubation at 37 °C prior to measurement at the subsequent time point.



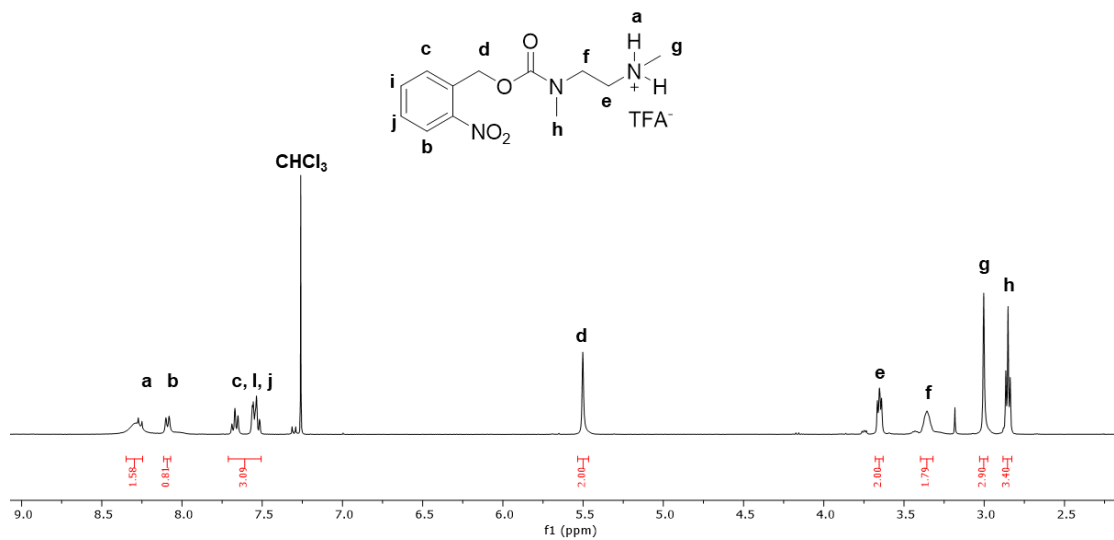
A6. (a) ^1H NMR (D_2O , 400 MHz), (b) degradation profile of non-irradiated **TEG-alkyne** in deuterated PBS: acetonitrile (100:1) incubated at 37 °C.



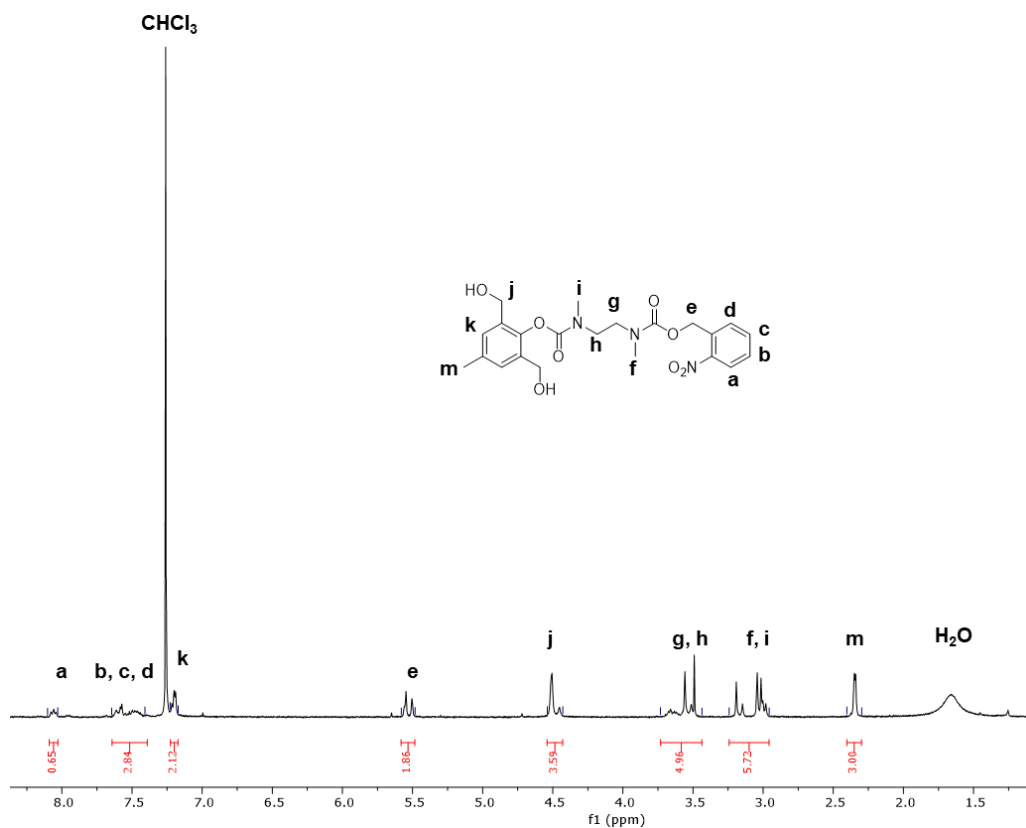
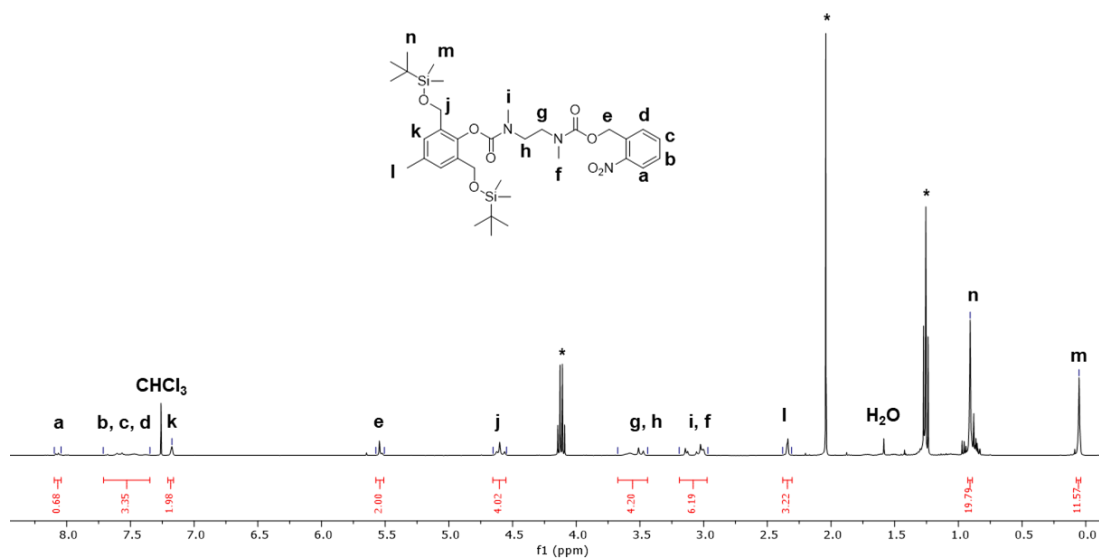
A7. (a) ^1H NMR (D_2O , 400 MHz), (b) degradation profile of UV-light irradiated TEG-alkyne in deuterated PBS: acetonitrile (100:1) incubated at 37°C . *denotes to 0.5 h of UV-light exposure.

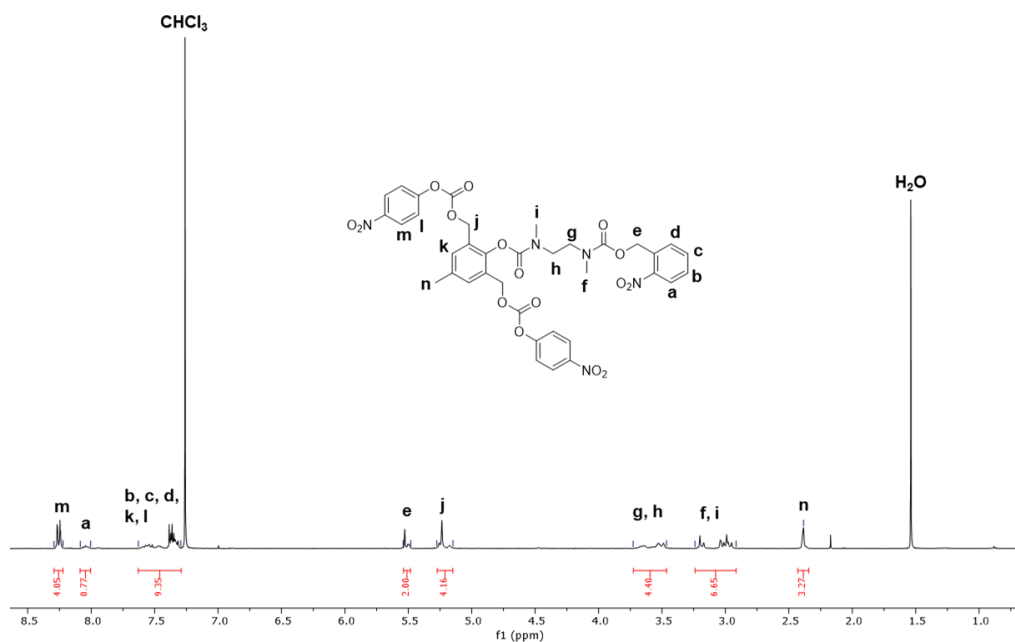


A8. ¹H NMR spectrum of compound **3** (400 MHz, CDCl₃). Asterisks correspond to ethyl acetate. Rotational isomers about the carbamate bond are observed.

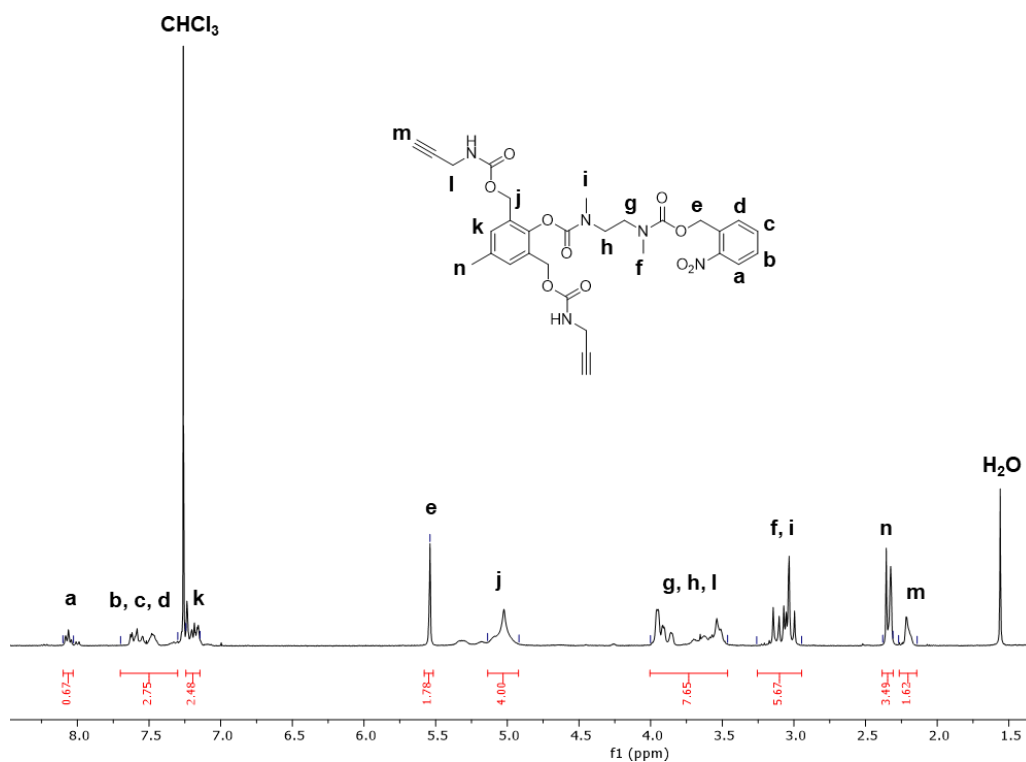


A9. ¹H NMR spectrum of compound **4** (400 MHz, CDCl₃). Rotational isomers about the carbamate bond are observed.

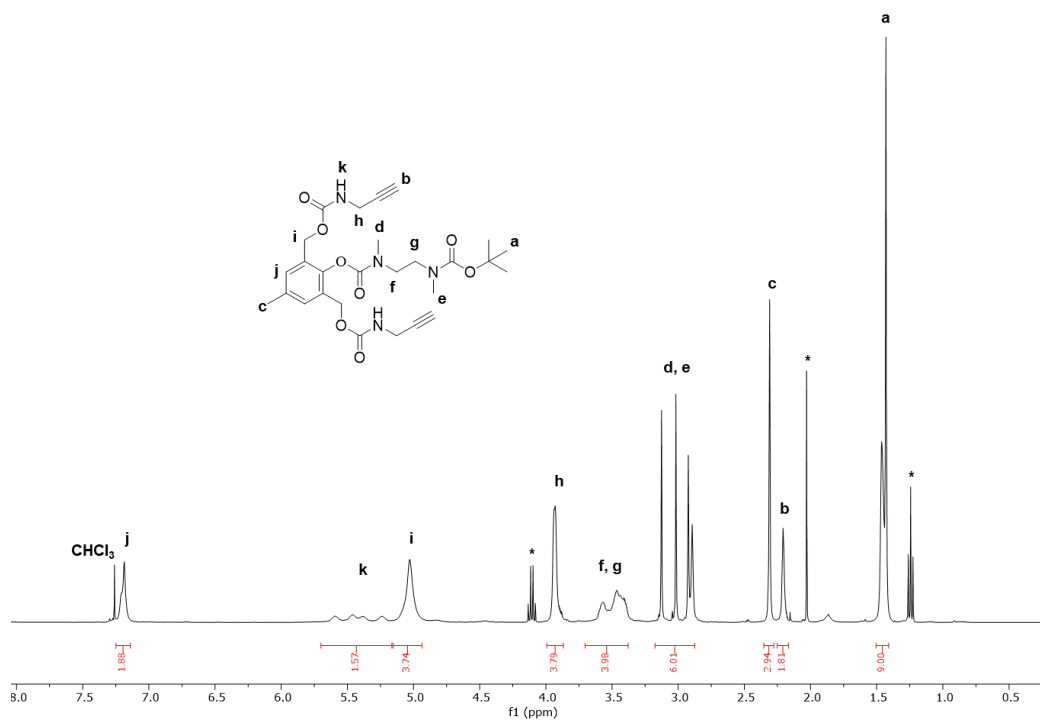




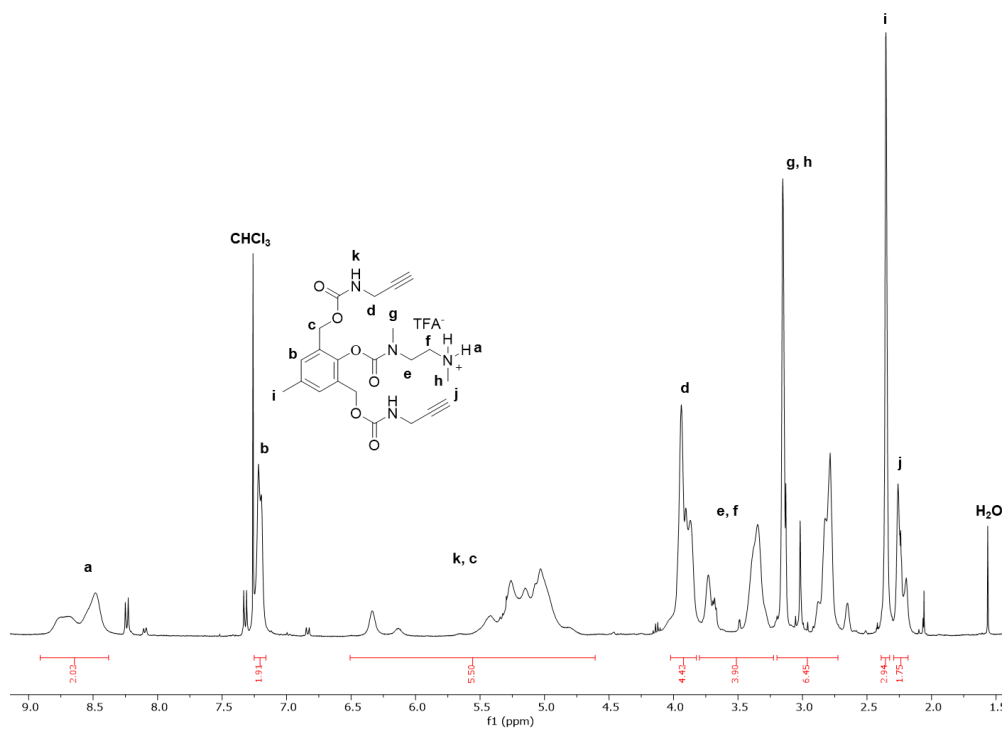
A12. ¹H NMR spectrum of compound **8** (400 MHz, CDCl₃). Rotational isomers about the carbamate bonds are observed.



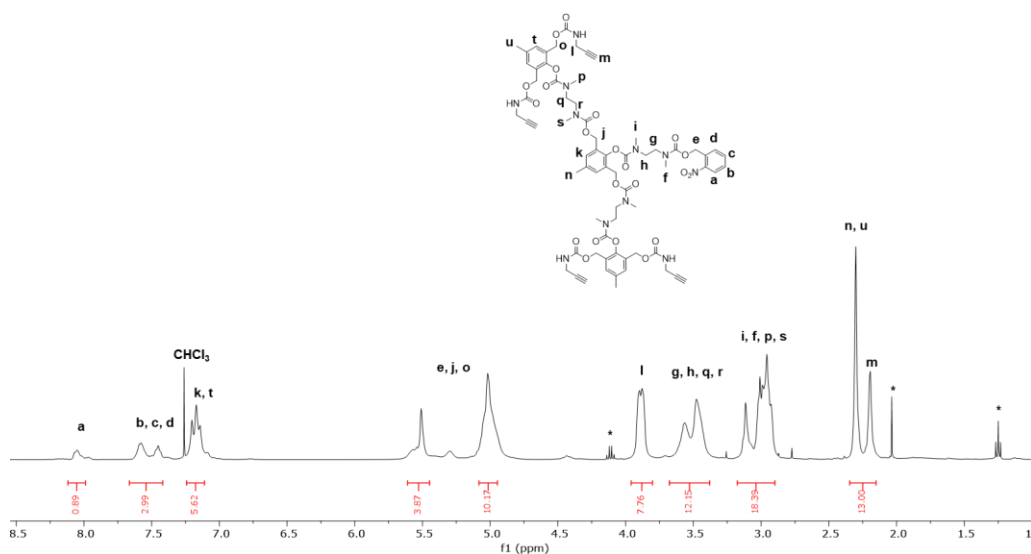
A13. ¹H NMR spectrum of **G1 SID** (400 MHz, CDCl₃). Rotational isomers about the carbamate bonds are observed.



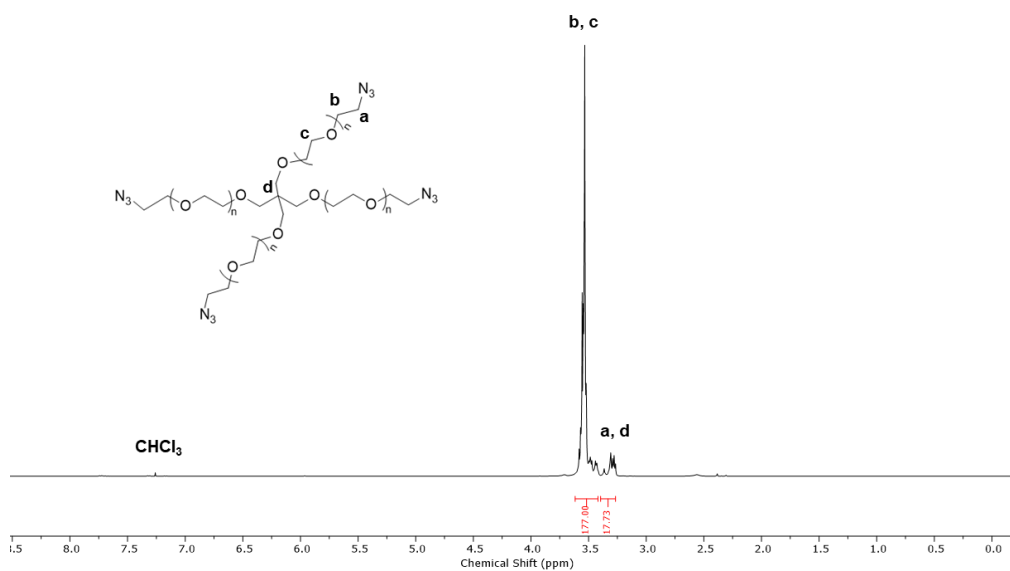
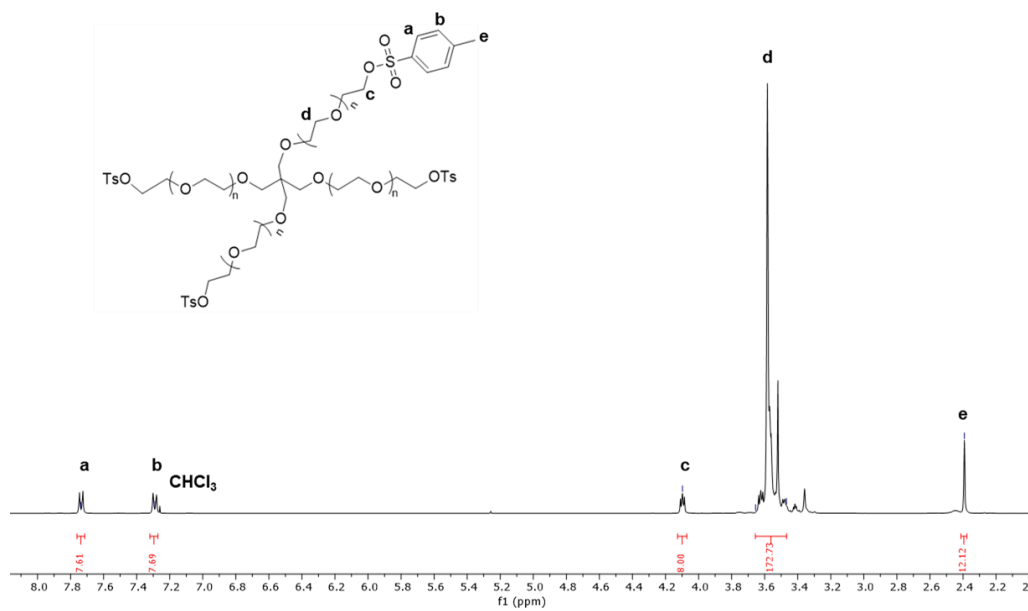
A14. ¹H NMR spectrum of compound **12** (400 MHz, CDCl₃). Asterisks correspond to ethyl acetate. Rotational isomers about the carbamate bonds are observed.

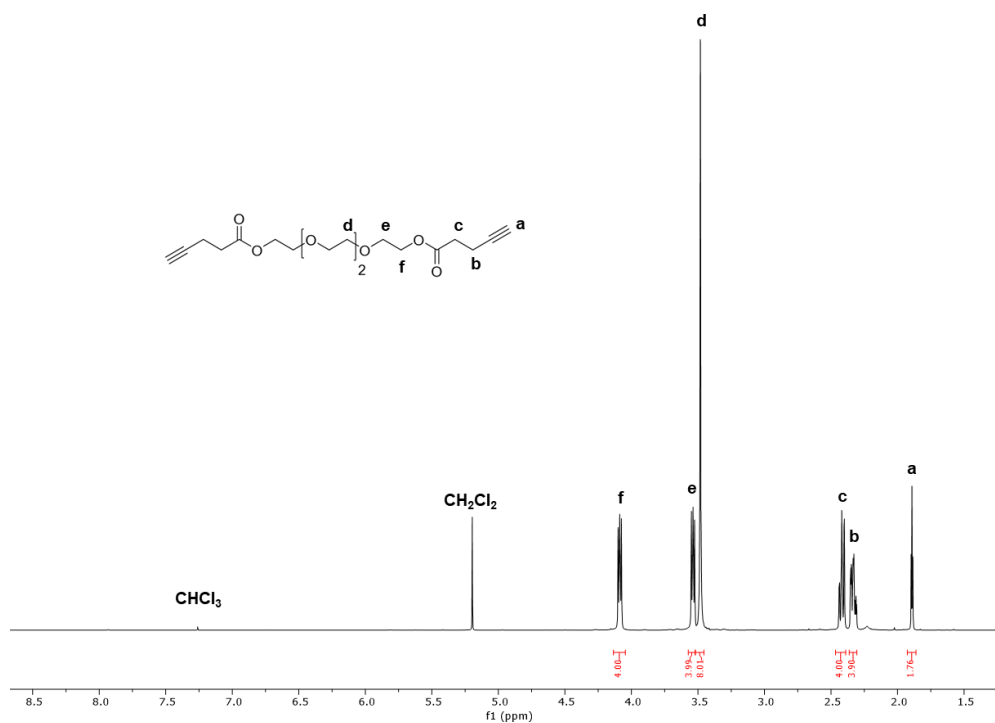


A15. ^1H NMR spectrum of compound **13** (400 MHz, CDCl_3). Rotational isomers about the carbamate bonds are observed.

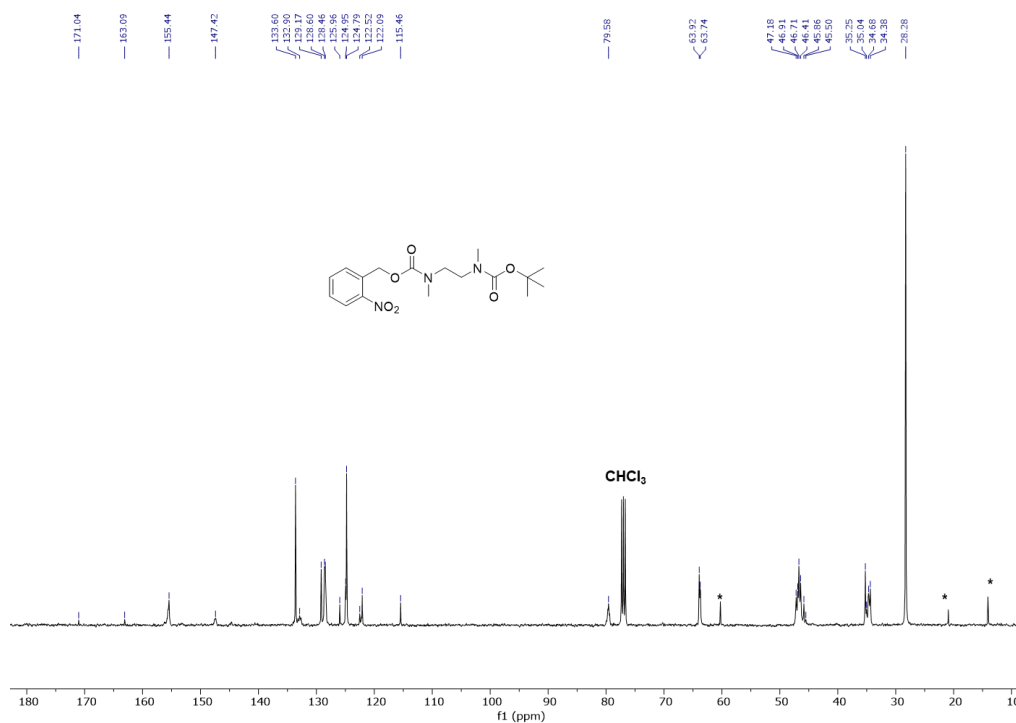


A16. ^1H NMR spectrum of **G2 SID** (400 MHz, CDCl_3). Asterisks correspond to ethyl acetate. Rotational isomers about the carbamate bonds are observed.

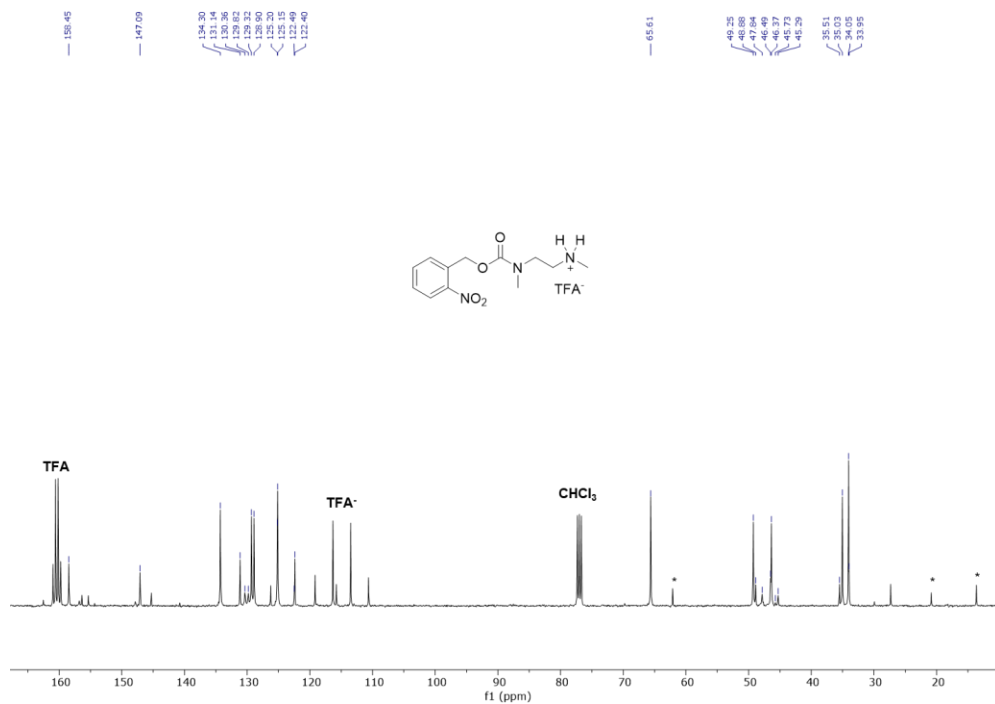




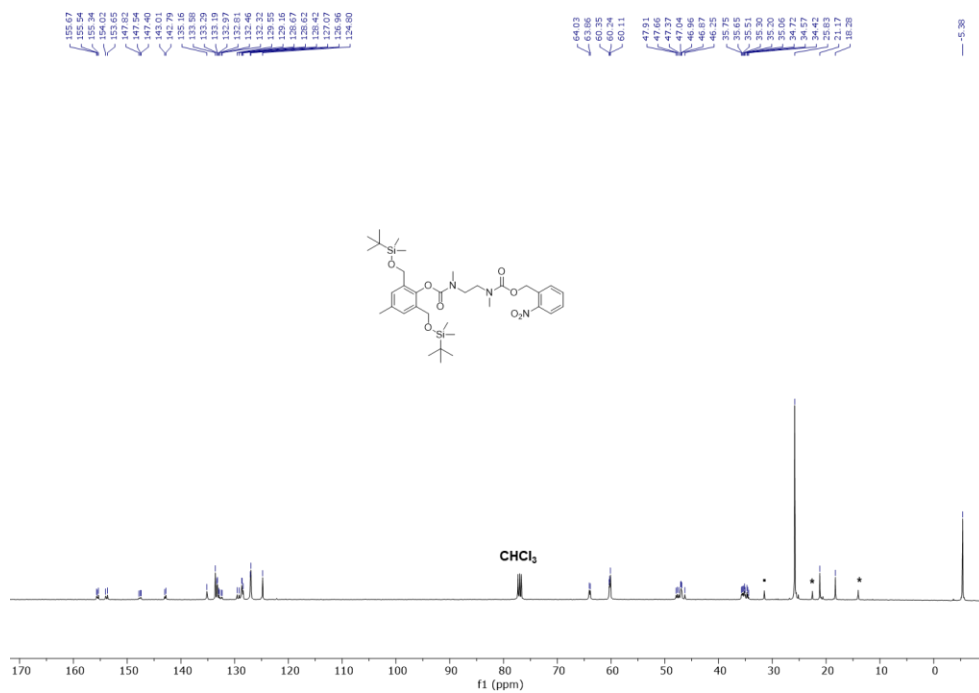
A19. ^1H NMR spectrum of **TEG-alkyne** (400 MHz, CDCl_3).



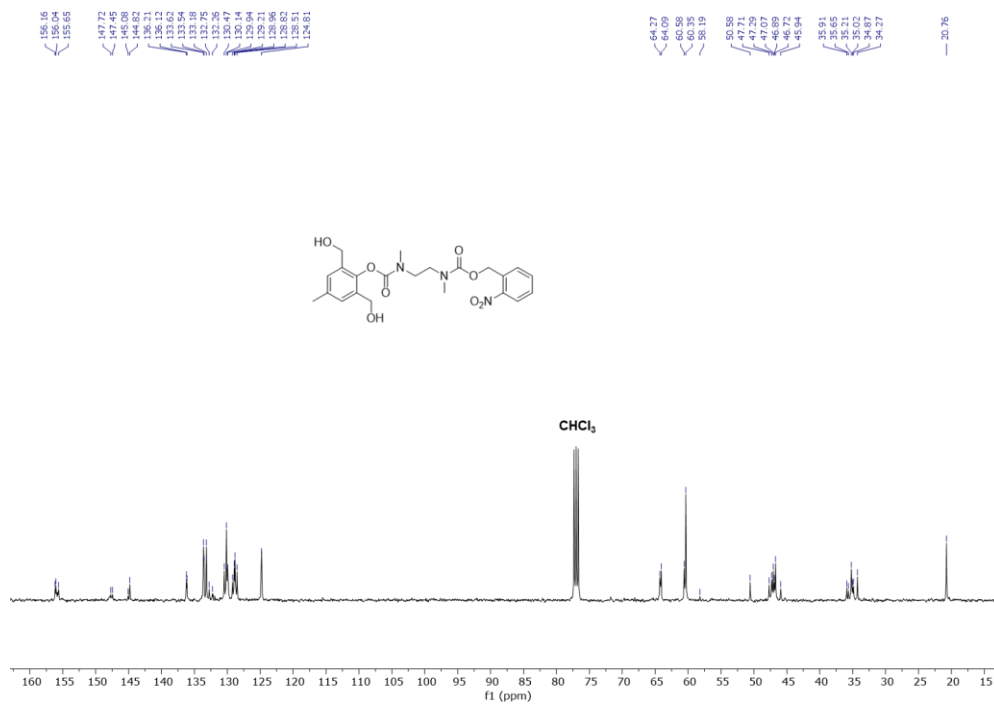
A20. ^{13}C NMR spectrum of compound **3** (100 MHz, CDCl_3). Asterisks correspond to ethyl acetate. Rotational isomers about the carbamate bonds are observed.



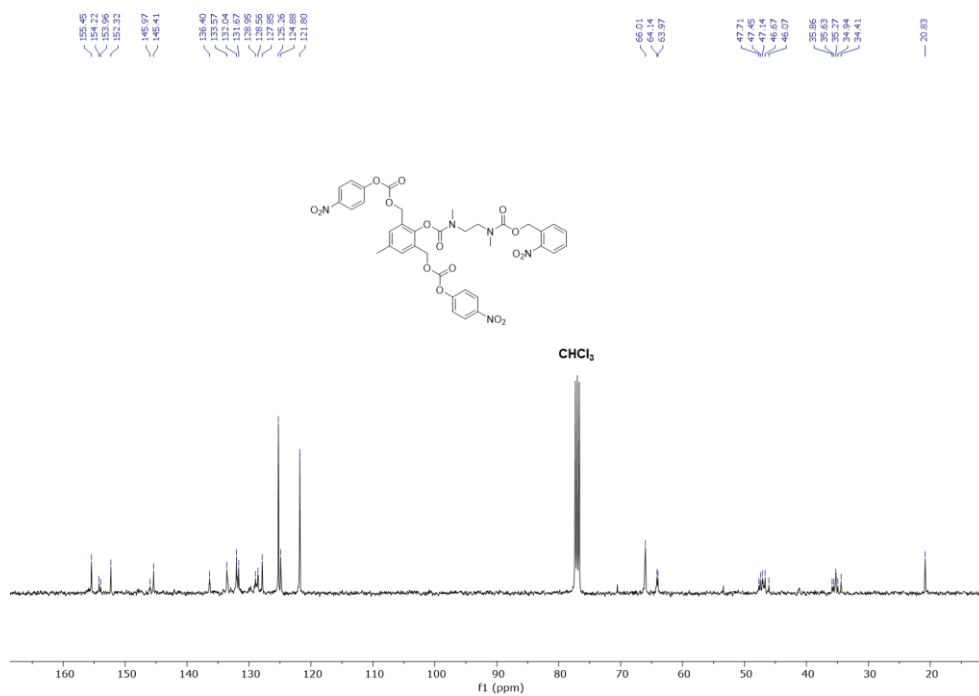
A21. ^{13}C NMR spectrum of compound **4** (100 MHz, CDCl_3). Asterisks correspond to ethyl acetate. Rotational isomers about the carbamate bonds are observed.



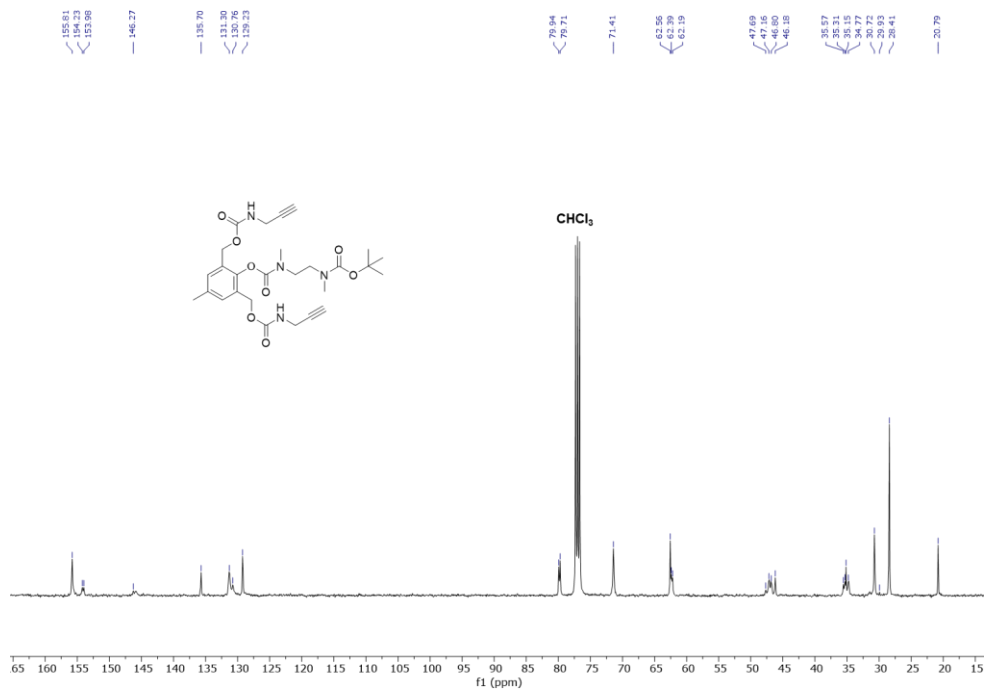
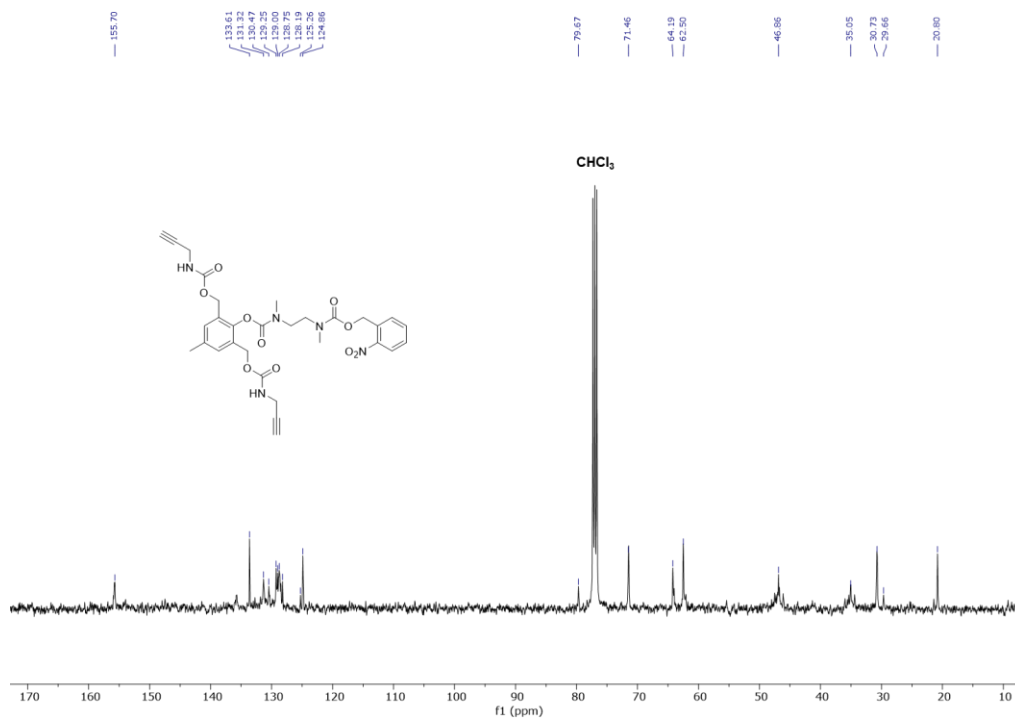
A22. ^{13}C NMR spectrum of compound **6** (100 MHz, CDCl_3). Asterisks correspond to ethyl acetate. Rotational isomers about the carbamate bonds are observed.

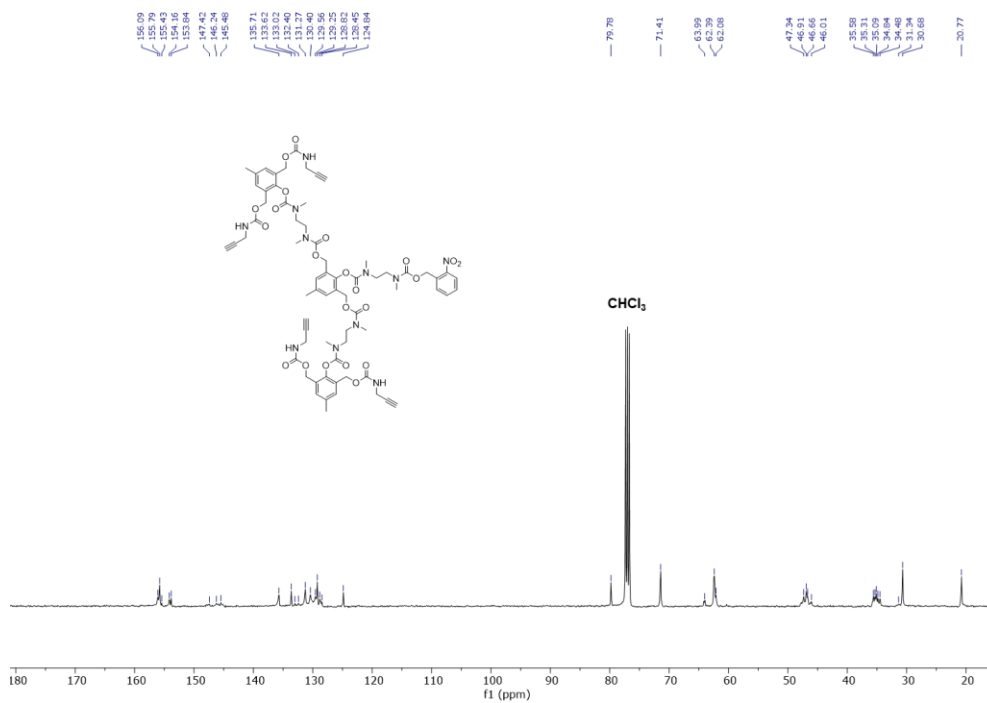
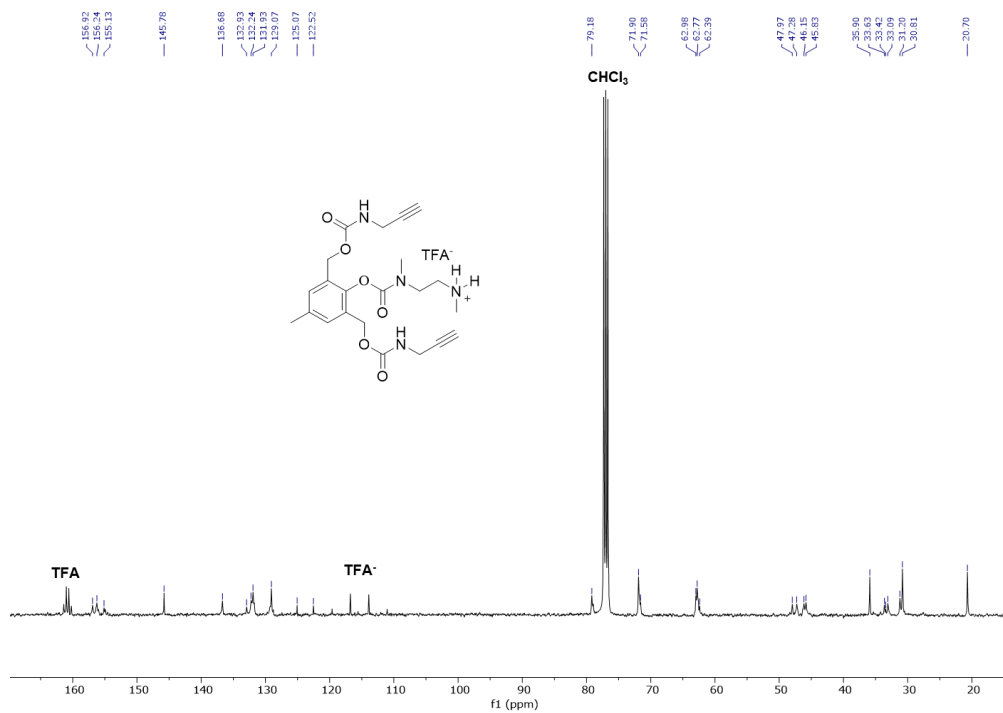


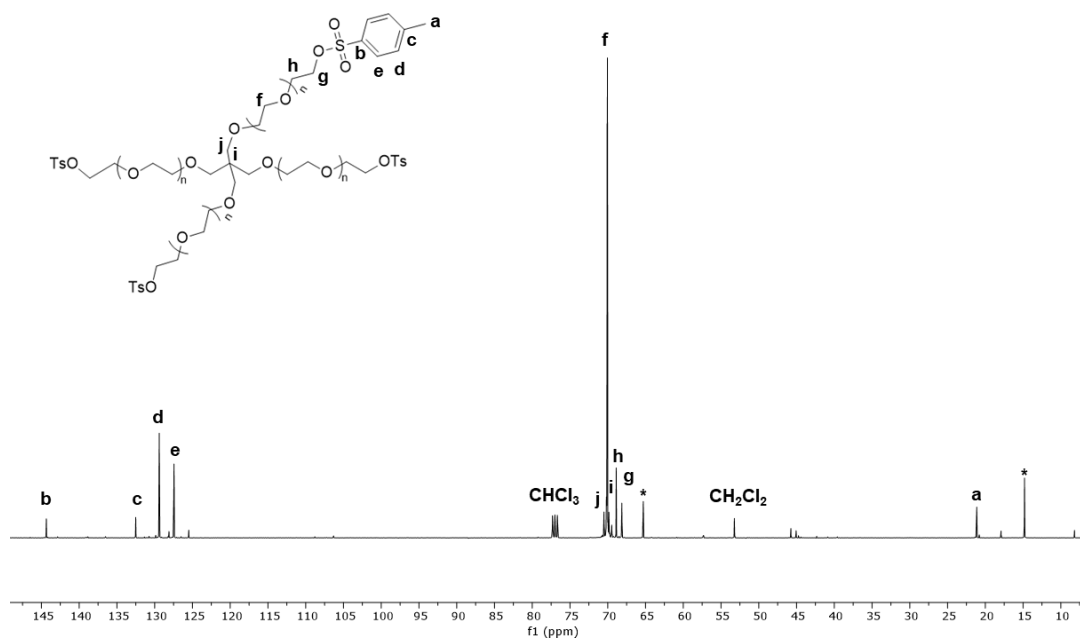
A23. ¹³C NMR spectrum of compound **7** (100 MHz, CDCl₃). Rotational isomers about the carbamate bonds are observed.



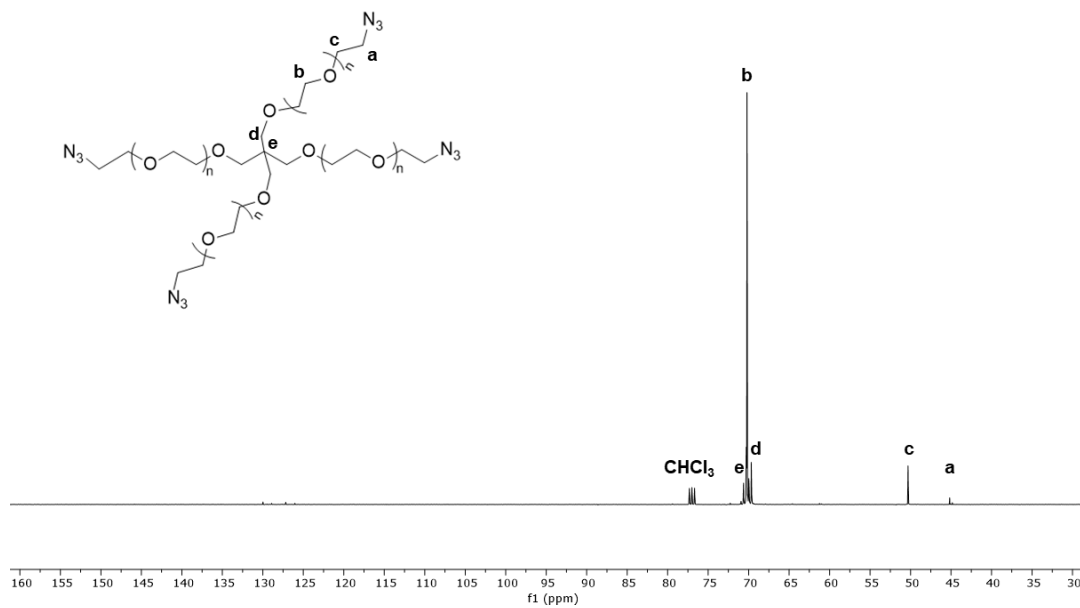
A24. ¹³C NMR spectrum of compound **8** (100 MHz, CDCl₃). Rotational isomers about the carbamate bonds are observed.



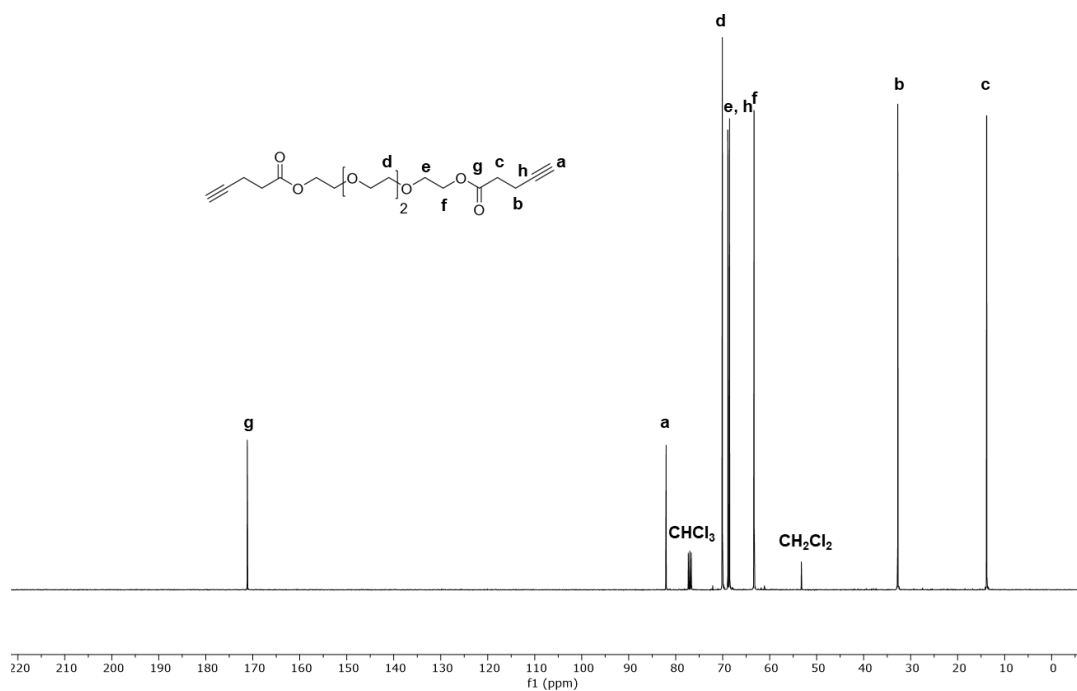




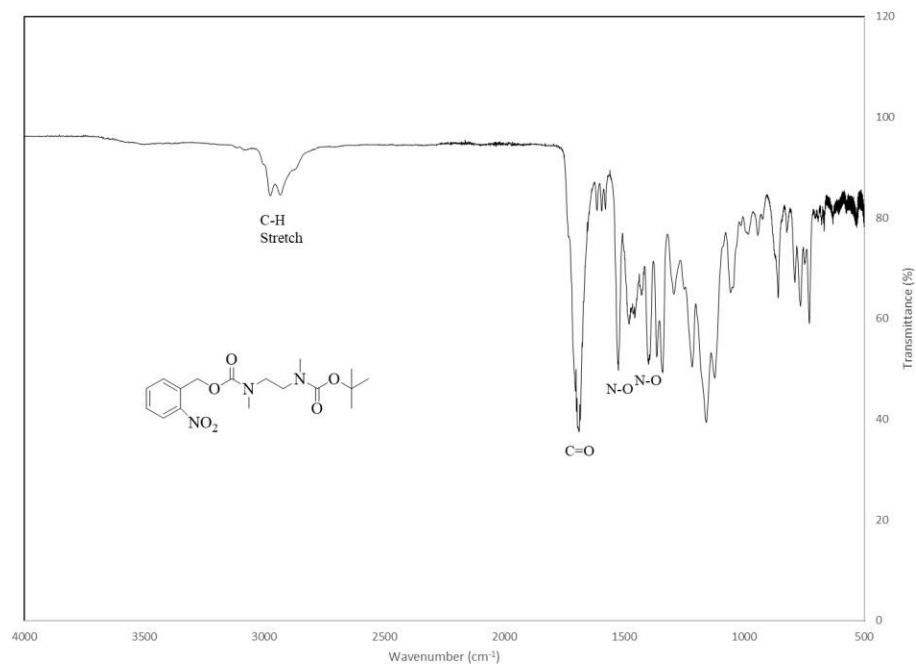
A29. ^{13}C NMR spectrum of compound **14** (100 MHz, CDCl_3). Asterisks correspond to diethyl ether.



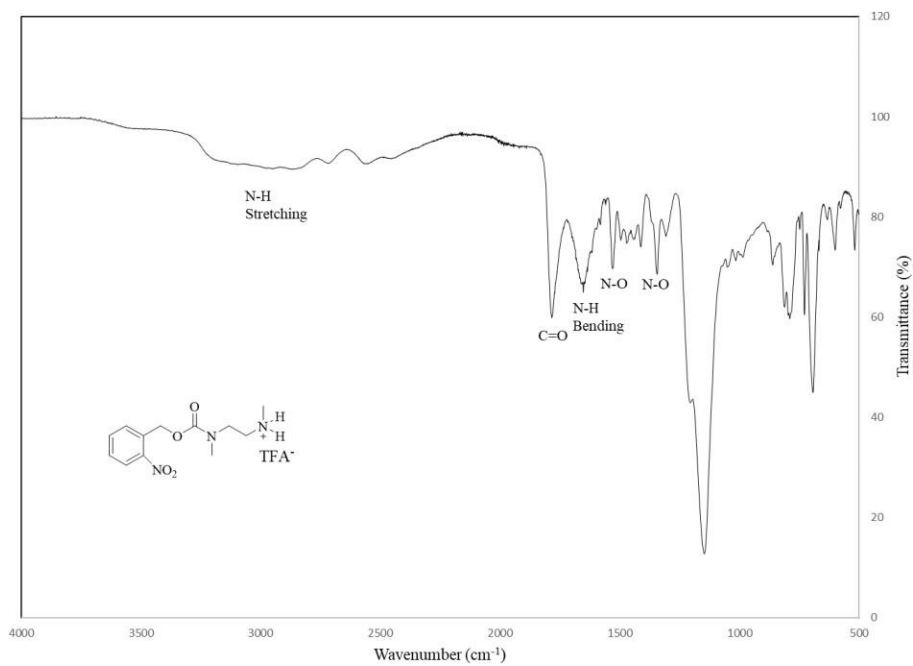
A30. ^{13}C NMR spectrum of 4-arm-PEG-azide (100 MHz, CDCl_3).



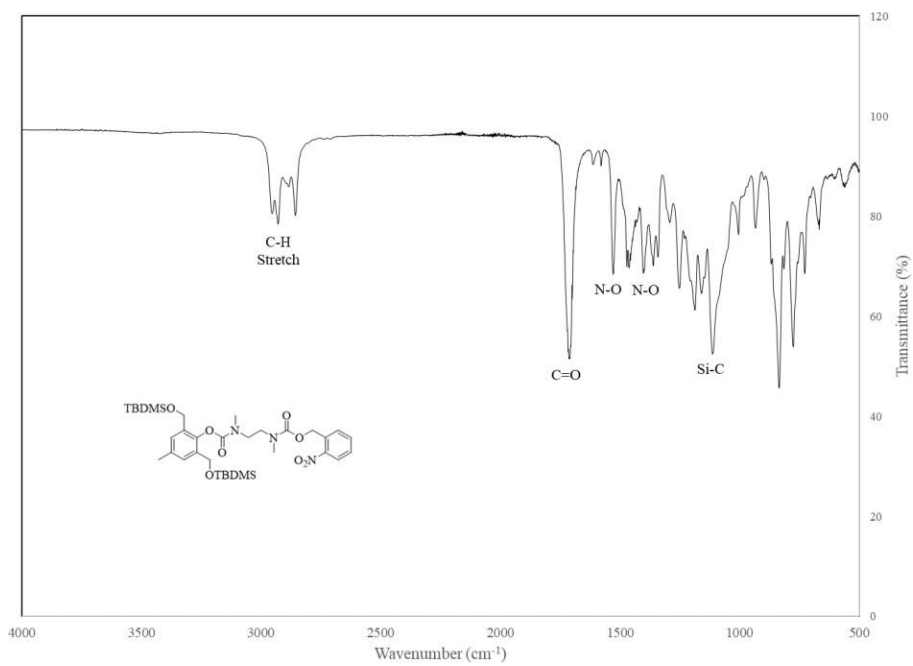
A31. ^{13}C NMR spectrum of **TEG-alkyne** (100 MHz, CDCl_3).



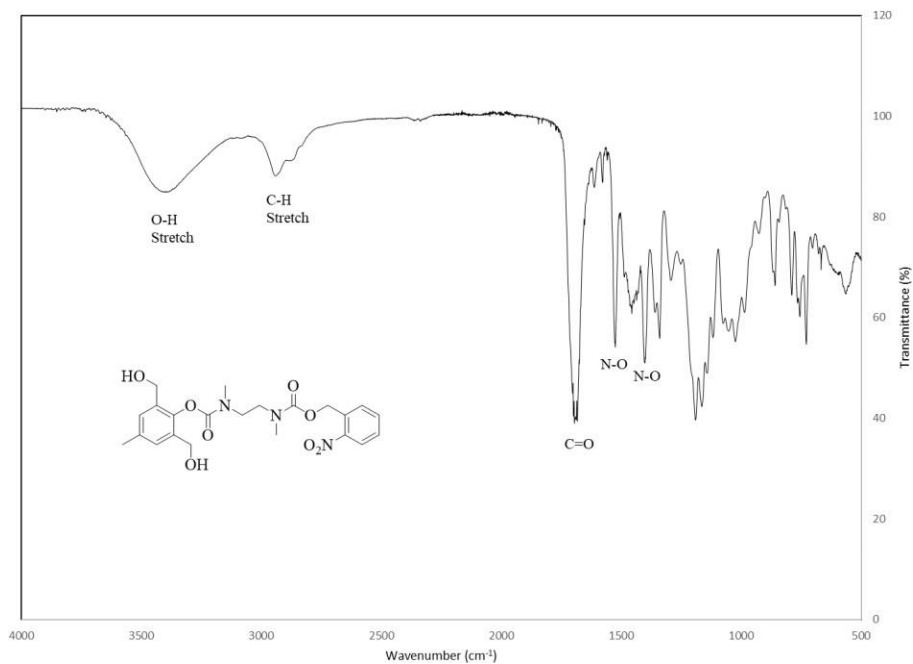
A32. FTIR of compound **3**.



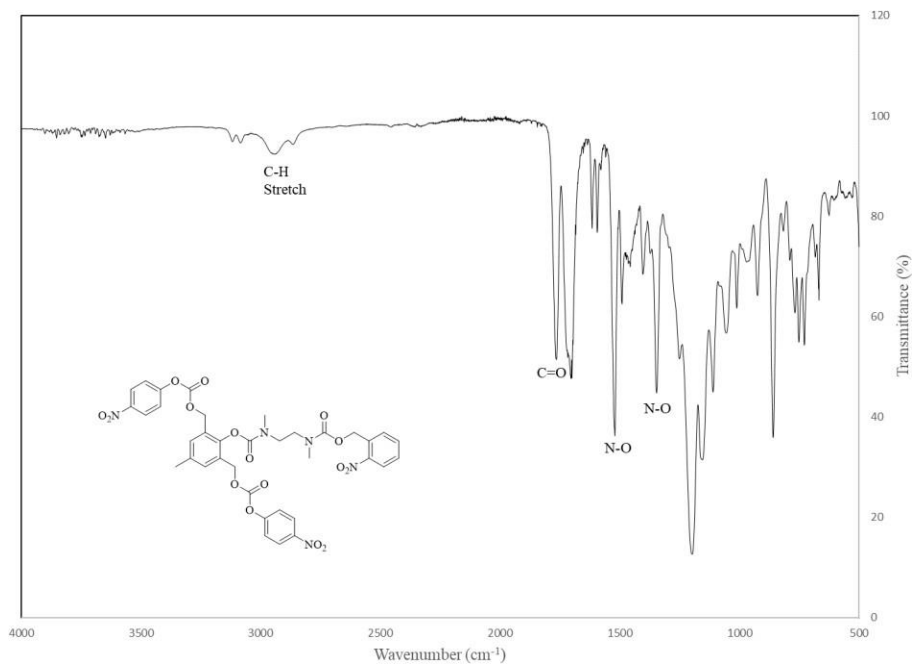
A33. FTIR of compound 4.



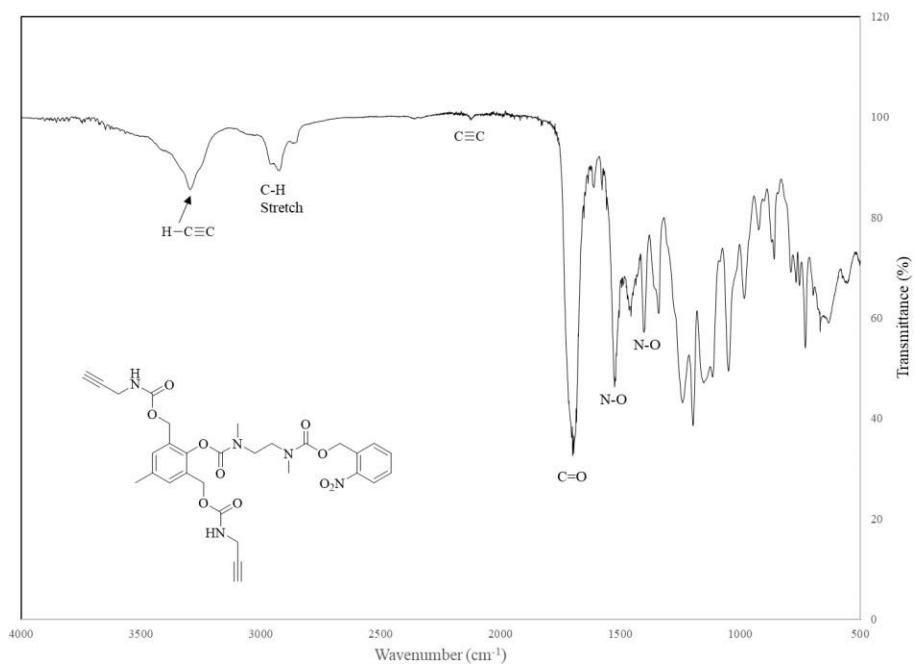
A34. FTIR of compound 6.



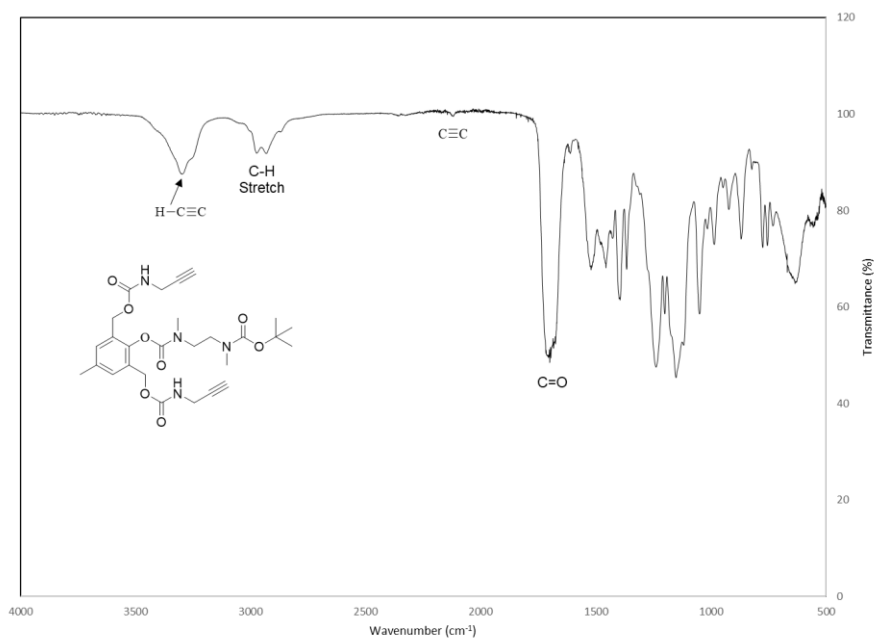
A35. FTIR of compound 7.



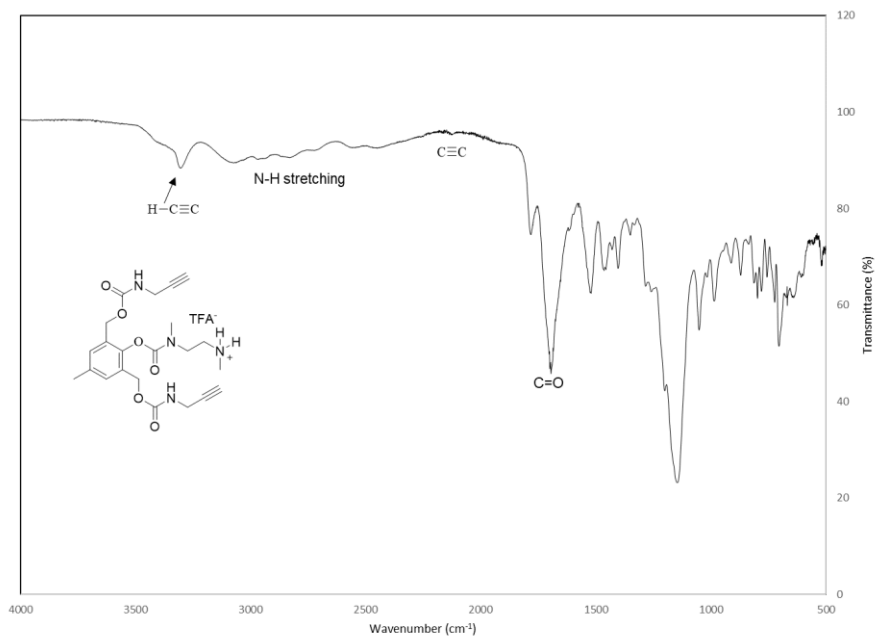
A36. FTIR of compound 8.



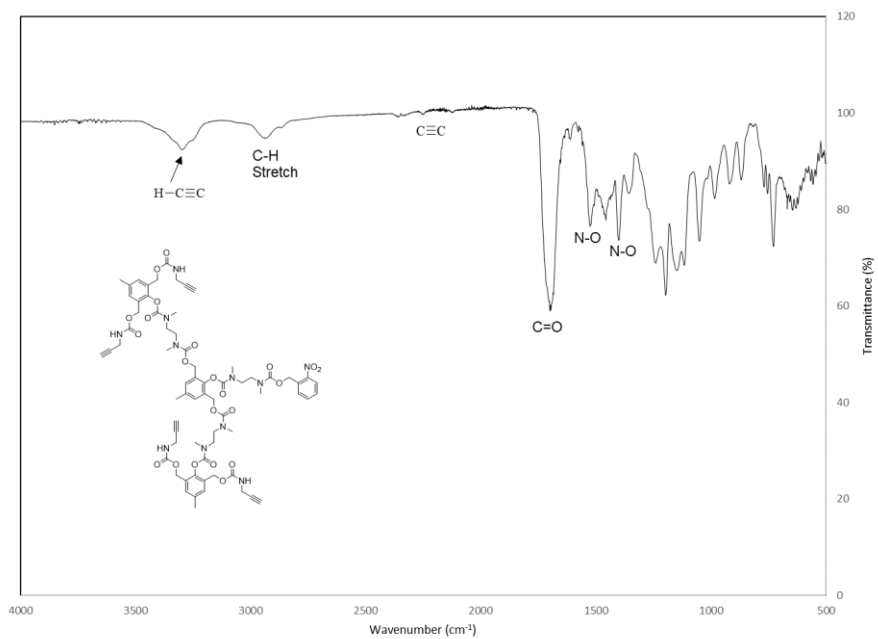
A37. FTIR of G1 SID.



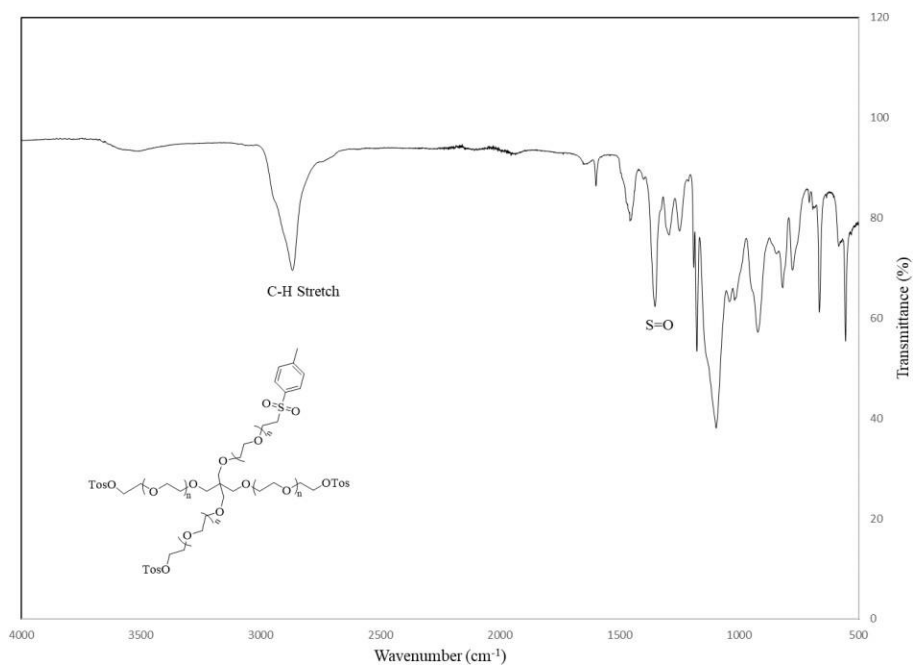
A38. FTIR of compound 12.



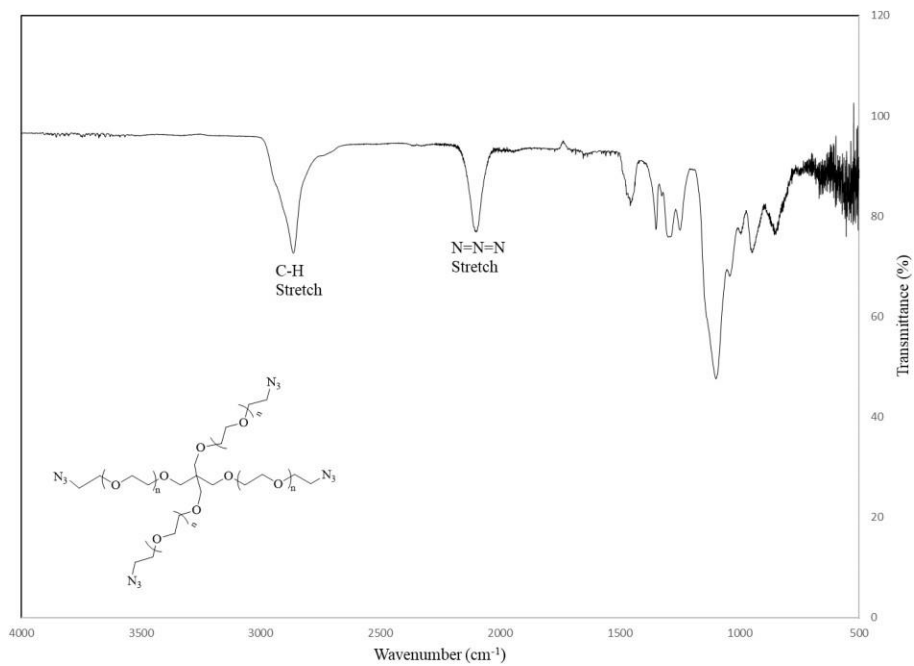
A39. FTIR of compound 13.



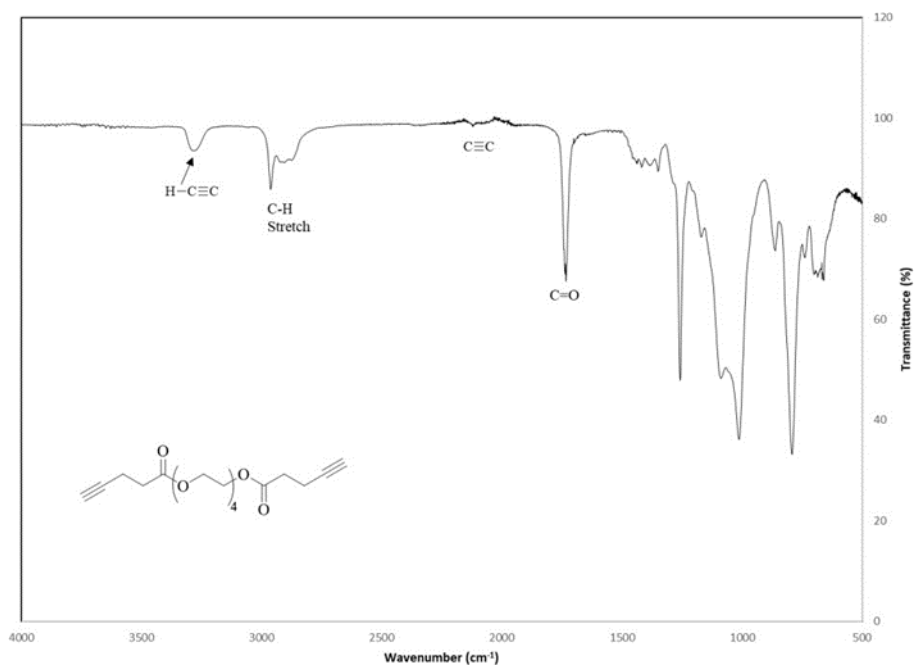
A40. FTIR of G2 SID.



A41. FTIR of compound 14.



A42. FTIR of 4-arm-PEG-azide.



A43. FTIR of TEG-alkyne.

Curriculum Vitae

Name: Karanpreet Gill

Post-secondary Education and Degrees: The University of Western Ontario
London, Ontario, Canada
2013-2018 B.Sc.

The University of Western Ontario
London, Ontario, Canada
2019-2021 M.Sc.

Honours and Awards: Western Scholarship of Excellence
2013

Dean's Honour List
2014, 2015, 2016, 2018

Queen Elizabeth II Science and Technology Scholarship
2020-2021

Related Work Experience Teaching Assistant
The University of Western Ontario
2019-2020

R&D Technologist
Presidium USA Inc.
2019

R&D Chemist
ARLANXEO
2016-2017